JOURNAL OF THE

Electrochemical Society

Vol. 110, No. 10 October 1963

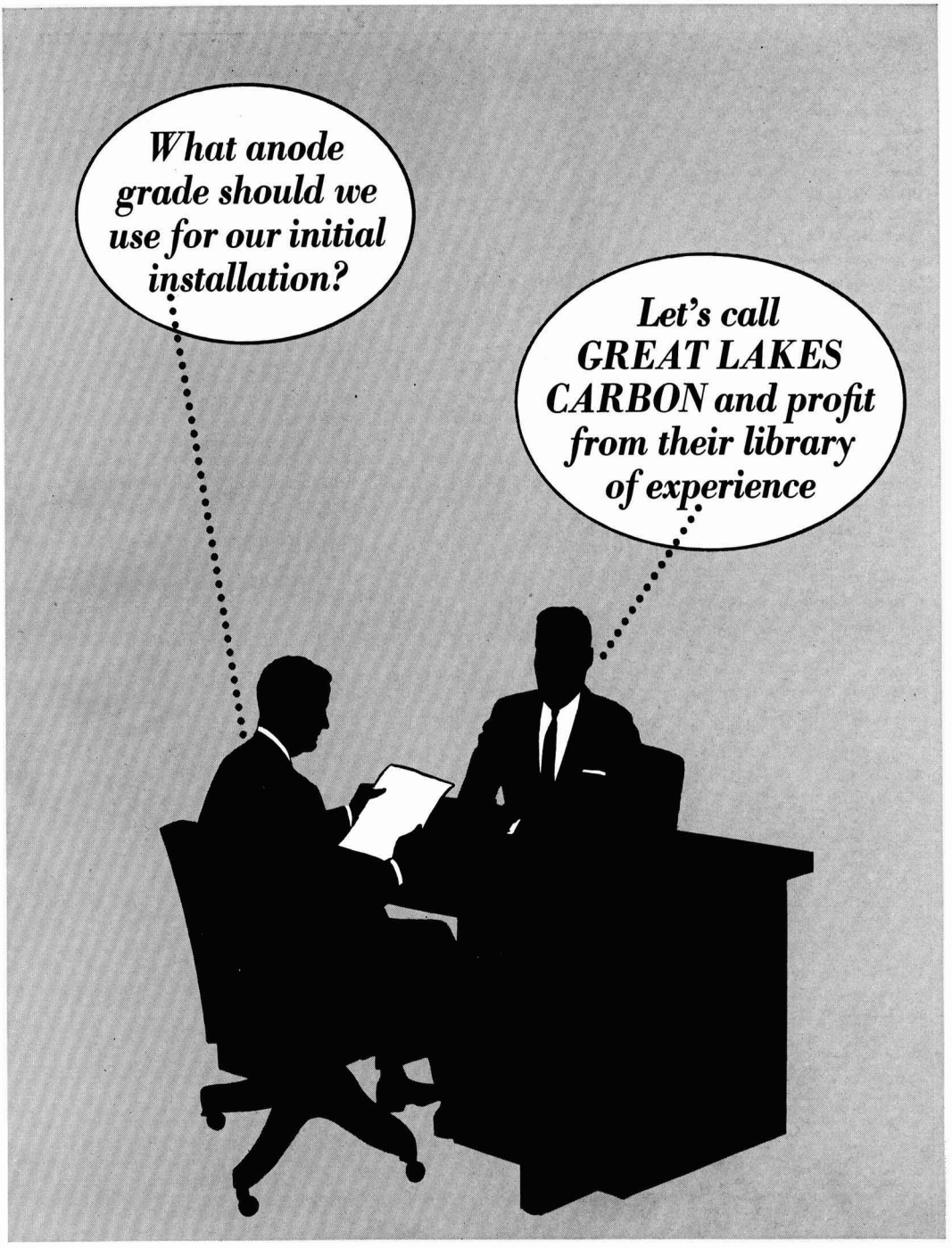

PRODUCTS YOU CAN TRUST
GRAPHITE PRODUCTS
GLC
DIVISION

GREAT LAKES CARBON CORPORATION

18 EAST 48TH STREET, NEW YORK 17, N.Y. OFFICES IN PRINCIPAL CITIES

Manuscripts submitted to the Journal should be sent, in triplicate, to the Editorial Office at 30 East 42 St., New York 17, N. Y. They should conform to the revised Instructions to Authors published on pp. 225C-226C of the Sept. issue. Manuscripts so submitted become the property of The Electrochemical Society and may not be published elsewhere, in whole or in part, unless permission is requested of and granted by the Editor.

The Electrochemical Society does not maintain a supply of reprints of papers appearing in its Journal. A photoprint copy of any particular paper, however, may be obtained by corresponding direct with the Engineering Societies Library, 345 E. 47 St., New York, N. Y.

Inquiries re positive microfilm copies of volumes should be addressed to University Microfilms, Inc., 313 N. First St., Ann Arbor, Mich.

Walter J. Johnson, Inc., 111 Fifth Ave., New York 3, N. Y., have reprint rights to out-of print volumes of the Journal, and also have available for sale back volumes and single issues, with the exception of the current calendar year. Anyone interested in securing back copies should correspond direct with them.

Journal of the Electrochemical Society

OCTOBER 1963 **VOL. 110 • NO. 10**

CONTENTS

Published monthly by The Electrochemical Society, Inc., at 215 Canal St. Manchester, N. H.; **Executive Offices, Editorial Office** and **Circulation Dept.,** and **Advertising Office** at 30 East 42 St., New York 17, N. Y., combining the JOURNAL and TRANSACTIONS OF THE ELECTROCHEMICAL SOCIETY. Statements and opinions given in articles and papers in the JOURNAL OF THE ELECTROCHEMICAL SOCIETY are those of the contributors, and The Electrochemical Society assumes no responsibility for them. Subscription to members as part of membership service; subscription to nonmembers $24.00 plus $1.50 for postage outside U.S. and Canada. Single copies $1.70 to members, $2.25 to nonmembers.

Entered as second-class matter at the Post Office at Manchester, N. H., under the act of August 24, 1912.

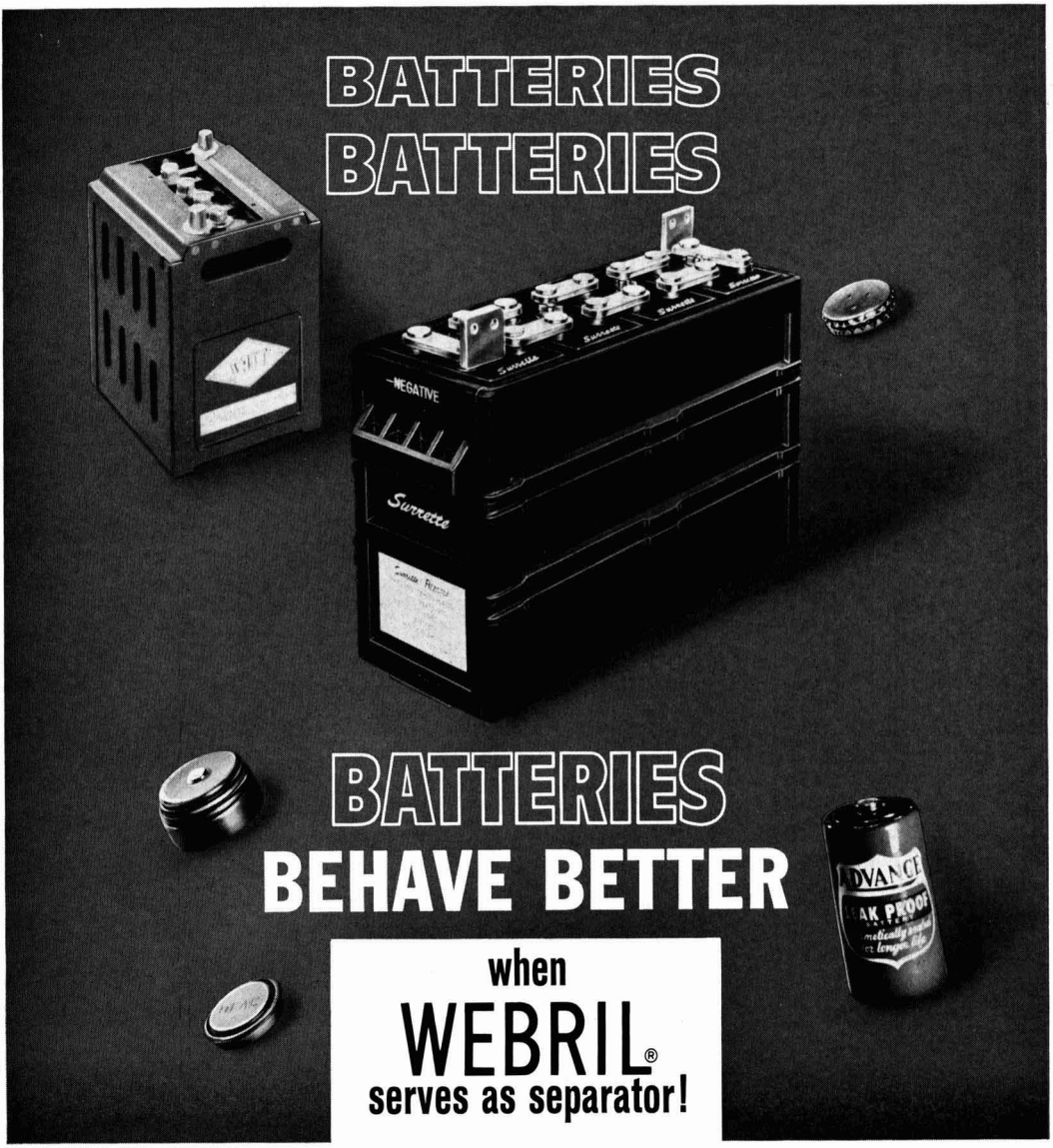

PRIMARY OR SECONDARY SYSTEMS, ACID OR ALKALINE, get greater life, more dependable operating characteristics with WEBRIL Non-Woven Separator Fabrics.

Proven by long time use in mercury, silver-zinc, silver-cadmium, nickel-cadmium, lead-acid and various specialty defense batteries. WEBRIL Non-Woven Separator Fabrics can consist of Polypropylene, Dynel*, Nylon, highly purified cotton, modified cellulose or other appropriate fibers. They provide longer life by

- Inhibiting dendrite growth and passage
- Holding active material on plates
- Allowing free ionic passage
- Avoiding separator degradation
- Assuring electrolyte contact with plates

Take a good look at WEBRIL Non-Woven Separator Fabrics—see what they can do to improve your battery design and performance. Write, wire or phone.

ELECTRICAL SPECIALTIES DEPARTMENT

THE **KENDALL** COMPANY
Fiber Products Division
WALPOLE, MASS., U. S. A.

* *Union Carbide Corp. trademark for its modacrylic fiber*

Las Cucarachas y las Chinches

SINCE the excitement created by Rachel Carson's book "Silent Spring" has somewhat abated and the various Committees have reported to the President, to Congress and to one or another government department, the pesticide situation can be considered more calmly. Insecticides are quite indispensable to modern civilization; without them there might be no more insects than at present, but there certainly would be fewer human beings. Having eliminated many enemies of the insects and created a favorable environment for certain types of pest, man must protect himself and his food and vegetation supplies as best he can. The time is long past when the farmer could pay the children 1¢ per hundred to pick Colorado potato beetles and drop them into kerosene, or to execute big green tobacco hornworms with a snap of the wrist. Lead arsenate took over, applied with a 2-row duster strapped over the shoulders and operated by turning a crank. Now, with tractor-drawn multirow sprayers and modern insecticides, the potato beetle is no longer a menace, and there is tobacco for everyone, lung cancer or no.

India has a large and growing population and not enough food for everyone. It is said that her greatest agricultural need is for insecticides and tools to apply them; the need for fertilizer comes second. Why try to raise a big crop if 80% of it is ruined by insects? China was in a similar position in 1947 (*Science*, 9 August 1963), and it is unlikely that the Communists have distributed insecticides, sprayers, and dusters since that time.

The recent investigations have made it clear that the dangerous chemical pesticides should be treated with much more respect and caution. These violent poisons should be properly labeled, and suburban gardeners and large-scale growers alike should receive education and information to protect themselves, their children, and the consumers of their products. Airplane dusting and other methods of application to large areas should be under strict control of competent authorities, and better techniques should be worked out. Finally, much research is needed on other methods of insect control, such as the isolation, analysis and synthesis of the "scents" which bring male and female together; and development of other lures which can be used to trap large numbers of insects, perhaps to be sterilized with radiation or chemicals and then released.

One appreciates the need for control of the spruce and pine budworms after seeing a few trees which have been stunted and deformed by the pest. The moth deposits eggs in the topmost bud, the "leader" which normally grows upward the following year, with a circle of side branches at its base. When the eggs hatch the worms destroy the bud and the tree grows no taller. In another year or two a shoot from a side branch takes over and the tree grows upward again, with a crooked trunk: that is, if the leading bud is not ruined again. With whole forests at stake it is tempting to dust from planes, even at the expense of decimating the useful insects and the birds, small animals, and fish. Too bad a trace of poison cannot be delivered to each bud concerned without contamination of the whole forest and the streams in and below it. There must be better ways to control the budworm, the *cucaracha* and the *chinche* too. Intensive research is needed in these areas.

—CVK

how do you look at ANODES?

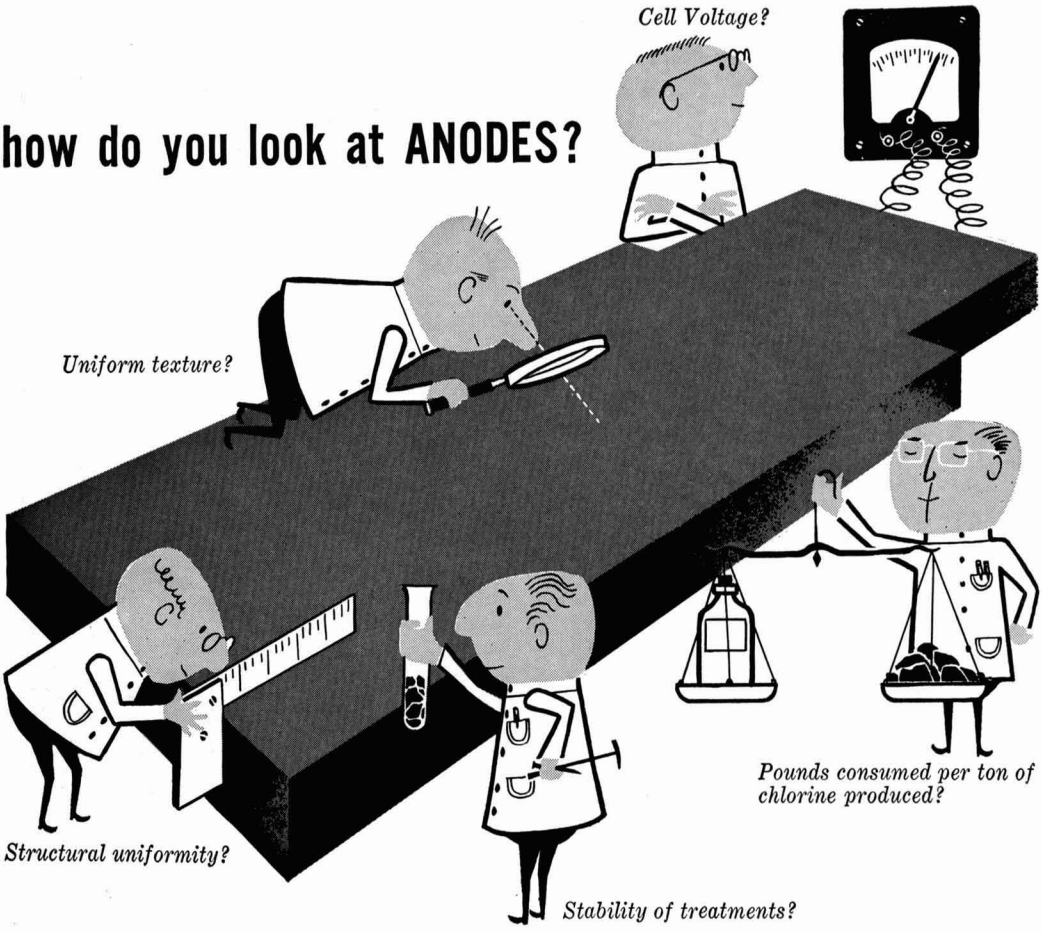

Judged by Cell Maintenance Costs Alone,

the highly stable impregnants used in Stackpole GraphAnode reduce diaphragm clogging to a bare minimum. The graphite is consumed slowly and evenly. Because GraphAnode anodes present uniform, low-porosity surfaces to the electrolyte, the graphite does not slough off to clog the diaphragm or to contaminate the cell.

Judged by Anode Cost and Performance,

Stackpole GraphAnode proves second to none whether you figure in terms of anode life, or in tons of chlorine produced per pound of graphite consumed. You get maximum anode life . . . and with the added advantage of low cell voltages. Stackpole engineers stand ready to offer a convincing demonstration on your equipment.

Stackpole Carbon Company, St. Marys, Pa.

STACKPOLE
GraphAnode®

ELECTROCHEMICAL ANODES FOR DIAPHRAGM, MERCURY, MANGANESE DIOXIDE, & SODIUM CHLORATE CELLS. OTHER TYPES FOR CATHODIC PICKLING, ALUMINUM ANODIZING, AND OTHER USES.

CATHODIC PROTECTION ANODES • FLUXING & DE-GASSING TUBES • SALT BATH RECTIFICATION RODS • ROCKET NOZZLES • RISER RODS • GRAPHITE BEARINGS & SEAL RINGS • ELECTRODES & HEATING ELEMENTS • WELDING CARBONS • VOLTAGE REGULATOR DISCS • "CERAMAGNET"® CERAMIC MAGNETS • ELECTRICAL CONTACTS • BRUSHES for all rotating electrical equipment • and many other carbon, graphite and electronic components.

Report from

BELL LABORATORIES

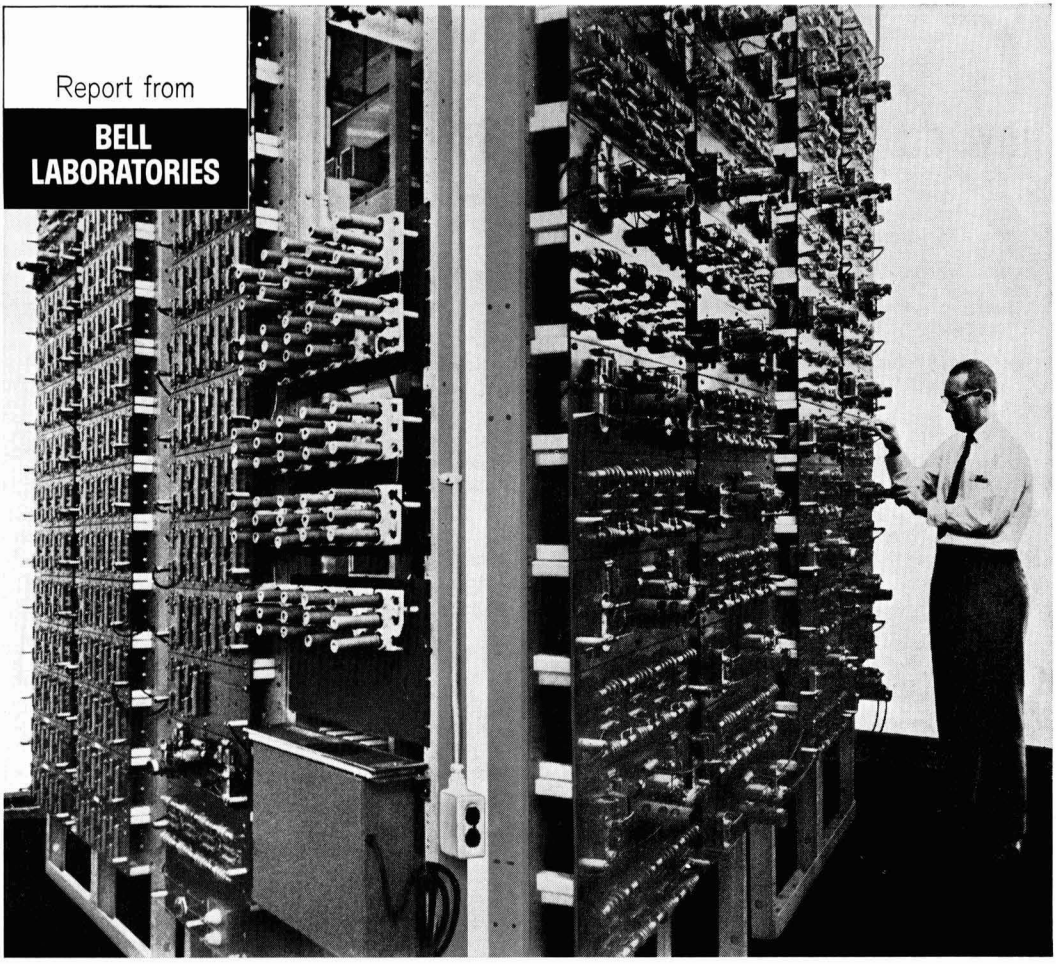

Engineer A. H. Evans measures the effect of voltage surges on Bell Laboratories' simulated undersea telephone cable. Simulating 180 amplifiers and 181 cable sections, with a total length of 3600 miles, the arrangement includes over 1100 electrical components. Photo merges two sides of the simulated cable so that both can be viewed at once.

THE UNDERSEA "CABLE" THAT NEVER GOES TO SEA

In undersea cable systems, electric power for the amplifiers is transmitted along the cable itself. To make this possible, precisely engineered circuits and devices must be designed into the system for protecting electron tubes and other components from sudden voltage surges which may result from accidental damage to the cable.

In systems such as these, the computation of the effects of such surges to establish the needed design parameters is extremely complex. Here, as in many other areas of our work, a solution to the problem has been found through electrical simulation.

Full-scale simulation is achieved by means of networks of electrical components. For the new 128-channel cable scheduled for transatlantic service this year, a network (above) was built to simulate the power path of a 3600-mile cable with its 180 amplifiers.

With the aid of this simulator, engineers can study the effects of voltage surges, the operation of electron tube protectors, and the performance of the power supply in the various contingencies that may occur in active service.

This study of unknown factors by means of electrical simulation is an example of how engineers at Bell Laboratories work to assure the performance and reliability of new communications systems before they are committed to service.

Bell Telephone Laboratories

World center of communications research and development

Monographs of The Electrochemical Society

ECS Series

The following are books developed and sponsored by The Electrochemical Society and published by John Wiley & Sons, Inc., 605 Third Ave., New York 17, N. Y. Members of The Electrochemical Society can receive a 33 1/3% discount by ordering volumes from Society Headquarters, 30 East 42 St., New York, N. Y., 10017. Book and invoice will be mailed by John Wiley & Sons. Nonmembers (including subscribers) should order direct from Wiley.

Corrosion Handbook. Edited by Herbert H. Uhlig. Published 1948, 1188 pages, **$16.00**

Modern Electroplating. Edited by Allen G. Gray. Published 1953, 563 pages, **$8.50** (Out of print; new edition to be published sometime in 1963)

Abstracts of the Literature on Semiconducting and Luminescent Materials and Their Applications. Compiled by Battelle Memorial Institute.

Vol. I, 1953 Issue—published 1955, 169 pages, **$5.00** (soft cover); **Vol. II, 1954 Issue**—published 1955, 200 pages, **$5.00** (soft cover); **Vol. III, 1955 Issue**—Edited by E. Paskell; published 1957, 322 pages, **$10.00** (hard cover); **Vol. IV, 1956 Issue**—Edited by E. Paskell, published 1959, 456 pages, **$12.00** (hard cover); **Vol. V, 1957 Issue**—Edited by C. S. Peet; published 1960, 449 pages, **$12.00** (hard cover); **Vol. VI, 1958 Issue**—Edited by J. J. Bulloff and C. S. Peet; published 1961, 528 pages, **$14.00** (hard cover); **Vol. VII, 1959 Issue**—Edited by J. J. Bulloff and C. S. Peet; published 1962, 728 pages, **$20.00 (hard cover).**

Electrochemistry in Biology and Medicine. Edited by Theodore Shedlovsky. Published 1955, 369 pages, **$11.50**

Vapor Plating (The Formation of Metallic and Refractory Coatings by Vapor Deposition), by C. F. Powell, I. E. Campbell, and B. W. Gonser. Published 1955, 158 pages, **$6.00**

High-Temperature Technology (Materials, Methods, and Measurements). Edited by I. E. Campbell. Published 1956, 526 pages, **$15.00** (Out of print; new edition in course of preparation)

Stress Corrosion Cracking and Embrittlement. Edited by W. D. Robertson. Published 1956, 202 pages, **$7.50**

Arcs in Inert Atmospheres and Vacuum. Edited by W. E. Kuhn. Published 1956, 188 pages, **$7.50**
(Papers Presented at the Symposium on Arcs in Inert Atmospheres and Vacuum of the Electrothermics and Metallurgy Division of The Electrochemical Society, April 30 and May 1, 1956, San Francisco, Calif.)

Technology of Columbium (Niobium). Edited by B. W. Gonser and E. M. Sherwood. Published 1958, 120 pages, **$7.00**
(Papers Presented at the Symposium on Columbium—Niobium of the Electrothermics and Metallurgy Division of The Electrochemical Society, May 15 and 16, 1957, Washington, D. C.)

The Structure of Electrolytic Solutions. Edited by Walter J. Hamer. Published 1959, 441 pages, **$18.50**
(Based on a Symposium held in Washington, D. C., in May 1957, sponsored by The Electrochemical Society, New York, and The National Science Foundation, Washington, D. C.)

Mechanical Properties of Intermetallic Compounds. Edited by J. H. Westbrook. Published 1959, 435 pages, **$9.50**
(A Symposium, Sponsored by the Electrothermics and Metallurgy Division of The Electrochemical Society, May 4, 5, and 6, 1959, Philadelphia, Pa.)

The Surface Chemistry of Metals and Semiconductors. Edited by Harry C. Gatos, with the assistance of J. W. Faust, Jr., and W. J. La Fleur. Published 1960, 526 pages, **$12.50**
[Proceedings of an International Symposium Sponsored Jointly by the Office of Naval Research and The Electrochemical Society, Inc. (Corrosion and Electronics Divisions), October 19, 20, and 21, 1959, Columbus, Ohio]

Transactions of the Symposium on Electrode Processes. Edited by Ernest Yeager. Published 1961, 374 pages, **$20.00** (The papers and discussions of the Symposium on Electrode Processes, sponsored jointly by the U. S. Air Force, Office of Scientific Research, and The Electrochemical Society, Inc., Philadelphia, Pa., May 1959).

Iodide Metals and Metal Iodides, by Robert F. Rolsten. Published 1961, 441 pages, **$17.50**

Other ECS Publications

Vacuum Metallurgy, third printing, 1958. **Edited by J. M. Blocher, Jr.; 216 pages; $5.00, less a 20% discount** to ECS members only. Available from Electrochemical Society Headquarters, 30 East 42 St., New York 17, N. Y. (Papers Presented at the Vacuum Metallurgy Symposium of the Electrothermics and Metallurgy Division of The Electrochemical Society held in Boston, Mass., October 6 and 7, 1954)

Rhenium, Edited by B. W. Gonser. Published by Elsevier Publishing Co., 1962. 225 pages; $11.00. (Papers Presented at the Symposium on Rhenium of the Electrothermics and Metallurgy Division of The Electrochemical Society, May 3 and 4, 1960, Chicago, Ill.) ECS Members can obtain a 30% discount by sending their orders direct to Society Headquarters, 30 East 42 St., New York 17, N. Y. Remittance, made payable to American Elsevier Publishing Co., 52 Vanderbilt Ave., New York 17, N. Y. should accompany the order. Nonmembers must order direct from the publisher.

Iron Ore Reduction, Edited by R. R. Rogers. Published by Pergamon Press Ltd., New York and London, 1962. 359 pages; $12.50. (Proceedings of a Symposium of the Electrothermics and Metallurgy Division of The Electrochemical Society, held in Chicago, Ill., May 3-5, 1960) Order direct from the publisher. Pergamon Press Ltd., 122 East 55 St., New York 22, N. Y.

Thermodynamics of Hydrocarbon Fuel Cells

E. J. Cairns, A. D. Tevebaugh, and G. J. Holm

Research Laboratory, General Electric Company, Schenectady, New York

ABSTRACT

Recently, there has been a great increase in activity in the field of hydrocarbon fuel cells. A rather neglected area has been that of the thermodynamics of the reactions in the anode compartment. The conditions under which a fuel cell must be operated in order to prevent carbon deposition have been calculated for the CHO system at 500°K under two important sets of conditions. Two literature methods for the calculation of the complex gas phase equilibria were evaluated, and an improved method extending one of these methods is presented. The calculations show that unexpectedly high and constant emf values are possible. Appreciable amounts (*ca.* 1%) of hydrogen were found to be present at equilibrium over a wide range of fuel compositions at 500°K. The levels of CO partial pressures at equilibrium were found to be about 10^{-5} atm.

In recent years, there has been a great upsurge of interest and activity in the field of hydrocarbon fuel cells. A great deal of effort has been expended in the search for optimum combinations of anode electrocatalysts, fuels, and electrolytes. A rather neglected area has been that of the thermodynamics of the reactions which take place or may take place in the anode compartment of a fuel cell using a hydrocarbon or a modified hydrocarbon (*e.g.*, CH_3OH) as the fuel. It is in this important area that the present work has been concentrated.

There are several areas relating to the theory and operation of hydrocarbon fuel cells where thermodynamics can make a contribution. The theoretical open-circuit voltage of a fuel cell at thermodynamic equilibrium may be calculated only if the composition of the anode gas is known. Usually, the assumption is made that the open-circuit voltage should correspond to that calculated by applying the Nernst equation to the inlet fuel composition. Hardly ever can this method be expected to yield an accurate result since the inlet fuel composition can be significantly different from the gas phase composition which would exist at chemical equilibrium. The maximum voltage attainable in a fuel cell during the process of oxidation, or during the procession of the fuel gas through a series of fuel cells (during which it is being oxidized) may be calculated, providing the composition of the gas is known as a function of the degree of oxidation. An important consideration, especially for fuel cells which are required to operate for extended periods of time, is whether or not it is thermodynamically possible for carbon to deposit from the fuel gas in the anode compartment during any stage of its oxidation. The deposition of carbon has been found to be a particularly troublesome problem to some fuel cell investigators (1-6). All of these problems and some others have been considered and are reported on here.

Making use of our recent results on the carbon deposition boundaries in the CHO system (7), it is now possible to calculate precisely the conditions under which carbon deposition at equilibrium can be avoided for any CH or CHO fuel system. These computations provide a starting point for the determination of the gas phase compositions and the maximum theoretical emf values for fuel cell operation outside the carbon deposition region. The two practical methods for avoiding carbon deposition are mixing water with the fuel and recycling the combustion products (CO_2 and H_2O) with the fuel. These general methods will be discussed for the case where methane is used as the fuel.

The calculation of the equilibria among the several important species in the anode compartment of a hydrocarbon fuel cell is not a simple task even using the so-called simplified methods. Because of the complexity of these calculations, it is desirable to discuss methods by which they may be carried out and the disadvantages of some procedures.

Thermodynamic Methods

Thermodynamic considerations may be used to determine the important chemical species which must be considered in calculating the equilibria of interest to fuel cell operation. The species most likely to be present in the greatest amounts are determined by their equilibrium constants of formation and the equilibria among these species under the conditions of interest. In the system containing the elements carbon, hydrogen, and oxygen at a pressure of 1 atm, the most important species are carbon, hydrogen, water, carbon dioxide, carbon monoxide, and methane, with other species such as ethane, methanol, and some of the other hydrocarbons being present in very much smaller amounts in the temperature range of 298°-1500°K. Details of the method establishing the above mentioned species as the only important ones have been given in an earlier paper (8).

Various simplified computational methods which have been applied to the CHO system containing only those species mentioned above are available in the literature (9-14). Some of these methods are largely graphical (9, 11, 12), while others are algebraic (10, 13, 14). These simple methods can be justified only when a limited number of results are

necessary, or when limited accuracy is desired. More sophisticated mathematical approaches, using computer methods (15, 16), are highly recommended where a large volume of high precision results is required.

Mayland and Hays (9) have presented a graphical method for determining the equilibrium gas phase composition for the CHO system in the absence of solid carbon. The preparation of a plot of log (CH_4/CO) *vs.* log (CO_2/CO) for various values of (H_2/CO) was described in detail. The procedure for the calculation of the amounts of H_2O and the various partial pressures was also described. Given this plot, it is necessary to perform subsequent calculations in order to obtain results applicable to a specific fuel cell system. These calculations will be described below.

Case I.—Prevention of carbon deposition by recycling oxidation products with methane as the fuel. The gas phase composition and the theoretical maximum emf are to be calculated for operation of a methane fuel cell at 500°K and 1 atm absolute pressure.

First, it is necessary to establish those conditions under which carbon cannot be present at equilibrium. Figure 1 shows some data selected from our recent work (8) which are pertinent to this example. Above the carbon deposition boundary, carbon will be present; below this boundary, all of the carbon is combined and is in the gas phase. The point representing CH_4 is shown on the H-C axis of Fig. 1. A straight line joining the CH_4 point to the 0 vertex shows the path of the over-all composition of the system during the oxidation process. The equilibrium gas phase composition during oxidation follows a path along the carbon deposition boundary until point a is reached. On further oxidation from point a, along the path aO to point b, carbon is no longer present at equilibrium. Point b (on the line joining CO_2 and H_2O) represents complete oxidation of the fuel mixture. It is along the path ab that the fuel cell will operate free of carbon at equilibrium (500°K, 1 atm total pressure).

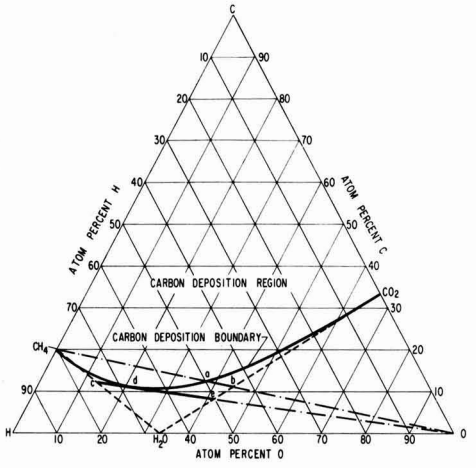

Fig. 1. Graphical determination of CH_4 fuel mixture compositions which will not deposit carbon at equilibrium (500°K, 1 atm).

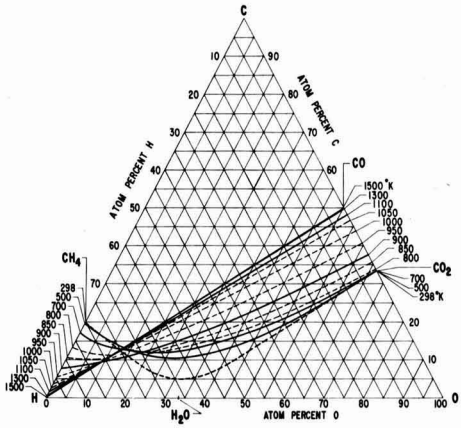

Fig. 2. Carbon deposition boundaries for the CHO system at 1 atm.

Point a in Fig. 1 determines the number of moles of oxidation products (1 CO_2 + 2H_2O) to be recycled with 1 mole of the methane fuel. This amount was calculated from Eq. [1] and the C:H:O ratio at point a.

$$\text{Point a} = 1\ (CH_4) + x(CO_2 + 2H_2O)$$

$$x = \frac{4 - 5f_{(H)}}{9f_{(H)} - 4} = \frac{4 - 5(0.5)}{9(0.5) - 4} = 3 \quad [1]$$

where $f_{(H)}$ = the hydrogen atom fraction at point a, Fig. 1. Thus, recycling three moles of the oxidation product mixture (1CO_2 + 2H_2O) with each mole of methane entering a fuel cell will (at equilibrium, 500°K, and 1 atm pressure) permit complete oxidation of the methane without the deposition of solid carbon.

The carbon deposition boundaries over the temperature range 298°-1500°K for 1 atm pressure are shown in Fig. 2 (7). The conditions under which a fuel cell may be operated outside the carbon deposition region at any temperature may be calculated by the use of this figure.

The calculation of the gas phase compositions along the fuel cell operating line ab (Fig. 1) was performed by an extension of the graphical method of Mayland and Hays (9). By comparison of the range of the C:H:O gas phase ratios for line ab with Fig. 1 of Mayland and Hays (9), it was found that the range of interest was not covered. Following their methods, the solid lines of Fig. 3 were then prepared to cover the desired range. Since the H_2/CO ratio is an important parameter in the use of Fig. 3, it was necessary to devise a method for determining H_2/CO along the line ab of Fig. 1.

Since all points along the line joining CH_4 to the 0 vertex in Fig. 1 have a constant H/C ratio equal to 4.00, this value of H/C is an important parameter in these calculations and was used to determine the path of the operating line ab when transferred to Fig. 3. Since the locus of all points of H/C = 4.00 in Fig. 3 corresponds to line ab of Fig. 1 it was necessary to locate the line on Fig. 3 corresponding to H/C = 4.00. In order to accomplish this, a crossplot of H/C *vs.* CH_4/CO from Fig. 3 was prepared

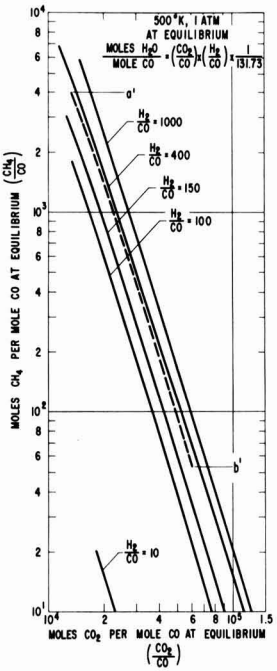

Fig. 3. Equilibrium gas compositions at 500°K and 1 atm for the CHO system.

for various constant values of CO_2/CO. The intersections of these lines with the line H/C = 4.00 then allowed the line a'b' to be plotted on Fig. 3. In order to determine the gas phase compositions from line a'b', it was necessary to know how H_2/CO varied along this line. This was accomplished by using a crossplot of H_2/CO *vs.* CH_4/CO for constant CO_2/CO values from the solid lines of Fig. 3. The CH_4/CO values from line a'b' were then used with this crossplot to determine H_2/CO at the various CO_2/CO values along line a'b'. Along the line a'b', H_2/CO was found to vary from 263 at a' to 261 at b'.

Using line a'b' and the values of H_2/CO, the relative partial pressures of H_2, CH_4, CO_2, and CO were known, and from Eq. [2]

$$K_1 = \frac{[H_2][CO_2]}{[CO][H_2O]}$$

$$\therefore\ [H_2O] = \frac{[H_2][CO_2]}{K_1[CO]} \qquad [2]$$

the relative H_2O partial pressure could be calculated. The true partial pressure of each species could then be calculated knowing that the total pressure was 1 atm.

Consistent with the previous discussion, point a of Fig. 1 was defined as the composition representing 0% combustion in the fuel cell, and corresponds to point a' of Fig. 3. The composition of the fuel mixture in the anode compartment during oxidation proceeds from a to b in Fig. 1 and from a' toward b' in Fig. 3. Various points along a'b' in Fig. 3 were chosen, and the gas phase compositions, cell potentials (from the Nernst equation), and per cents oxidation were calculated. The results will be discussed in detail in the next section.

Although this graphical method is straightforward, it was found necessary to prepare very large-scale plots and crossplots. In addition, it was required that the values obtained from the graphs be refined by trial and error calculation in order to maintain an error of less than 1%. These disadvantages cause the method to be very cumbersome and time consuming.

Case II.—Prevention of carbon deposition by mixing water with the methane fuel. The gas phase composition and the theoretical maximum emf are to be calculated for the operation of a methane fuel cell at 500°K and 1 atm absolute pressure.

The conditions under which carbon cannot be present at equilibrium were determined in a manner similar to that for case I. All mixtures of CH_4 and H_2O lie along the line joining the points CH_4 and H_2O in Fig. 1. In order to determine the fuel composition which is richest in CH_4, yet avoids carbon deposition during oxidation, a line is constructed from the O vertex such that it intersects the CH_4-H_2O line and is tangent to the 500°K carbon deposition boundary. The line cdeO was located in this manner. Point c represents a methane-water mixture, which can be oxidized completely (to point e) without carbon deposition at equilibrium. The water-methane mole ratio corresponding to point c, Fig. 1 was calculated (see case I) to be 1.039.

Due to the disadvantages encountered in the method of Mayland and Hays (cited in case I), the algebraic method of Montgomery *et al.* (10) appeared attractive. It was found that their equation 10b would not yield a correct solution for this case, although it was stated their equations applied to ". . . the general case with completely arbitrary feed ratios . . .". It was found, however, that equation 10b of Montgomery *et al.* (10) did yield correct results for H/C = 4.0, and that their material balance equations [13b] and [14b] were also correct. It was therefore decided to combine the equation

$$CH_s + nO_2 \rightarrow xCH_4 + aH_2O + \left(\frac{s}{2} - a - 2x\right)H_2 + (b-x)CO + (1-b)CO_2 \qquad [3]$$

and their material balance equations

$$b = K_8\left[\frac{K_1}{r}\left(\frac{s}{2} - 2x + rx\right) - 1\right] \qquad (10)\ [13b]$$

$$a = (1-b)\frac{r}{K_1} \qquad (10)\ [14b]$$

where

$$r = \frac{[H_2]}{[CO]} \text{ at equilibrium}$$

$$K_1 = \frac{[CO_2][H_2]}{[CO][H_2O]}$$

and

$$K_8 = \left[\frac{[CO_2][H_2]}{[CO][H_2O]} - 1\right]^{-1}$$

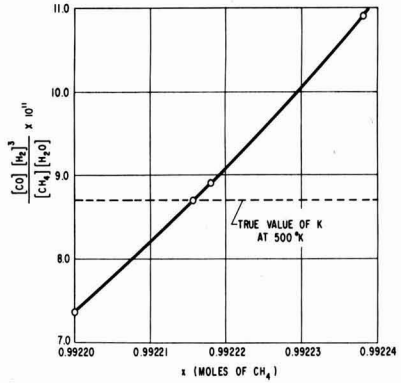

Fig. 4. Graphical solution for the equilibrium partial pressure of methane.

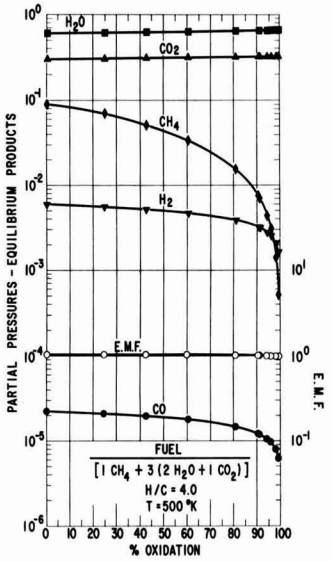

Fig. 5. Equilibrium gas compositions and cell potential as a function of per cent oxidation for a ($1CH_4 + 2H_2O + 1CO_2$) fuel, 500°K, 1 atm.

with a graphical method, plotting x *vs.* the deviation of the calculated equilibrium constants from the true values (see Fig. 4). As a guide in these calculations, the values of $[H_2]/[CO]$ at 0 and 100% oxidation were desired. These values for $[H_2]/[CO]$ were readily calculated. At 100% oxidation, the gas phase is primarily $CO_2 + H_2O$, and from material balance constraints and the equilibrium

$$CO + H_2O \rightleftharpoons CO_2 + H_2 \qquad K_1 \quad [4]$$

the $[H_2]/[CO]$ ratio can be calculated as follows:

$$\frac{\text{moles of } H_2O \text{ at 100\% oxidation}}{\text{moles of } CO_2 \text{ at 100\% oxidation}} = \frac{1.039 + 2.000}{1.000} = 3.039$$

$$K_1 = 131.73 = \frac{[CO_2]}{[H_2O]} \times \frac{[H_2]}{[CO]}$$

from which

$$\frac{[H_2]}{[CO]} = 400.3$$

The calculation of $[H_2]/[CO]$ at 0% oxidation is somewhat more involved than in the example above. As a first approximation, the problem can be approached in a manner similar to that above if one assumes that the methane and water do not react with each other; this yields a $[H_2]/[CO]$ ratio of 1,547 which can be used as a rough guide in the calculations from 100% oxidation to about 5% oxidation. When gas phase composition data have been calculated for approximately 5% oxidation, a more reliable boundary value for $[H_2]/[CO]$ at 0% oxidation can then be calculated. For example, using our results for 5.72% oxidation, material balance constraints, and the equilibrium constant equation K_1, the ratio of $[H_2]/[CO]$, as an upper limit, was calculated to be 17,030 for 0% oxidation of the fuel. The value 17,000 was used in the calculations and it was found that this value would correspond to a negative 0.47% oxidation; hence the true value of $[H_2]/[CO]$ for 0% oxidation is less than 17,000.

The combined algebraic and graphical method described above was found to be more rapid and simpler than the solution of the fourth order equation 10b of Montgomery *et al.*, and was very much faster than the all graphical method described for case I. A complete solution of the combined graphical and algebraic method for one set of conditions could be obtained on a desk calculator in 3 to 4 hr,

Table I. Case I: $1CH_4 + 2H_2O + 1CO_2$, 500°K, 1 atm

% Oxidation	Partial pressures, atm					Emf, v
	CH_4	H_2	CO	H_2O	CO_2	
0.069	9.01×10^{-2}	5.92×10^{-3}	2.27×10^{-5}	6.01×10^{-1}	3.03×10^{-1}	1.0355
24.6	7.03×10^{-2}	5.60×10^{-3}	2.14×10^{-5}	6.14×10^{-1}	3.10×10^{-1}	1.0338
42.5	5.17×10^{-2}	5.21×10^{-3}	1.99×10^{-5}	6.27×10^{-1}	3.16×10^{-1}	1.0319
60.2	3.45×10^{-2}	4.74×10^{-3}	1.81×10^{-5}	6.39×10^{-1}	3.21×10^{-1}	1.0294
80.6	1.60×10^{-2}	3.93×10^{-3}	1.50×10^{-5}	6.52×10^{-1}	3.27×10^{-1}	1.0252
90.4	7.86×10^{-3}	3.30×10^{-3}	1.26×10^{-5}	6.58×10^{-1}	3.30×10^{-1}	1.0210
90.8	7.19×10^{-3}	3.23×10^{-3}	1.23×10^{-5}	6.59×10^{-1}	3.31×10^{-1}	1.0204
94.0	4.58×10^{-3}	2.88×10^{-3}	1.10×10^{-5}	6.61×10^{-1}	3.31×10^{-1}	1.0180
95.8	3.18×10^{-3}	2.63×10^{-3}	1.00×10^{-5}	6.62×10^{-1}	3.32×10^{-1}	1.0160
97.9	1.46×10^{-3}	2.17×10^{-3}	8.26×10^{-6}	6.64×10^{-1}	3.32×10^{-1}	1.0118
99.0	5.29×10^{-4}	1.68×10^{-3}	6.40×10^{-6}	6.65×10^{-1}	3.33×10^{-1}	1.0063

Table II. Case II: 1 CH_4 + 1.039 H_2O, 500°K, 1 atm

% Oxidation	Partial pressures, atm					Emf, v
	CH_4	H_2	CO	H_2O	CO_2	
−0.47	4.83×10^{-1}	2.43×10^{-2}	1.43×10^{-6}	4.89×10^{-1}	3.79×10^{-3}	1.0708
5.72	4.31×10^{-1}	1.46×10^{-2}	6.34×10^{-6}	5.24×10^{-1}	3.00×10^{-2}	1.0579
10.0	3.96×10^{-1}	1.29×10^{-2}	8.63×10^{-6}	5.43×10^{-1}	4.77×10^{-2}	1.0545
13.5	3.69×10^{-1}	1.21×10^{-2}	1.09×10^{-5}	5.57×10^{-1}	6.12×10^{-2}	1.0525
21.3	3.15×10^{-1}	1.09×10^{-2}	1.25×10^{-5}	5.86×10^{-1}	8.87×10^{-2}	1.0492
39.0	2.13×10^{-1}	9.18×10^{-3}	1.53×10^{-5}	6.38×10^{-1}	1.40×10^{-1}	1.0437
55.8	1.38×10^{-1}	8.00×10^{-3}	1.60×10^{-5}	6.76×10^{-1}	1.78×10^{-1}	1.0398
71.1	8.16×10^{-2}	6.89×10^{-3}	1.53×10^{-5}	7.05×10^{-1}	2.06×10^{-1}	1.0353
91.2	2.15×10^{-2}	4.87×10^{-3}	1.19×10^{-5}	7.37×10^{-1}	2.37×10^{-1}	1.0269
94.7	1.24×10^{-2}	4.24×10^{-3}	1.05×10^{-5}	7.42×10^{-1}	2.41×10^{-1}	1.0238
97.9	4.42×10^{-3}	3.28×10^{-3}	8.17×10^{-6}	7.47×10^{-1}	2.45×10^{-1}	1.0181
99.8	1.45×10^{-4}	1.40×10^{-3}	3.49×10^{-6}	7.51×10^{-1}	2.48×10^{-1}	0.9999

with an accuracy of 3 or more significant figures in the calculated equilibrium constants.

Results and Discussion

Case I.—The results of the all-graphical method discussed above as applied to the case where carbon deposition was prevented by recycling the oxidation products with methane as the fuel (at 500°K) are presented in Table I and are plotted in Fig. 5. One of the most interesting aspects of Fig. 5 is that the emf remains surprisingly constant throughout nearly the full oxidation range, varying from 1.036v at 0.0% oxidation to 1.006v at 99.0% oxidation. Of course, the voltage must decrease very rapidly as 100% oxidation is very closely approached. The partial pressure of H_2 at equilibrium is sufficiently high in the above methane fuel mixture that the fuel cell performance on this fuel should be nearly equivalent to the performance on hydrogen alone if chemical equilibrium can be maintained, and if there are no gas phase mass transport limitations. Figure 5 also shows that the CO partial pressure is low enough at equilibrium that electrodes sensitive to its presence (*e.g.*, Pt) should not be "poisoned."

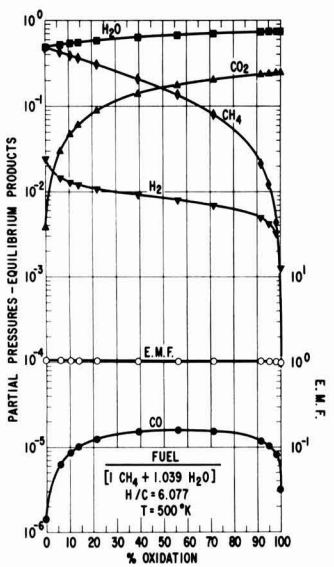

Fig. 6. Equilibrium gas compositions and cell potential as a function of per cent oxidation for a (1CH_4 + 1.039 H_2O) fuel, 500°K, 1 atm.

Case II.—The results of the combined algebraic and graphical method discussed earlier as applied to the case where carbon deposition was prevented by mixing water with the methane fuel (at 500°K) are presented in Table II and Fig. 6.

As in case I, it was found that the emf remained quite constant over nearly the full combustion range, varying from 1.0697v at 0.0% to 1.0135v at 99.0% oxidation. Again, the partial pressure of hydrogen is sufficiently high that the fuel cell performance might be expected to be considerably enhanced by its presence. On the average, the H_2 partial pressure for case II is about 1.7 times higher than for case I. An unexpected result was that the CO partial pressure showed a maximum, about an order of magnitude higher than its value at 0% oxidation. The general level of CO partial pressure is however very low from the standpoint of possible electrode "poisoning." In contrast to case I, CO_2 increases in partial pressure by about two orders of magnitude as the oxidation proceeds. This large change in CO_2 partial pressure is due to the fact that the fuel mixture of case I initially contained much more (combined) oxygen than was present in case II.

Theoretical Fuel Cell Potentials

The comparison of the emf values calculated for cases I and II as a function of per cent oxidation is shown in Fig. 7. These theoretical cell potentials were calculated from the equilibrium gas phase

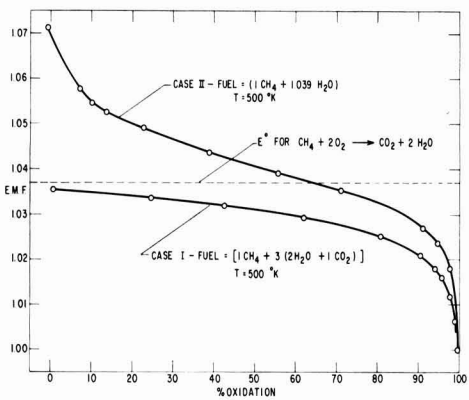

Fig. 7. Theoretical cell potentials for two fuel mixtures as a function of per cent oxidation (carbon free at equilibrium) at 500°K.

composition and the Nernst equation for a cell operating with 1 atm of oxygen at the cathode. As a reference, the dotted line in Fig. 7 shows the E° value at 500°K for the reaction

$$CH_4 + 2\,O_2 \rightarrow CO_2 + 2H_2O \qquad [4]$$

For case II, where water alone was added to the methane fuel, the theoretical cell potential lies above the E° value for reaction [4] up to 64.5% oxidation.

Summary and Conclusions

The conditions under which a fuel cell must be operated in order to prevent carbon deposition were calculated from our recent carbon deposition data for the CHO system. Two literature methods for calculations of CHO gas phase compositions in the absence of carbon were evaluated. An improved method based partially on one of the above methods was developed and illustrated. Examples of the two important methods for avoiding carbon deposition in a methane fuel cell at 500°K were calculated and compared in detail.

The conclusions drawn from the calculation are

1. Unexpectedly high and constant emf values (over a wide per cent oxidation range) were found for both of the methods of avoiding carbon deposition.

2. Appreciable (*ca.* 1%) amounts of hydrogen were present at equilibrium over essentially the full oxidation range. This could greatly enhance fuel cell performance on methane.

3. The levels of CO partial pressures at equilibrium were found to be very low ($\sim 10^{-5}$ atm) for all conditions considered, hence CO "poisoning" of fuel cell electrodes should not be a matter of concern so long as equilibrium is maintained.

Acknowledgments

The authors wish to thank H. A. Liebhafsky for his encouragement and support in this work. This work was supported in part by the Advanced Research Projects Agency (Order No. 247-61) through the United States Army Engineer Research and Development Laboratories, Ft. Belvoir, Va., under Contract No. DA-44-009-ENG-4853.

Manuscript received March 14, 1963; revised manuscript received May 10, 1963. This paper was presented at the Pittsburgh Meeting, April 15-18, 1963.

Any discussion of this paper will appear in a Discussion Section to be published in the June 1964 JOURNAL.

REFERENCES

1. V. S. Daniel-Bek, M. Z. Mints, V. V. Sysoeva, and M. V. Tikhonova, *Zhur. Priklad. Khim.*, **32**, 649 (1959).
2. C. G. Conway and H. H. Chambers, Proceedings from the International Symposium on Batteries, Christchurch, Hants, England (Oct. 1958).
3. G. H. J. Broers, Dissertation, Univ. of Amsterdam (1958).
4. H. H. Chambers and A. D. S. Tantram, Paper presented at Am. Chem. Soc. Meeting, Atlantic City (Sept. 1959).
5. D. L. Douglas, *Ind. Eng. Chem.*, **52**, 308 (1960).
6. E. B. Shultz, Jr., K. S. Vorres, L. G. Marianowski, and H. R. Linden, Paper presented at Am. Chem. Soc. Meeting, Chicago (Sept. 1961).
7. E. J. Cairns and A. D. Tevebaugh, Submitted to *J. Chem. Phys.*
8. E. J. Cairns and A. D. Tevebaugh, *ibid.*
9. B. J. Mayland and G. E. Hays, *Chem. Eng. Progr.*, **45**, 452 (1949).
10. C. W. Montgomery, E. B. Weinberger, and D. S. Hoffman, *Ind. Eng. Chem.*, **40**, 601 (1948).
11. R. E. Reitmeier, K. Atwood, H. A. Bennett, Jr., and H. M. Baugh, *ibid.*, **40**, 620 (1948).
12. K. Muraosa, *Kogyo Kagaku Zasshi*, **64**, 1782 (1961).
13. M. Greyson, J. J. Demeter, M. D. Schlesinger, G. E. Johnson, J. Jonakin, and J. W. Myers, Bur. of Mines Report 5137 (1955).
14. British Gas Research Board Communications, Vols. 11-20 (1944-1948).
15. S. R. Brinkley, Jr., and B. Lewis, Bur. of Mines Report 4806 (1952).
16. L. M. Naphtali, *J. Chem. Phys.*, **31**, 263 (1959).

On the Theory of Simultaneous Discharge of Metal Ions in Real Conjugated Systems

A. T. Vagramyan and T. A. Fatueva

Institute of Physical Chemistry, Academy of Sciences of the U.S.S.R., Moscow, U.S.S.R.

ABSTRACT

A differentiation is made in the theory of codischarge of ions in unconjugated and conjugated electrochemical reactions. It is shown that during simultaneous discharge of metal ions mutual effect takes place due to change in the state of ions in solution, change in concentration of discharged ions in the double layer, change in the substrate nature and the state of the electrode surface. As a result of these changes the reduction rates during simultaneous discharge of metal ions are different from those of separate discharge. An example of the electrodeposition of nickel and cobalt, nickel and iron showed that the reactions of coreduction of these ions are conjugated, and the usual theory of unconjugated systems is not applicable to them.

Simultaneous Discharge of Ions in Unconjugated Systems

According to the existing laws of electrode processes (1), the necessary condition for the simultaneous discharge of several types of ions is the equality of their potentials of reduction[1]

$$\psi_1^\circ + \frac{RT}{n\mathbf{F}} \ln a_1 - \eta_1 = \psi_2^\circ + \frac{RT}{n\mathbf{F}} \ln a_2 - \eta_2 \qquad [1]$$

where ψ_1^o, ψ_2^o, a_1, a_2, η_1, η_2 are, respectively, normal potentials, activities, and overvoltage for the first and second types of metal ions.[2] If it is assumed that the speed of the electrochemical reaction i [3] changes due to electrode potential (ψ) as follows $i = kce^{-\frac{\alpha\psi F}{RT}}$, then with a given electrode potential, it is possible to find the rate ratio of discharge of metal ions (2).

$$\frac{i_1}{i_2} = \frac{k_1 c_1 e^{-\frac{\alpha_1 \psi F}{RT}}}{k_2 c_2 e^{-\frac{\alpha_2 \psi F}{RT}}} \qquad [2]$$

Here it is assumed that the character of rate dependence of individual electrode reactions on the electrode potential remains the same, whether the ions are reduced separately or simultaneously.

Simultaneous Discharge of Ions in Conjugated Systems

As experimental results (3-5) indicate, during simultaneous discharge of metal ions under real conditions of electrolysis their mutual influence should be taken into consideration, since during codeposition changes take place in the substrate nature, the concentration of each ion in the double layer, and the state of ions in the solution.

Effect of Substrate Nature and the State of Electrode Surface on Speed of Ion Reduction

The effect of the nature of the substrate of the electrode on the reduction of metal ions may be of two kinds: (*a*) decrease in the potential of the electrode during simultaneous discharge in comparison with the equilibrium potential, owing to the alloy formation (depolarization) (6);[4] (*b*) increase in the electrode potential in comparison with the equilibrium potential due to the retardation of the electrochemical reaction (polarization).

In the case of the best known process of reduction of hydrogen ions, the rate of the electrochemical reaction, which depends on the electrode potential, changes in accordance with equation $i = ke^{-\frac{\alpha\psi F}{RT}}$; if we replace $k = e^{-a/b}$ and transform the equation, we get the well-known Tafel equation (8)

$$\psi - \psi^o = \eta = a + b \ln i$$

where a shows the degree of retardation of the electrochemical reaction and depends on the substrate nature and the state of the metal surface; for instance, at 1 ma/cm^2 a varies from 1.56v for lead to 0.1 — 0.03v for the platinum group (9). Hence, it follows that a changes drastically depending on the nature of the metal.

It is obvious that constant a depends also on the state of the electrode surface. In some cases the reduction of the metal ions on the electrode surface adsorbed by foreign particles or on an oxidized surface is so difficult that metal practically does not deposit (10). For instance, the reduction of chromate ions on an oxidized surface in a solution of chromic acid is very difficult, and therefore it is the discharge of hydrogen ions that essentially takes place, in spite of the fact that the reduction potential is more negative. When the electrode surface is effectively scraped during the electrolysis cathode polarization decreases drastically and instead of the reduction of hydrogen ions a reaction $Cr^{6+} \rightarrow Cr^{3+}$ occurs. If the electrode that had been scraped off is left for some time in the electrolyte without current, it becomes passivated again, and the reduction of the chromate ion is retarded even when the electrode is polarized considerably higher. The effect of the electrode surface state on the electrode process during codeposition of nickel and molybdenum has been studied by Krasovsky (7). The important influence of the electrode surface state on the reduction rate of metal ions is also evident when studying electrodeposition of silver (10), nickel (11), manganese (12), alloys, etc.

Since, during codischarge of metals, the nature and surface state of the electrode differ from those which take place during deposition of separate components, it is necessary to substitute values (η_1) and (η_2) in Eq. [1] by the corresponding values of overvoltage on the alloy (η_1 alloy) and (η_2 alloy).

Change is Concentration of Ions Discharged in Double Layer

The rate of reduction of ions depends on their concentration in the double layer, but not on the concentration in the solution. As is well known, the ion concentration in the double layer (C_s) related to the concentration in the solution (C_v) for the simplest case by the following equation (8)

$$C_s = C_v e^{-\frac{F\psi}{RT}}$$

When the electrode polarization is constant, the concentration of each ion type in the double layer during codischarge of ions is less than during separate reductions, due to partial replacement of some ions by others. The degree of replacement of one type of ions in the double layer by ions of another type depends on the ion nature (radius, valency of ions, degree of ion hydration-factor α). It is evident that $\epsilon\alpha_i = 1$. As a result of this replacement the concentration of each type of discharging ion in the double layer decreases at a given overvoltage. This results in lowering the reduction rate of each type of metal ion during simultaneous discharge in comparison with separate reduction.

Figure 1 shows the dependence of nickel ion reduction rate on concentration of cobalt sulfate additions. The curves were obtained potentiostatically at 650 mv (*vs.* NHE) in 1*N* solution of nickel sulfate with *p*H 1.9 and with a different concentration of cobalt sulfate.

Curve 1 shows the change in the current used to discharge the ions with the addition of cobalt sulfate.

[1] It is obvious that this condition is not applicable when interaction of the reduced ions in the solution or of metal atoms in the deposit takes place.

[2] Hereafter ion concentration is given instead of ion activity.

[3] Reaction speed in the kinetics of the electrode processes is characterized by current density, *i*.

[4] A record of the depolarization action of the substrate during simultaneous discharge was proposed by Krasovsky (7).

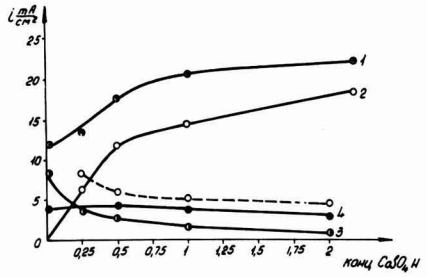

Fig. 1. Change of current for discharging Ni^{2+}, Co^{2+} and H^+ ions, depending on concentration of $CoSO_4$ added to solution of $NiSO_4$ during electrolytic codeposition. ψ_{const} 650 mv (NHE), pH 1.9, temperature 25°: curve 1, over-all curve; 2, discharge of Co^{2+} ions; 3, discharge of Ni^{2+} ions; 4, discharge of H^+ ions; dotted curve, calculated values.

Curves 2, 3, and 4 show the current used to discharge cobalt, nickel, and hydrogen, respectively. The rate of hydrogen reduction practically does not depend on the concentration of the salt additions (curve 4). When cobalt salts are added to the electrolyte in the amount of, say, 0.5*N*, the total current density increases from 12.2 to 17.5 ma/cm². However, the current used to reduce nickel decreases from 8.3 to 2.5 ma/cm² which is 3.3 times lower.

A similar retardation is observed in the course of a potentiostatic study of the reduction rate of the cobalt ions caused by the addition of nickel sulfate (Fig. 2). As can be seen from these curves, the addition of nickel salts sharply decreases the total current (curve 1) as well as that part of the current which is used to discharge the cobalt ions (curve 2), although the total concentration of ions in the electrolysis not only does not decrease, but even increases. The lowering in rate of cobalt ions reduction in this case can be accounted for only by the fact that part of the cobalt ions in the double layer are replaced by nickel ions, the reduction of which requires higher activation energy than the reduction of cobalt ions.

If we assume that with the concentration being equal the probability of nickel and cobalt ions getting into the double electrical layer is the same, it

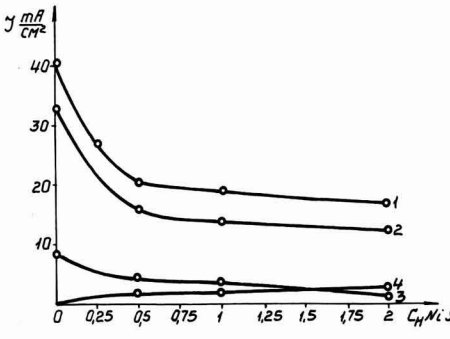

Fig. 2. Change of current for discharging Co^{2+}, Ni^{2+}, and H^+ ions, depending on concentration of $NiSO_4$ added to 1*N* solution $CoSO_4$ during electrolytic codeposition. ψ_{const} 606 mv (NHE), pH 1.9, temperature, 25°: curve 1, over-all curve; 2, discharge of Co^{2+} ions; 3, discharge of H^+ ions; 4, discharge of Ni^{2+} ions.

is possible to calculate the partial polarization of each ion type during codeposition. It is evident that it will be proportional to their concentration ratio in the electrolyte, if the rate of the electrochemical process is not limited by diffusion of the ions. The decrease in polarization of one ion type with the entry of another ion type into the double electric layer, taking into consideration penetration factor α, will amount to

$$\frac{RT}{n\mathbf{F}} \ln C_1 - \frac{RT}{n\mathbf{F}} \ln \frac{\epsilon\alpha_i C_i}{\alpha_1 C_1} = \frac{RT}{n\mathbf{F}} \ln \frac{\alpha_1 C_1}{\epsilon\alpha_i C_i} C_1$$

It is evident that in accordance with the decrease in this partial potential the reduction rate of a given ion type will decrease, if the total potential is maintained strictly constant.

If we assume that $\alpha_{Ni} = \alpha_{Co}$ and that the substrate nature does not substantially effect the deposition rate of cobalt and nickel ions, *i.e.*, that no depolarization takes place, it is possible to calculate the decrease of reduction rate of one ion type when codischarged with other ions. The dotted line on Fig. 1 corresponds to this calculated value. It can be seen from Fig. 1 that the calculated value (dotted line), although considerably different from the experimental data, yields the same general character of relationship.[5] In view of the fact that the reduction rates of metal ions when codischarged differ from those that are discharged separately, due to the changes of ion concentration in the double layer, it is necessary to substitute $RT/n\mathbf{F} \ln C$ in Eq. [1] by

$$\frac{RT}{n\mathbf{F}} \ln \frac{\alpha_1 C_1}{\epsilon\alpha_i C_i} C_1.$$

Galvanostatic studies of the speed of simultaneous and separate discharge of cobalt and nickel ions (Fig. 3) have shown that not only is the rate of nickel reduction decreased, but the character of dependence of the discharge speed on the potential also changes in comparison with the separate reduction of nickel. For instance, when $\psi = -650$ mv (Fig. 3), the rate of nickel discharge is reduced 10.5 times when codeposited with cobalt; at a potential of 550 mv the discharge speed of cobalt is decreased 16 times; at higher potentials the speed of cobalt discharge from a 2*N* solution is considerably higher and is incommensurable with the conjugated curve, as can be seen on Fig. 3. The change in rate correlation of the reduction of nickel and cobalt ions and the electrode potential shows that the delay in the process depends not only on the change in the ion concentration near the electrode layer, but on the change of the substrate nature as well. The discrepancy between experimental and calculated data (Fig. 1) also indicates that the change in the substrate nature affects the reduction rate of the metal ions.

In view of the above it would be correct, instead of using Eq. [1], to use the following expression which characterizes the condition for codischarge of ions in real conjugated systems (5):

[5] This discrepancy may be partially due to the fact that the calculation did not take into account the concentration of hydrogen ions.

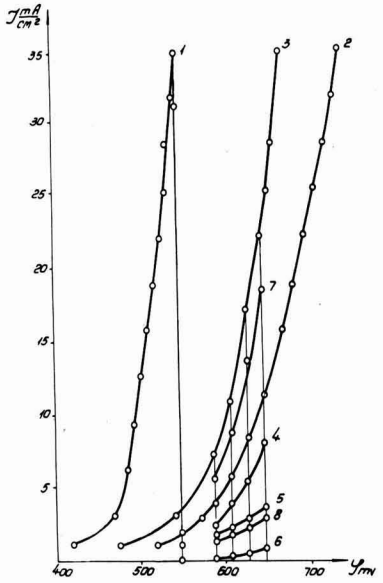

Fig. 3. Variation in current with electrode potential used to discharge Co^{2+}, Ni^{2+}, and H^+ ions in their simultaneous and separate deposition: curve 1, curve for the discharge of Co^{2+} from 2*N* $CoSO_4$; 2, over-all curve for the discharge of Ni^{2+} and H^+ from 1*N* $NiSO_4$; 3, over-all curve for the discharge of Ni^{2+}, Co^{2+}, and H^+ from 1*N* $NiSO_4$ + 1*N* $CoSO_4$; 4, partial curve for the discharge of Ni^{2+} from 1*N* $NiSO_4$; 5, partial curve for the discharge of H^+ from 1*N* $NiSO_4$; 6, partial curve for the discharge of Ni^{2+} from 1*N* $NiSO_4$ and 2*N* $CoSO_4$; 7, partial curve of the discharge of Co^{2+} from 1*N* $NiSO_4$ and 2*N* $CoSO_4$; 8, partial curve for the discharge of H^+ from 1*N* $NiSO_4$ and 2*N* $CoSO_4$

$$\psi_1^{\circ} + \frac{RT}{n\mathbf{F}} \ln \frac{\alpha_1 C_1}{\epsilon \alpha_i C_i} \cdot C_1 - \eta_1 \text{ alloy} = \psi_2^{\circ} + \frac{RT}{n\mathbf{F}} \ln \frac{\alpha_2 C_2}{\epsilon \alpha_i C_i} \cdot C_2 - \eta_2 \text{ alloy} \quad [3]$$

Since, during simultaneous discharge, overvoltage may either increase or decrease, depending on the changes in the substrate nature, the following cases are possible in real conditions of codeposition of metals:

1. When

$$\eta_1 \text{ alloy} + \eta_2 \text{ alloy} << \psi_1^{\circ} + \frac{RT}{n\mathbf{F}} \ln \frac{\alpha_1 C_1}{\epsilon \alpha_i C_i} \cdot C_1 + \psi_2^{\circ} + \frac{RT}{n\mathbf{F}} \ln \frac{\alpha_2 C_2}{\epsilon \alpha_i C_i} \cdot C_2$$

the rate of discharge of more electropositive metal ions is higher than the speed of discharge of more electronegative ions.

2. When

$$\eta_1 \text{ alloy} + \eta_2 \text{ alloy} >> \psi_1^{\circ} + \frac{RT}{n\mathbf{F}} \ln \frac{\alpha_1 C_1}{\epsilon \alpha_i C_i} \cdot C_1 + \psi_2^{\circ} + \frac{RT}{n\mathbf{F}} \ln \frac{\alpha_2 C_2}{\epsilon \alpha_i C_i} C_2 \text{ and } \eta_1 \text{ alloy} > \eta_2 \text{ alloy}$$

the rate of discharge of more electronegative metal ions is higher than the rate of more electropositive ions.

Thus, in real conjugated systems, as a result of the influence of the substrate nature on the overvoltage, a change in the reduction speed of both more positive and more electronegative metal ions over a wide range is possible.

Indeed, as has been observed by Glasstone, Symes, and others (13, 14), when nickel and iron are codeposited, the iron concentration in the alloy is much higher than that of nickel, although the reduction potential of the nickel ion, when deposited separately, is more positive than when iron ions are reduced.

In order to compare the reduction rate of nickel and iron during simultaneous and separate reduction, we have studied the dependence of the speed of these reactions on the electrode potential. Results of separate deposition of nickel (curve 1) and iron (curve 3) as well as of their codischarge (curve 2) are shown in Fig. 4.

Figure 4 shows that the discharge rate of iron ions when codeposited with nickel (curve 6) is considerably higher than that of nickel (curve 7). According to Eq. [1] there should be an inverse relationship between the deposition rates of nickel and iron.

From the data given in Table I it can be seen that at a cathode potential of $\psi = -730$ mv (with reference to the hydrogen electrode) the rate of discharge of iron ions determined by the current density corresponds to 4.5 ma/cm² during separate reduction and to 13.6 during coreduction. Thus, when iron is

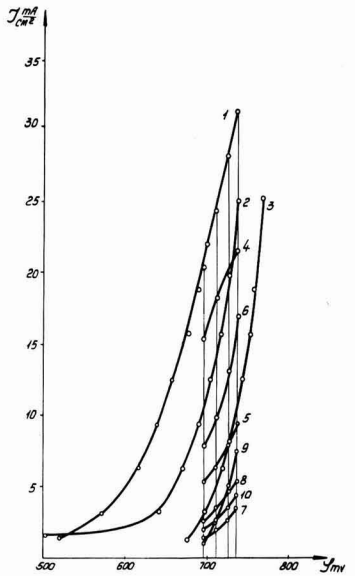

Fig. 4. Dependence of speed of reduction of ions of iron and nickel on electrode potential, pH 1.9, temperature, 25°: curve 1, over-all curve for discharge of Ni^{++} and H^+ ions from 1*N* $NiSO_4$; curve 2, over-all curve for discharge of Fe^{++}, Ni^{++}, and H^+ ions from solution 1*N* in $FeSO_4$ and 1*N* in $NiSO_4$; 3, over-all curve for discharge of Fe^{++} and H^+ ions from 1*N* $FeSO_4$; 4, partial curve of discharge of Ni^{++}: ions from 1*N* $NiSO_4$; 5, partial curve for discharge of H^{++} ions from 1*N* $NiSO_4$; 6, partial curve for discharge of Fe^{++} ions from 1*N* $FeSO_4$ and 1*N* $NiSO_4$; 7, partial curve for discharge of Ni^{++} ions from 1*N* $NiSO_4$ and 1*N* $FeSO_4$; 8, partial curve for discharge of H^+ ions from 1*N* $NiSO_4$ + 1*N* $FeSO_4$; 9, partial curve for discharge of Fe^{+++} ions from 1*N* $FeSO_4$; 10, partial curve for discharge of H^+ ions from 1*N* $FeSO_4$.

Table I. Distribution of current between separate reactions when electrodeposition of iron and nickel is carried out both separately and together

(cathode potential, —730mv)

Type of electrodeposition	Speed of ion reduction, ma/cm² Fe^{2+}	H^+	Ni^{2+}	Total speed of electrodeposition, ma/cm²
Iron without nickel	4.5	4.4	—	8.9
Nickel without iron	—	7.9	20.8	28.7
Iron with nickel	13.6	4.5	2.6	20.7

reduced together with nickel, the rate of reduction of iron ions becomes three times as high and the rate of discharge of nickel ions decreases at this potential from 20.8 to 2.6 ma/cm² which is approximately eight times as low. The rate of discharge of hydrogen ions with simultaneous reduction of nickel is 7.9 ma/cm², and that of reduction of hydrogen with iron 4.4 ma/cm²; in the case of codischarge of the ions of nickel and iron it is 4.5 ma/cm². From these data it is evident that hydrogen with nickel is reduced at a much higher rate than with iron. During the simultaneous reduction of iron and nickel ions, the reduction rate of the hydrogen ions is far less than in the case of nickel and somewhat higher than in the case of iron.

The results of codeposition of nickel and iron show the "anomalous" retardation of the discharge speed of nickel ions and the "facilitation" of the discharge of iron ions. This anomaly depends on the various degrees of retardation of the discharge of metal ions during codeposition. Therefore, when conditions allow the decrease of overvoltage during reduction, it may be expected that this anomaly will be eliminated.

High overvoltage during the reduction of metal of the iron group, as was shown in a number of papers (10, 15), depends on the inhibiting action of foreign substances (hydroxide, hydrogen) adsorbed on the electrode surface, which influence the reduction rate of the metal ions. With an increase in temperature, the irreversible adsorption of hydrogen (16) and hydroxides is drastically decreased; hence the inhibiting action of foreign particles and overvoltage (17) is also decreased. Therefore, when co-

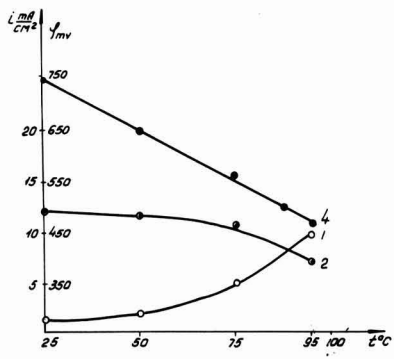

Fig. 5. Dependence of speed of reduction of Ni^{2+} ions (curve 1) and Fe^{2+} (curve 2) during codischarge upon temperature and change of electrode potential ψ (curve 4) in solution 1*N* $NiSO_4$, 1*N* $FeSO_4$. 30 g/l H_3BO_3, pH 1.9.

depositing nickel with iron at a low voltage, the anomaly referred to may be eliminated, *i.e.*, the alloy will contain more nickel than iron (5).

As can be seen from Fig. 5, with the temperature increase the potential of alloy deposition decreases and the discharge of the nickel ions is facilitated. Therefore, when the electrolyte temperature is about 100° at a current density of 20 ma/cm², the alloy contains more nickel than iron.

Thus the "anomalous" reduction rates of iron and nickel ions in accordance with Eq. [3] depend on the change of the overvoltage during codischarge. The overvoltage in this case depends on the state of the electrode surface during electrolysis, but not on the retarding effect on the change of metastable to stable nickel with the result that the further deposition of this metal is inhibited (13). Therefore, any addition agent which is not reduced on the electrode, but affects the state of the electrode surface and the overvoltage, may change the metal relationship in the alloy.

The above experimental results show that the theory of real conjugated systems makes a better allowance for the regularity of codischarge of metal ions.

Summary

1. It has been shown that when nickel and cobalt are codeposited the rate of each electrochemical reaction is retarded compared with the separate reduction of each ion.

2. It has been established that, for a given overall electrode polarization during codischarge, retardation of the separate reactions depends on the decrease of the ion concentration in the double layer.

3. It has been shown that the anomalous correlation of rates during codeposition of nickel and iron depends on causes which produce high overvoltage of the discharge of ions. During electrolysis, when the overvoltage is sharply reduced, this anomaly is eliminated.

4. An equation has been proposed which makes a better allowance for the conditions of metal deposits in real conjugated systems.

Manuscript received June 29, 1962; revised manuscript received April 30, 1963. This paper was presented before the Boston Meeting, Sept. 16-20, 1962.

Any discussion of this paper will appear in a Discussion Section to be published in the June 1964 JOURNAL.

REFERENCES

1. S. Glasstone, "An Introduction to Electrochemistry," D. Van Nostrand Company, Inc., New York (1942); C. L. Faust, "Modern Electroplating," p. 64 A. G. Gray, Editor, John Wiley & Sons, Inc., New York (1953); R. Kremann and R. Muller, "Elektromotorische Krafte Elektrolyse und Polarisation," Part 2, Akademische Verlagsges m.b.H., Leipsig (1931); V. V. Skorshelletti, "Teoreticheskaya Elektrokhimiya," (Theoretical Electrochemistry), Gosudarst. Nauch. Tekhn. Izdatel. Khim. Lit., Leningrad (1959).
2. O. A. Esin, *Z. Fiz. Khim.*, **6**, 795, (1935); **7**, 1071 (1936); **8**, 326 (1937); V. L. Kheifetz and A. L. Rotinyan, *Proc. Institute "Gipronikel,"* (1958).
3. A. T. Vagramyan and A. T. Fatueva, *Zhur. Neorg. Khimii*, **4**, 1281 (1959).
4. A. A. Fatueva and A. T. Vagramyan, *Doklady Akad. Nauk SSSR*, **128**, 773 (1959); A. T. Vagramyan

and T. A. Fatueva, *Z. physik Chem.* (Leipzig), **216**, 163 (1961).
5. A. T. Vagramyan and T. A. Fatueva, *Doklady Akad. Nauk SSSR*, **135**, 1413 (1960).
6. Haber and Sack, *Z. Elektrochem.*, **8**, 251 (1902); Bredig and Haber, *Ber.*, **31**, 2741 (1898).
7. A. I. Krasovsky, Proc. Fourth Conference on Electrochemistry, Izdat Akad. Nauk SSSR, 530 (1959).
8. Tafel, *Z. phys. chem.*, **50**, 641 (1905).
9. A. N. Frumkin, B. S. Bagotsky, Z. A. Ioffe, and B. N. Kabanov, "Kinetics of Electrode Processes," Izdat. MGU (1952).
10. A. T. Vagramyan and L. A. Uvarov, *Trans. Inst. Met. Finishing*, **39**, 56 (1962); A. T. Vagramyan, *Z. Fiz. Khim.*, **19**, 305 (1945); A. B. Price and D. A. Vermilyea, *J. Chem. Phys.*, **28**, 720 (1958).
11. A. I. Krasovsky, G. I. Kobosnidze, and A. T. Vagramyan, *Z. Fiz. Khim.*, **36**, 714 (1962).
12. A. T. Vagramyan, A. I. Krasovsky, Y. S. Petrova, and Z. A. Solovieva, *ibid.*, **34**, 1255 (1960).
13. S. Glasstone and T. E. Symes, *Trans. Faraday Soc.*, **23**, 213 (1927); **24**, 370 (1928).
14. R. Kremann and R. Maas, *Monatshefte f. Chemic.*, **35**, 731 (1914); H. W. Toepffer, *Z. Elektrochem.*, **6**, 324 (1899); F. W. Kuester, *ibid.*, **7**, 257 (1900).
15. A. T. Vagramyan and L. A. Uvarov, *Doklady Akad. Nauk SSSR*, **146**, 635 (1962).
16. N. Kavtaradze, *Z. Fiz. Khim.*, **32**, 909, 1214 (1958).
17. A. T. Vagramyan and Yu. S. Petrova, "Physico-Mechanical Properties of Electrodeposits" (in Russian), Izdat. Akad. Nauk SSSR, Moscow (1960). English translation, Consultants Bureau, New York (1962); A. T. Vagramyan and Z. A. Solovieva, "Technology of Electrodeposition," p. 398, Robert Draper Ltd., Teddington (1961).

The Kinetics of the Electrodeposition and Dissolution of Metal Monolayers as a Function of Dislocation Density

A. Damjanovic and J. O'M. Bockris

The Electrochemistry Laboratory, The University of Pennsylvania, Philadelphia, Pennsylvania

ABSTRACT

The mechanism and the kinetics of the short time metal deposition and dissolution has been analyzed on the basis of a model which includes transfer of ions across the double layer, diffusion of adions over the metal surface, and incorporation of ions into the lattice at steps one atom high. It is shown that it is possible to obtain data on the exchange current density of the reaction and on the equilibrium adion concentration from the initial portion of the potentiostatic transients. Steady-state current density is analyzed. Conditions necessary for the surface diffusion of adions or for the transfer of ions across the double layer to be the rate-controlling step in the over-all reaction are formulated and discussed. Current density at each potential depends on distances between the steps suitable for the incorporation of adions into the lattice, which distances are related in turn to the dislocation density. On an ideal surface, without nucleation, the steady-state current density should be zero. Conditions for two-dimensional nucleation are analyzed and discussed.

Some attention has been given recently to the problem of determining the path and rate-controlling step in mechanisms of electrochemical metal dissolution and deposition from solutions.

Concepts, *e.g.*, surface diffusion, growth steps (1-4), and dislocation densities (5) previously used in the theory of the growth of metals from the vapor (6-8), have been introduced into the electrode kinetics associated with metal deposition and dissolution. Lorenz (2) obtained a relation between current density and distance between growth steps for steady-state deposition, under surface diffusion control. Mehl and Bockris (1) analyzed deposition mechanisms under galvanostatic transient and steady-state conditions, near the reversible potential, and showed that (for Ag in $AgClO_4$ + $HClO_4$ solutions) rise times of the potential much greater than those to be expected for rate-determining charge transfer are consistent with rate-determining surface diffusion. They deduced for the first time the concentration of adions on the electrode surface. At high current densities, charge transfer was found to become rate-controlling. Independently, and with a different mathematical treatment, Gerischer (4) also suggested the same rate-controlling step for low current densities. Despic and Bockris (3) showed that, with a constant potential on the electrode surface, the local current density at steady state changes with position in respect to a step and can be much higher near growth steps than elsewhere. Kita, Enyo, and Bockris (5) related the number of growth steps to the dislocation density and showed that depending on the overpotential not all the steps may be active [cf. Cabrera and Burton (7)].

Fleischmann and Thirsk (9) considered transient and steady-state kinetics with rate-controlling surface diffusion and developed an expression for the steady-state deposition velocity as a function of the distance between spiral arms. Mott and Watts-Tobin (10) deduced conditions under which surface diffusion will occur [cf. Mehl and Bockris (1)]; they confirmed the conclusion of Despic and Bockris (3) concerning the concentration of current close to growth steps under surface diffusion control, but considered that deposition could occur directly from

the Helmholtz layer onto a kink site [cf. Conway and Bockris (11)]. Vermilyea (12) showed that on a dislocation free surface no deposition should occur below a critical overvoltage, and established this point experimentally using copper whiskers (13). Many examinations have been made of electrochemical crystal growth (the steps following those considered in this paper), but little progress has been made in the determination of molecular mechanisms of this process [cf. Seiter, Fischer, and Albert (14) and Pick, Storey, and Vaughan (18)].

A number of problems remain unsolved from these recent investigations of the kinetics of the formation of "monolayers." The effect of dislocation density on the kinetics is unexplored (5). Conditions for the onset of nucleation have not been worked out. The current-time transient as a function of dislocation density has not been developed. The transition from surface diffusion control to transfer control remains unexplained. Utilizing the model of Despic and Bockris these problems are here analyzed.

Transient Potentiostatic Polarization

Basic equation for the rate of charge transfer as a function of time and position.—Initially, after the commencement of polarization, the surface adion concentration is near to equilibrium. If, however, the rate constant for surface diffusion is much less than i_o, a change of adion concentration between growth steps with time will occur. In this section, the variations of the adion concentration with time and distance from the growth steps are analyzed. The cathodic partial current density (between growth steps) is considered independent of the distance from a growth step for low coverages with adions; the anodic partial current density is, however, proportional to the adion concentration, and thus is a function of time and the position between growth steps [cf. Despic and Bockris (3)]. Hence, the net, Faradaic current density also changes with time and the distance from a growth step. The variation of adion concentration with time t and at position x (see Fig. 1) is equal to the sum of the net charge transfer rate and of the divergence of the adion flux at the same position (2, 3, 9)

$$\frac{\partial c(x,t)}{\partial t} = \frac{i(x,t)}{zF} + D\frac{\partial^2 c(x,t)}{\partial x^2} \qquad [1]$$

The diffusion coefficient, D, is taken independent of adion concentration, $c(x,t)$. The net current density of charge transfer, $i(x,t)$ is, for the conditions stated above, given by (3, 9)

$$i(x,t) = i_o\left\{\exp\left(\frac{-\beta zF\eta}{RT}\right) - \frac{c(x,t)}{c_o}\exp\left[(1-\beta)\frac{zF\eta}{RT}\right]\right\} \qquad [2]$$

where β, z, F, R, and T have their usual meaning, η is the constant overpotential, and c_o is the equilibrium adion concentration.

It is assumed that the adion concentration at steps does not change with time and is always at the equilibrium concentration, which is tantamount to the assumption that the incorporation of adions into the lattice at steps is very fast. If the origin of the coordinate system is chosen at the mid-point between two growth steps, at distance $2x_o$ apart (Fig. 1), then the initial and boundary conditions for the differential Eq. [1] are

$$c(x,0) = c_o,$$
$$c(\pm x_o,t) = c_o, \text{ and}$$
$$\left[\frac{\partial c(x,t)}{\partial x}\right]_{x=0} = 0 \qquad [2a]$$

The third boundary condition states that at $x = 0$ the adion concentration reaches a maximum (in the cathodic area) or a minimum value (in the anodic case). With these, the solution of Eq. [1] is (see Appendix)

$$c(x,t) = A + B\cosh(mx) + \frac{2B'm^2x_o^2}{\pi}\sum_{0}^{\infty}\frac{(-1)^n\cos[(n+1/2)\pi x/x_o]}{(n+1/2)[(n+1/2)^2\pi^2+m^2x_o^2]}\cdot\exp\left[\left(-\frac{(n+1/2)^2\pi^2D}{x_o^2}-p\right)t\right] \qquad [3]$$

where

$$A = c_o\exp\left(-\frac{zF\eta}{RT}\right)$$
$$B = \frac{c_o\left[1-\exp\left(-\frac{zF\eta}{RT}\right)\right]}{\cosh(mx_o)}$$
$$B' = c_o\left[1-\exp\left(-\frac{zF\eta}{RT}\right)\right]$$
$$p = \frac{i_o}{zFc_o}\exp\left[(1-\beta)\frac{zF\eta}{RT}\right]$$

and

$$m = \sqrt{\frac{p}{D}} \qquad [3a]$$

Equation [3] gives the change of adion concentration with time at any point between growth steps.

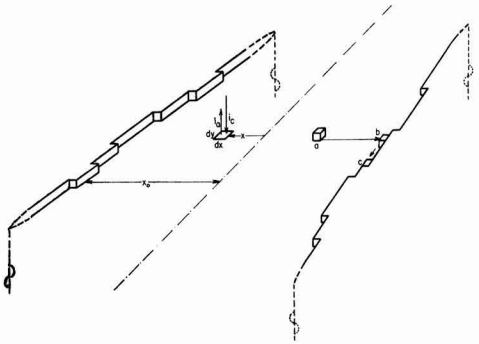

Fig. 1. Illustration of the model for electrodeposition. At the element of the electrode surface dxdy, number of arriving ions, represented as i_c, is greater than the number of ions escaping back to the solution, represented as i_a. The net charge transfer across the double layer at the point x on the surface is given by the difference $i_c - i_a$. Adions (a), diffuse to the step (a to b) formed between two screw dislocations of opposite sign, and along the step to the kink site (b to c) where they become incorporated into the lattice.

Since short time polarization only is considered, the surface structure will not be altered appreciably (see section on Rise time under potentiostatic conditions, below). The distance between growth steps, $2x_o$, can then be simply related to the density of dislocations. A surface is intersected by a number of dislocations with screw component perpendicular to it, and steps are produced between two emerging screw dislocations of opposite sign. In order to minimize the surface energy, the steps should tend to become straight when an electrode surface remains in contact with a solution, in the absence of net current. Straightening of a step in solution should be fast [~ order of minutes (12)] particularly if the exchange current, i_o, is high. Assuming a random distribution of dislocations the average distance between straight steps may then be related to the number of dislocations per square centimeter, N, terminating on the surface and producing growth steps.[1] Thus, to a first approximation

$$x_o = \frac{1}{2\sqrt{N}} \qquad [4]$$

By replacing x_o with $\frac{1}{2\sqrt{N}}$ and rearranging, Eq. [3] transforms to

$$c(x,t) = A + B\cos(mx) + \frac{2B'p}{\pi} \cdot \sum_{n=0}^{\infty} \frac{(-1)^n \cos[(2n+1)\pi x\sqrt{N}]}{(n+1/2)[(2n+1)^2\pi^2 ND + p]} \cdot \exp\{-[(2n+1)^2\pi^2 ND + p]t\} \qquad [5]$$

The net current density as a function of time and position, $i(x,t)$, is obtained from [2] and [5] as

$$i(x,t) = zF\left\{-Bp\cos(mx) - \frac{2B'p^2}{\pi} \cdot \sum_{n=0}^{\infty} \frac{(-1)^n \cos[(2n+1)\pi x\sqrt{N}]}{(n+1/2)[(2n+1)^2\pi^2 ND + p]} \cdot \exp\{-[(2n+1)^2\pi^2 ND + p]t\}\right\} \qquad [6]$$

At a sufficiently early time after application of a constant potential, [6] reduces in the limit $t \to 0$, to[2]

$$i(x,o^+) = i_o\left\{\exp\left(-\frac{\beta zF\eta}{RT}\right) - \exp\left[\left(1-\beta\right)\frac{zF\eta}{RT}\right]\right\} \qquad [7]$$

where o^+ represents the time just after the cessation of double layer charging. (The time necessary to charge the double layer can be made less than 1 μsec.) Thus, at this time, transfer across the double layer is the rate-controlling step, and the local charge transfer rate is independent of the distance from the growth step. With increasing time, the local current density at steps (in the sense of rate of charge transfer), as obtained by replacing x with x_o in Eq. [6], remains constant and is given by the right hand side of Eq. [7]. At the midpoints between growth steps, the current density changes with time and is given by

$$i(o,t) = zF\left\{-Bp - \frac{2B'p^2}{\pi}\sum_{n=0}^{\infty} \frac{(-1)^n \exp\{-[(2n+1)^2\pi^2 ND + p]t\}}{(n+1/2)[(2n+1)^2\pi^2 ND + p]}\right\} \qquad [8]$$

This equation shows that the net rate of charge transfer at midpoints between steps decreases with time toward the steady-state value both during deposition and dissolution. The ratio of the current densities at $x = 0$ and $x = x_o$

$$\frac{i(o,t)}{i(x_o,t)} = \operatorname{sech}\sqrt{\frac{p}{4ND}} + \frac{2p}{\pi}\sum_{n=0}^{\infty} \frac{(-1)^n \exp\{-[(2n+1)^2\pi^2 ND + p]t\}}{(n+1/2)[(2n+1)^2\pi^2 ND + p]} \qquad [9]$$

is less than unity and similarly decreases with time. The current density at the midpoint between two growth steps depends on the values of N, D, and of overpotential, and can reach very low values.

In Fig. 2, $c(x,t)$ and $i(x,t)$ are plotted *vs.* x for two values of ND and for η values + 30 mv and − 30 mv. These results are discussed later.

Average rate of charge transfer as a function of time.—The average rate of charge transfer over the whole surface (per square centimeter) as a function of time, $i(t)$, can be obtained by integrating [6] from 0 to x_o and dividing by x_o

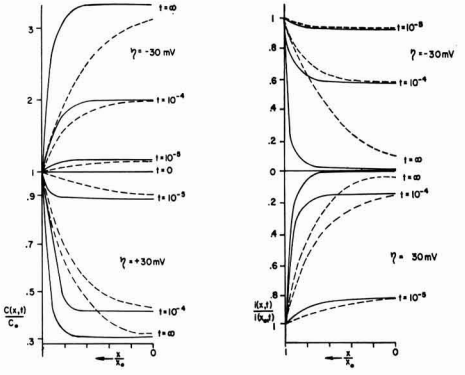

Fig. 2. Illustration of the change of adion concentration and current density with time (in seconds) and with the distance from the growth steps for two values of ND and overpotential of ± 30 mv. The current density close to steps is controlled by transfer reaction. Full lines are for ND = 1 sec^{-1}, dashed lines for ND = 10^2 sec^{-1}. i_o is taken as 100 ma/cm^{-2} and c_o as 10^{-10} mole/cm^2.

[1] N will be less than the density of dislocation, probably by an order of magnitude, since only a fraction of dislocations emerging on the surface produce steps suitable for growth. The objective here is to calculate the change of adion concentration with dislocation density under the nonequilibrium conditions. At equilibrium, the adion concentration is taken as independent of the dislocation density. In this treatment, all the steps are considered available for growth and hence are "active," or in other words, no potential dependence of the "activity" of growth steps is considered [*e.g.*, Kita, Enyo, and Bockris (5)]. The effect of the potential on the "activity" of growth steps is important only in the detailed interpretation of phenomena at low overpotentials and for high dislocation densities, and need not, therefore, be taken into account here.

[2] It can be shown that:

$$1 - \frac{\cosh(mx)}{\cosh(mx_o)} = \frac{2p}{\pi}\sum_{n=0} \frac{(-1)^n \cos[(2n+1)\pi x\sqrt{N}]}{(n+1/2)[(2n+1)^2\pi^2 ND + p]}$$

$$i(t) = -2zF\mathrm{B}'\sqrt{ND}p \tanh\sqrt{\frac{p}{4ND}} - \frac{2zF\mathrm{B}'p^2}{\pi^2} \sum_{n=0}^{\infty} \frac{\exp\{-[(2n+1)^2\pi^2ND+p]t\}}{(n+1/2)^2[(2n+1)^2\pi^2ND+p]^3} \quad [10]$$

During potentiostatic transients two processes may be distinguished: (*a*) the adion concentration will change; and (*b*) the adions will diffuse to steps and will become incorporated into the lattice, if deposition is considered; or, atoms in the steps will leave the lattice to form adions, if dissolution is considered. The average rate at which the adion concentration builds up or decreases is expressed in terms of current density as

$$i_{\mathrm{ad},t} = -\frac{2zF\mathrm{B}'p}{\pi^2} \sum_{n=0}^{\infty} \frac{\exp\{-[(2n+1)^2\pi^2ND+p]t\}}{(n+1/2)^2} \quad [11]$$

Correspondingly, the rate at which adions diffuse to, or away from, steps is given by

$$i_{\mathrm{lat},t} = 2LzFD\left[\frac{\partial c(x,t)}{\partial x}\right]_{x=-x_0} \quad [12]$$

Here, L is the total length of steps per cm^2, and to a first approximation can be related to the distance between steps, $2x_0$, by the equation

$$L \cdot 2x_0 = 1 \quad [13]$$

Differentiating [5] with respect to x, and using [13], Eq. [12] becomes

$$i_{\mathrm{lat},t} = -2zF\mathrm{B}'\sqrt{NDp}\tanh\sqrt{\frac{p}{4ND}} + 8zF\mathrm{B}'NDp \sum_{n=0}^{\infty} \frac{\exp\{-[(2n+1)^2\pi^2ND+p]t\}}{(2n+1)^2\pi^2ND+p} \quad [12a]$$

For the first instant ($t = 0^+$) after application of a constant overpotential, the right hand side of Eq. [12a] reduces to zero,[4] and Eq. [10] and [11] reduce to Eq. [7], meaning that, at this time, transfer across the double layer is rate controlling (see above), and all the current is used to change the adion concentration. With increasing time, $i_{\mathrm{ad},t}$ (Eq. [11]), and the second term in Eq. [12a] diminish, attaining zero value at steady-state. Thus, no further build up of adions occurs, and the rate of the process is controlled by the rate of adion diffusion to, or away from, the steps.

Therefore, it may be concluded that whenever surface diffusion of adions is a slow process in comparison with the transfer of ions across the double layer, the rate of deposition or dissolution process during the potentiostatic transients will be controlled at the beginning by the transfer of ions across the double layer, and later on by surface diffusion of adions. Conditions under which surface diffusion will be the fast process are discussed in the section on Anodic polarization, below.

[3] Fleischmann and Thirsk (9) arrived at an expression superficially similar to [10], but the model considered involved the assumption of the presence of steps due to spirals.

[4] Relevant relationships for transformation can be found in ref. (15).

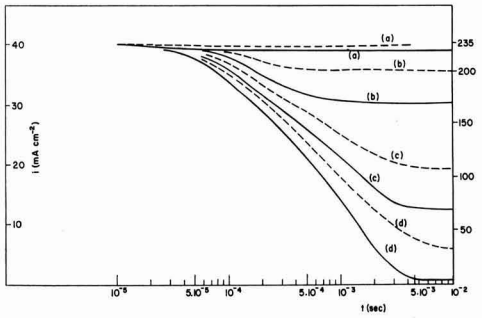

Fig. 3. Potentiostatic transient representing the calculated dependence of the average current density on time. Full lines, $\eta = -10$ mv, current plotted on the left-hand scale; dashed lines, $\eta = -50$ mv, current plotted on the right-hand scale. Curves a, b, c, and d are for $ND = 10^4$, 10^3, 10^2, and 10 sec^{-1}, respectively. i_0 is taken as 100 ma cm^{-2}, and c_0 as 10^{-10} mole/cm^2.

In Fig. 3, the average current densities for two overpotentials and various ND values are plotted against time. With decreasing density of dislocations, $i(t)$ decreases considerably; this is discussed further below.

Exchange current density and equilibrium adion concentration.—The usual method of determining the exchange current density, i_o, from the steady-state data by extrapolation of the linear part of log i—η curve to η=0, although sufficiently accurate for most purposes, may be subject to certain inaccuracy when surface diffusion of adions and the structure of the electrode surface are expected to be still important factors in determining the rate of the reaction even at higher (~50 mv) overpotentials (see Eq. [20]). This possible inaccuracy may be avoided if the nonsteady-state data of potentiostatic transients are considered. The current density at the first instant after application of a constant potential, ($i_{t=o+}$), since independent of the structure of the electrode surface, and on the surface-diffusion of adions, and determined only by the transfer rate in the over-all reaction (Eq. [7]), may be more suitable for obtaining the exchange current density than is the steady-state current density.

Also, the equilibrium value of the adion concentration, c_o, can be obtained from the potentiostatic transient. At a sufficiently early time after application of a constant potential, the slope on the i_t—t curve is given from [10] by

$$\left[\frac{di(t)}{dt}\right]_{t=o+} = \frac{[i(t)_{t=o+}]^2}{2zFc_o \sinh\left(\frac{zF\eta}{2RT}\right)} \exp\left(\frac{zF\eta}{2RT}\right) \quad [14]$$

from which c_o can be evaluated.

Rise time under potentiostatic conditions.—The time necessary to reach the steady state when constant overpotential is applied across the electrode can be obtained from the second, nonsteady state part of Eq. [10]. Terms under the summation sign rapidly decrease when the time is near to, or larger than

$$\tau = \frac{2}{\pi^2 ND + p} \qquad [15]$$

When $t = \tau$, the second term ($n = 1$) in Eq. [10] can be neglected, since it is at least 10 times smaller than the first ($n = 0$), which itself is already at τ small (less than 10%) compared with the steady-state current density. Thus, τ represents the rise time. When, in the steady state, surface diffusion of adions is rate controlling, and $\pi^2 ND$ is less than p (see section on Average current density for cathodic polarization, below), the rise time depends on p, and therefore on the exchange current density, i_o. The reverse also holds, *i.e.*, when transfer is rate controlling in the steady state, τ depends on the rate of surface diffusion. Thus, in potentiostatic transients the rise time depends on the rate of the faster reaction.

In order to compare the rise time of the potentiostatic transients with that of galvanostatic transients, the nonlinear distribution of adions should be considered in both cases. However the expression for the galvanostatic rise time with the nonlinear distribution of adions has not yet been obtained. With the linear distribution of adions (Mehl and Bockris' model), the galvanostatic rise time, when surface diffusion is rate controlling, is given by (1)

$$\tau_g = \frac{c_o}{2v_o} \qquad [16]$$

where v_o, the surface diffusion flux, is equal to Dc_o/x_o^2 and, with $x_o = \frac{1}{2\sqrt{N}}$, to $4NDc_o$. Thus, contrary to the potentiostatic case, the rise time for the galvanostatic transient, when surface diffusion is rate controlling, depends on the rate of surface diffusion. Hence one can compare the galvanostatic rise time with that for the corresponding potentiostatic case, *i.e.*, that obtained from a linear distribution of adions with distance between the growth steps. It can easily be shown to be

$$\tau_p = \frac{2}{8ND + p} = \frac{2c_o}{2v_o + pc_o} \qquad [17a]$$

or, for low overpotentials

$$(\tau_p)_{\eta \to o} = \frac{2c_o}{2v_o + i_o/zF} \qquad [17b]$$

It is interesting to notice that there is no significant difference between the expressions for the potentiostatic rise time obtained with the linear and nonlinear adion distributions. The ratio between rise times for galvanostatic and potentiostatic transients for linear distribution of adions is therefore

$$\left(\frac{\tau_g}{\tau_p}\right)_{\eta \to o} = 1 + \frac{i_o}{2zFv_o} \qquad [18]$$

and is expected not to differ significantly from the ratio which would be obtained with nonlinear distribution of adions. Here, 90% rise time ($\tau = c_o/v_o$) is considered. Thus, it offers a possibility for establishing the rate-determining step in a given system by measuring the rise time under galvanostatic and potentiostatic conditions. When surface diffusion is the rate-determining step, $i_o/2zFv_o$ is greater than 1, and τ_g/τ_p should be reasonably greater than 2. Also, the value of i_o/v_o may be obtained directly from the above ratio.

The total number of atoms which diffuse to the steps and become incorporated into the lattice during the cathodic rise time, for instance, can be obtained by integration of the Eq. [12a] from $t = 0$ to $t = \tau$. The analysis shows that during the rise time the number of atoms incorporated into the lattice is only a fraction of the total number of atoms which have crossed the double layer. It can be shown that the number of adions which diffuse to steps and become incorporated into the lattice during the rise time is greater for galvanostatic than for potentiostatic case, and, therefore, to reach the same steady-state conditions, more ions have to cross the double layer in galvanostatic than in potentiostatic case. Even during the galvanostatic transient, the total number of ions crossing the double layer is equivalent to only a fraction of a monolayer (1,3), and only a part of these will diffuse to steps to be incorporated there into the lattice. During the potentiostatic transient the advance of steps therefore will not be significant, *i.e.*, the present approach allows a study of the kinetics of the build up and decay of monolayers to be made under conditions in which a difficult experimental feature of metal deposition kinetics, the change of electrode surface with time, is avoided.

Steady State

Steady-state distribution of current density.—In the steady state, the distribution of the net charge transfer rate between growth steps can be obtained by suitable transformation from the first, steady-state part of Eq. [6]

$$i(x) = -zF\mathrm{B}p\cosh(mx) = i_o \left\{ \exp\left(-\frac{\beta zF\eta}{RT}\right) - \exp\left[(1-\beta)\frac{zF\eta}{RT}\right] \right\} \frac{\cosh(mx)}{\cosh\sqrt{\frac{p}{4ND}}} \qquad [19]$$

The dependence of this net charge transfer rate on the distance between growth steps, $2x_o$, in the steady state, has already been treated by Despic and Bockris (3), who derived an essentially similar equation. In Fig. 4, the current density distribution between two steps is given for various overpotentials and ND values. When surface diffusion is the rate-controlling step, that is, at all anodic current densities and at sufficiently low cathodic current densities, the rate of charge transfer at midpoints between growth steps is small compared to that at the growth steps themselves, *i.e.*, a large part of the current is confined to the near vicinity of growth steps. This does not, however, imply that deposition, for instance, occurs predominantly directly from solution to kink sites at the steps, not only because the collisional probability is small, but because the required activation energy for trans-

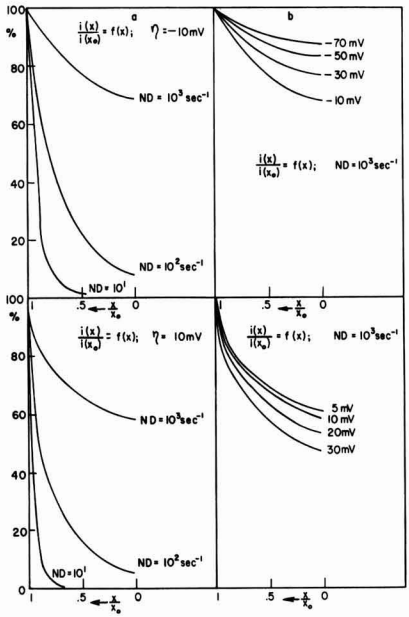

Fig. 4. Variation of the current density with the distance from the growth step: a, for various values of *ND* and $\eta = \pm$ 10mv; b, for *ND* = 10^4 sec^{-1} and various values of overpotentials, both cathodic and anodic.

fer directly to a kink site is prohibitively large (11, 16). The local rate of charge transfer can never be greater than that given by transfer as a rate-controlling step for the given overpotential. Were deposition to occur directly onto kink sites (10), the local rate of charge transfer would be by some orders of magnitude greater than that allowed for charge transfer [*cf.* also the identity of the current densities for liquid and solid electrodes in the rate-controlling charge transfer region (17).

Average current density for cathodic polarization.—The average current density, i, both for deposition and dissolution, can be obtained by integrating [19] from 0 to x_o and dividing by x_o. It is

$$i = i_o \left\{ \exp\left(-\frac{\beta z F \eta}{RT}\right) - \exp\left[(1-\beta)\frac{zF\eta}{RT}\right] \right\} \sqrt{\frac{4ND}{p}} \tanh\sqrt{\frac{p}{4ND}} \quad [20]$$

For $ND \geq p$, $\sqrt{\frac{4ND}{p}} \tanh\sqrt{\frac{p}{4ND}} \simeq 1$, and Eq. [20] reduces to

$$i = i_o \left\{ \exp\left(-\frac{\beta z F \eta}{RT}\right) - \exp\left[(1-\beta)\frac{zF\eta}{RT}\right] \right\} \quad [20a]$$

This accounts for the gradual transition from rate-controlling surface diffusion at low cathodic overpotentials (p large) to rate-controlling transfer step at more cathodic overpotentials (p small), observed by Mehl and Bockris (1). As the overpotential becomes increasingly negative, the adion concentration increases, so that $\left|\frac{dc}{dx}\right|_{x=\pm x_o}$ increases and, hence, the surface diffusion rate increases to a nonrate-controlling value. The overpotential at which transition from rate-controlling surface diffusion to rate-controlling transfer during deposition occurs, depends on N and D. At more perfect crystal surfaces (N is small) the transition will occur at more negative overpotentials. For surface diffusion to be the rate-controlling step, it is necessary that (*cf.* Eq. [20])

$$ND < p = \frac{i_o}{zFc_o} \exp\left[(1-\beta)\frac{zF\eta}{RT}\right] \quad [21]$$

or, at low overpotentials

$$ND < \frac{i_o}{zFc_o}$$

Thus, for silver electrodes in a solution of 0.2N $AgClO_4$, for instance, with $i_o = 0.1$ amp/cm², and $c_o = 10^{-10}$ mole/cm², surface diffusion will be rate controlling if ND is less than 10^4 sec^{-1}. In fact, from Fig. 5 it can be seen that, for $ND = 10^4$ sec^{-1} and $\eta = -10$ mv, the steady-state currents are only a few per cent smaller than they would be if transfer were the rate-controlling step. It is possible to estimate the value of the diffusion coefficient of silver adions, for instance, in the system used by Mehl and Bockris (1). The best fit with their experimental data (see Fig. 6) can be obtained if in Eq. [20] ND is $3.4 \cdot 10^3$ sec^{-1}. A reasonable value of N for their electrodes can be taken as 10^9 cm^{-2}, and then D is approximately equal to $5 \cdot 10^{-6}$ cm^2 sec^{-1}. The accuracy with which the value of D can be obtained depends also on the accuracy with which c_o is determined. Here, c_o is taken as 10^{-10} mole/cm². With decreasing N values, surface diffusion will tend increasingly to become rate controlling. In Fig. 5, as an illustration, a family of $i - \eta$ curves is given for various ND values, $i_o = 100$ ma/cm², and $c_o = 10^{-10}$ mole/cm². In Fig. 6 the experimental results of Mehl and Bockris (1) on silver are plotted together with the theoretical curve obtained with Eq. [20].

Anodic polarization.—When surface diffusion is rate controlling, Eq. [20] indicates that the disso-

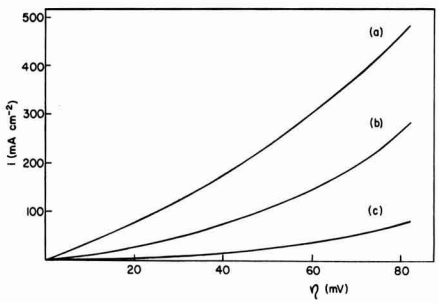

Fig. 5. Calculated average current density at the steady-state deposition as function of overpotential. Curves a, b, and c correspond to *ND* = 10^4, 10^2, and 10 sec^{-1}, respectively; i_o = 100 ma cm^{-2} and $c_o = 10^{-10}$ mole/cm².

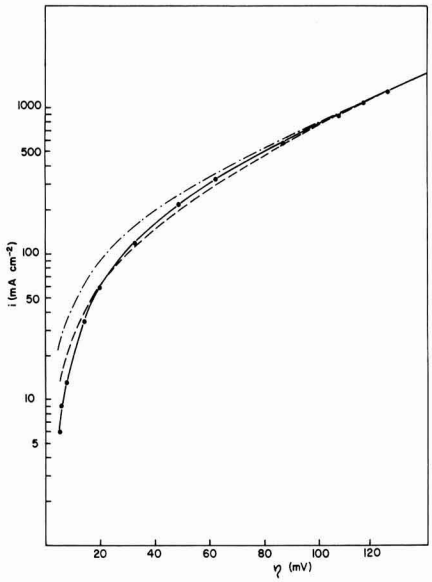

Fig. 6. Log i — η plot of experimental results of Mehl and Bockris full line. Dashed line, surface diffusion-controlled current according to the present analysis with i_o = 120 ma/cm², c_o = 10^{-10} mole/cm², and ND = 3.4 x 10^3 sec^{-1}v. Dashed and dotted line is the closest fit for transfer control.

lution current density is not symmetrical with that of deposition, and i_{cath} is greater than i_{an}. It should be pointed out that Despic and Bockris (3) observed a dissymmetry in the i — η curves at low overpotentials ($|\eta| < 20$ mv) in the sense that the currents on the anodic side, for a nonactivated electrode became less than those on the cathodic side. Furthermore, the condition for surface diffusion $ND < p$ implies that surface diffusion will stay rate controlling for higher anodic overpotentials if it is rate controlling at low overpotentials. Moreover, Eq. [20] shows that, contrary to the deposition case, rate-controlling transfer at low overpotentials eventually should be replaced by surface diffusion rate controlling at higher overpotentials. There is, however, evidence (3) that, at higher anodic overpotentials, the log i — η relation on the anodic side has a gradient equal to that on the cathodic. This inconsistency may perhaps be interpreted by reference to the fact that at higher anodic overpotentials with surface diffusion control the adion concentration between the growth steps will decrease considerably (cf. Eq. [22]). The path of the reaction may then change so that the origin of the adions is no longer the growth steps only but the planes themselves. New growth steps will be thus created at numerous points, and this would effectively increase N in Eq. [20] and transfer will become rate controlling.

It may be pointed out that the process of formation of new steps by dissolving atoms in the surface can occur at relatively low overpotentials. Vermilyea (13) observed pitting in the extreme case of copper whiskers (N very low) and sudden rise in the dissolution current already at 20 mv. This would agree with a model in which the initial difficulty in dissolution from plane surface is relieved by the introduction of new growth steps. For activated electrodes, symmetry of the cathodic and anodic lines is observed (3), and this is consistent with transfer control on these electrodes, for anodic as well as cathodic currents, as will occur from [20] if N is large. Despic and Bockris' electrodes were activated by anodic dissolution which may have caused the creation of steps also at the edges of the crystals.

Adion concentration in the steady state.—The concentration of adions at the midpoints between two growth steps is given by (see Eq. [3])

$$c_{x=o} = c_o\left\{\exp\left(-\frac{zF\eta}{RT}\right) + \left[1-\exp\left(-\frac{zF\eta}{RT}\right)\right]\frac{1}{\cosh(mx_o)}\right\} \quad [22]$$

For the same overpotential, the concentration of adions varies with N. Thus, for the cathodic case, with η = — 50 mv, and $D = 5.10^{-6}$ cm²/sec, ratio $c_{x=o}/c_o$ changes from approximately 1 to 7 when N changes from 10^{10} to 10^6 cm^{-2}. On surfaces with high dislocation densities, when growth steps are close to each other, no appreciable change of adion concentration occurs during deposition or dissolution above or below that of the equilibrium concentration even at the midpoints between two growth steps. On more perfect crystal faces, however, the increase of adion concentration during deposition may be so large that a new process, two-dimensional nucleation, may be expected at higher overpotentials. The variation of adion concentration with the distance between growth steps for various values of ND and overpotentials is illustrated in Fig. 7.

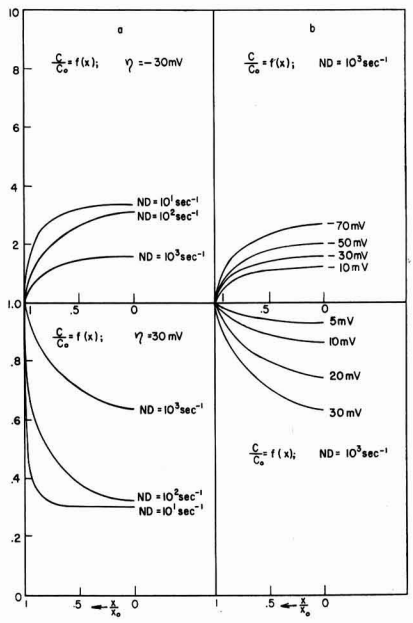

Fig. 7. Variation of adion concentration with the distance from the growth step; a, for various values of ND and $\eta = \pm$ 10 mv; b, for various overpotentials, both cathodic and anodic, and ND = 10^3 sec^{-1}.

Two-Dimensional Nucleation During Deposition

Free energy change in the formation of a two-dimensional nucleus and its critical radius.—During deposition, the adion concentration, particularly at the midpoints between steps, and if the density of growth steps is below a certain level, may reach a value at which nucleation will commence. The effect of the nucleation will be to form new growth steps, and this in turn will reduce x_o, and hence decrease the adion concentration and increase the rate of surface diffusion (see Eq. [12a] and [13]).

Adion clusters, or embryos, are in equilibrium with adions. An embryo may either disappear or grow. When it reaches a critical size, it becomes a nucleus. The free energy change for the formation of an embryo from adions is made up of two terms, one due to "condensation" of adions into the inner part of the embryo (edge ions are excepted), and the other due to the formation of the edge of the embryo. The first term decreases the free energy with respect to that of the number of adions concerned and is proportional to the number of ions in the embryo (except for those in the edge) and hence to the area of the embryo diminished by the edge contribution; the second increases the free energy change and is proportional to the number of ions in the periphery of the embryo

$$\Delta F = \left(\frac{2\pi r^2}{\sqrt{3}\, d^2} - \frac{2r - d}{d}\, \pi \right) \Delta F_1 + \frac{2r - d}{d}\, \pi \Delta F_2 \quad [23]$$

Here, ΔF_1, (< 0), is the free energy of the ion in the embryo diminished by that of an adion; and ΔF_2, (> 0), is the free energy of the ion in the edge diminished by that of an adion, d is the interatomic distance in the embryo, and r is the radius of the embryo. The factor $2/\sqrt{3}$ in the first term accounts for the close packing of atoms in the embryo on the (111) plane of fcc metals. A stable nucleus will be formed if the radius of an embryo exceeds a critical size. From the condition $\frac{d\Delta F}{dr} = 0$, the critical radius of the nucleus is obtained

$$r_c = -\frac{\sqrt{3}d(\Delta F_2 - \Delta F_1)}{2\Delta F_1} = -\frac{\sqrt{3}d}{2} \cdot \frac{\Delta F_3}{\Delta F_1} \quad [24]$$

where ΔF_3 is free energy of an ion in the edge diminished by that in the nucleus.

To a first approximation, assuming in the calculation of the heat content part that the binding energies (of first nearest neighbors only) are additive and considering the entropy of mixing only, expressions for the free energy changes per atom may be written in the form

$$\Delta F_1 = -\frac{L}{2} - kT \ln \frac{n}{N - n} + \Delta F_4 \quad [25a]$$

and

$$\Delta F_3 = \frac{2.5}{12} L + \Delta F_5 \quad [25b]$$

where L is the heat of sublimation of the metal, n the number of adions/cm^2, N the number of available sites/cm^2 ($\sim 1.5 \times 10^{15}$), ΔF_4 is the free energy of hydration of an ion in the nucleus diminished by that of an adion, and ΔF_5 is the free energy of hydration of an ion in the edge diminished by that in the nucleus. On the (111) plane, the number of neighbors of an ion in the edge of the nucleus is either six or seven, and of an ion in the nucleus itself 9. In ΔF_3, the factor 2.5 is the difference $9 - 6.5$, as average.

Possible modes of hydration at various sites on the surface have been considered by Conway and Bockris (16), and their estimates for hydration of adions as well as of ions in the edge of the nucleus and in the plane itself can be used for numerical evaluations of the free energy changes.

At equilibrium ($n = n_o$), the free energy change ΔF_1 is equal to zero, and with this condition Eq. [25a] reduces to

$$\Delta F_1 = -kT \ln \frac{n(N - n_o)}{n_o(N - n)} \quad [26]$$

where n_o is the number of adions/cm^2 at equilibrium. Assuming $N >> n > n_o$, and with $n/n_o = c/c_o$, where c and c_o are adion concentrations at a given overpotential and at the zero overpotential, respectively, the radius of the critical nucleus becomes

$$r_c = \frac{\sqrt{3}}{2} \frac{d^2\gamma}{kT \ln c/c_o} \quad [27]$$

where γ, the edge energy in ergs per centimeter of the circumference of the nucleus, is defined as

$$\gamma = \frac{\Delta F_3}{d} \quad [28]$$

and can be obtained numerically, providing the hydration energy term, ΔF_5, in Eq. [25b] can be estimated.

Frequency of nucleation.—An embryo having the critical radius, r_c, may become a stable nucleus after the elapse of time necessary for a further adion to join it. This is

$$\frac{1}{2\pi r_c v\, n} \quad [29]$$

where v is the average velocity of adions in a given direction. If 1 cm^2 of the surface contains N_c embryos of critical radius in equilibrium with n adions, all of them will become nuclei in $(2\pi r_c v\, n)^{-1}$ sec. Hence, in 1 sec, the number of embryos per cm^2 which become nuclei is

$$R = N_c \left(\frac{1}{2\pi r_c v\, n} \right)^{-1} = 2\pi r_c N_c n \cdot \sqrt{\frac{kT}{2\pi m}} \quad [30]$$

which is the rate of nucleation in nuclei per cm^2 sec^{-1}. Here, v is taken equal to $\sqrt{\frac{kT}{2\pi m}}$. Thus, as

$$N_c = n \cdot \exp\left[-\frac{\Delta F_c}{kT} \right] \quad [31]$$

where ΔF_c is the free energy change for the formation of a critical nucleus, the rate of nucleation becomes

$$R = 2\pi r_c n^2 \cdot \sqrt{\frac{kT}{2\pi m}} \cdot \exp\left[-\frac{\Delta F_c}{kT} \right] \quad [32]$$

The term ΔF_c, obtained from Eq. [23] when r is replaced by r_c, is equal to

$$\Delta F_c = \pi \Delta F_3 \left[\frac{r_c}{d} - 1 \right] \qquad [33]$$

In addition, allowance has to be made for the energy of activation for surface migration E, so that, just after nucleation begins,

$$R = 2\pi r_c n^2 \sqrt{\frac{kT}{2\pi m}} \cdot \exp\left[-\frac{\Delta F_c + E}{kT} \right] \qquad [34]$$

where both r_c and ΔF_c are dependent on the adion concentration which is a potential dependent quantity (cf. Eq. [22]). The rate of nucleation is thus strongly dependent on overpotential and, for a given overpotential, on the dislocation density.

Deposition on a step-free surface after the nucleation has commenced.—After application of a constant overpotential across a crystallographically flat surface ($N = 0$), net ion flow across the double layer will take place, but only until the adion concentration has reached the value (cf. Eq. [22])

$$c = c_0 \exp\left(-\frac{zF\eta}{RT} \right) \qquad [35]$$

At this point, unless the conditions for nucleation are created, no further net flow will occur. Analysis of the equation for the rate of the nucleation (Eq. [34]) shows that significant nucleation may be expected in the case of silver, for instance, if the overpotential is of the order of 80-100 mv (cf. Fig. 8). Experimentally, it is found that with copper whiskers there is no deposition current unless overpotentials of the order of 100 mv are reached [cf. Vermilyea (13)]. The current density which would be observed just after the commencement of nucleation is not, however, that obtainable from R (Eq. [34]). It is governed by surface diffusion-control and can now reach significant values as the nucleation has provided the steps to which ions can diffuse. The problem of calculating the current density after nucleation has commenced, however, is complex, not only because the nuclei grow, coalesce, and spread across the surface and thus change the distance between "steps," but also because, once nucleation has started, the adion concentration will change and moreover, due to small diameters of nuclei (~20Å), the adion concentration at "steps" of the nuclei cannot be taken as the equilibrium adion concentration, c_0. Further, the rate of nucleation itself decreases after commencement because adion concentration decreases. It is therefore possible to obtain only an approximate upper limit for the rate of deposition just after the first nuclei are formed. This is

$$i = i_0 \left\{ \exp\left(-\frac{\beta z F\eta}{RT} \right) - \exp\left[(1-\beta) \frac{zF\eta}{RT} \right] \right\} \frac{2\sqrt{N_c} \tanh\left(\frac{m}{2\sqrt{N_c}} \right)}{m} \qquad [36]$$

and is obtained from Eq. [20] when N is replaced by N_c, where N_c is the number of critical nuclei per cm^2.

Deposition on stepped surface after nucleation has commenced.—The possibility of nucleation on stepped surfaces is much less than on the crystallographically flat surface, as adion concentration even at the midpoint between steps is less than that at a step-free surface, under the same conditions (cf. Eq. [22]). Analysis of the rate of nucleation (Eq. [34]) shows that on a surface with high density of dislocation ($N \sim 10^{10}$ cm^{-2}), no nucleation is possible unless the overpotentials are over 150 mv. In Fig. 8 the rates of nucleation are plotted for various ND values. Due to nucleation, the net rate of charge transfer across the double layer will increase over that given by the steady-state equation (Eq. [20]), because of the effective decrease of adion concentration following nucleation. However, it is difficult to calculate this change, as the appearance of the first nuclei will make the kinetics of deposition complex for the reasons stated in the last section above. Nevertheless, a very rough estimate of the change of charge transfer rate across the double layer after nucleation has started can be made by assuming that the distances between the growth steps are effectively halved, as the nuclei will preferentially be formed at midpoints between steps.

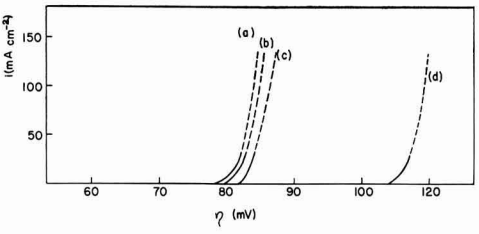

Fig. 8. Current density expected at the first instant after nucleation has commenced as function of overpotential. Curves a, b, c, and d correspond to ideally flat surface, $ND = 10$ sec^{-1}, $ND = 10^2$ sec^{-1}, and $ND = 10^3$ sec^{-1}, respectively.

Summary

The kinetics of the formation and decay of metal monolayers by electrochemical processes is considered for metal surfaces with steps due to emerging screw dislocations. The rate of ion transfer at low overpotentials across the double layer, integrated over the whole surface, varies considerably with the density of dislocations for the same overpotential, as does the rise time. Just after application of constant overpotential, the current density is independent of the fine structure of the substrate and the transfer reaction is always rate controlling. This enables a direct determination of the exchange current density to be made from measurements of the current-time transient immediately after double layer charging. The equilibrium adion concentration can be obtained from $(di/dt)_{t \to 0, \eta}$.

Contrary to the galvanostatic case, when transfer is rate controlling in the steady state, the rise time for potentiostatic charging is governed by the rate of diffusion of adions to growth sites and *vice versa*. A comparison of the rise times obtained in the po-

tentiostatic and galvanostatic transients allows distinction between the rate-controlling transfer and surface diffusion and the evaluation of the relative rate constants for transfer and surface diffusion. At low overpotentials, the steady-state cathodic current density under surface diffusion control is greater than the corresponding anodic value.

The steady-state current density, expressed in terms of a model which allows for the nonlinear distribution of adions with distance between the growth sites, gives rise to an interpretation of the observed gradual transition from surface diffusion control at low overpotentials, to transfer control at high overpotentials in deposition, and predicts diffusion to be rate controlling at all potentials in dissolution if it is controlling at low overpotentials, providing no dissolution from crystallographically flat surfaces or from edges of crystals occurs.

On surfaces with a high density of dislocations, diffusion of adions is relatively unimportant to rate control, since ions reaching the surface will diffuse quickly to the steps. The net rate of charge transfer is then the same all over the surface. At more perfect surfaces, when surface diffusion is rate controlling, the net current is confined to the near vicinity of growth steps, particularly at low current densities. Correspondingly, it is unlikely that deposition occurs directly from solution to kink sites.

Expressions are deduced for the rate of nucleation as a function of dislocation density and overpotential. On surface with a high dislocation density (say 10^{10} cm^{-2}), nucleation is improbable until an overpotential of the order of 100 mv is reached.

Acknowledgment

The authors wish to thank the National Science Foundation for the financial support of this work.

Manuscript received Nov. 28, 1962; revised manuscript received March 29, 1963.

Any discussion of this paper will appear in a Discussion Section to be published in the June 1964 JOURNAL.

REFERENCES

1. W. Mehl and J. O'M. Bockris, *Can. J. Chem.*, **37**, 190 (1959); *J. Chem. Phys.*, **27**, 818 (1957).
2. W. Lorenz, Z. *Elektrochem.*, **57**, 382 (1953); Z. *Naturforsch.*, **9a**, 716 (1954).
3. A. R. Despic and J. O'M. Bockris, *J. Chem. Phys.*, **32**, 389 (1960).
4. H. Gerischer, *Z. Elektrochem.*, **62**, 256 (1958).
5. H. Kita, M. Enyo, and J. O'M. Bockris, *Can. J. Chem.*, **39**, 1670 (1961).
6. F. C. Frank, *Discussion Faraday Soc.*, **5**, 48 (1949); W. R. Burton and N. Cabrera, *ibid.*, **5**, 33 (1949); W. R. Burton, N. Cabrera, and F. C. Frank, *Phil. Trans. Roy. Soc., London*, **A243**, 299 (1951).
7. N. Cabrera and W. K. Burton, *Discussion Faraday Soc.*, **5**, 40 (1949).
8. A. R. Verma, "Crystal Growth and Dislocations," Butterworths, London (1953).
9. M. Fleischmann and H. R. Thirsk, *Electrochim. Acta*, **2**, 22 (1960).
10. N. F. Mott and R. J. Watts-Tobin, *ibid.*, **4**, 79 (1961).
11. B. E. Conway and J. O'M. Bockris, *Proc. Roy. Soc.*, **A248**, 394 (1958).
12. D. A. Vermilyea, *J. Chem. Phys.*, **25**, 1254 (1956).
13. D. A. Vermilyea, *ibid.*, **27**, 814 (1957).
14. H. Seiter, H. Fischer, and L. Albert, *Electrochim. Acta*, **2**, 97 (1960).
15. E. T. Whittaker and G. N. Watson, "A Course of Modern Analysis," p. 136, Cambridge University Press (1920).
16. B. E. Conway and J. O'M. Bockris, *Electrochim. Acta*, **3**, 340 (1961).
17. J. O'M. Bockris and M. Enyo, *This Journal*, **109**, 48 (1962).
18. H. J. Pick, G. G. Storey, and T. B. Vaughan, *Electrochim. Acta*, **2**, 165 (1960).

APPENDIX

After introducing $i(xt)$ from Eq. [2] into [1], and setting

$$u(xt) = [c_\infty - c(xt)] \cdot e^{pt} \qquad \text{[A-1]}$$

Eq. [1] reduces to

$$\frac{\partial u}{\partial t} = D\frac{\partial^2 u}{\partial x^2} \qquad \text{[A-2]}$$

c_∞ is the steady-state distribution of adion concentration and is easily and directly obtainable from [1] and [2] when $\partial c/\partial t$ is placed equal to zero, and second and third condition of [2a] are used. Solution for c_∞ is then

$$c_\infty = A + B\cosh(mx) \qquad \text{[A-3]}$$

where A, B and m, and also p in [A-1] are given by [3a].

For the solution of [A-2], the initial and boundary conditions [2a] transform to

$$u(x,o) = c_\infty - c_o \qquad \text{[A-4]}$$

$$u(\pm x_o,t) = 0 \qquad \text{[A-5]}$$

and

$$\frac{\partial u(o,t)}{\partial x} = 0 \qquad \text{[A-6]}$$

By separation of variables and expanding in Fourier series, the general solution of [A-2] is

$$u(xt) = \sum_\alpha e^{-\alpha t}\left[a\cos\sqrt{\frac{\alpha}{D}}x + b\sin\sqrt{\frac{\alpha}{D}}x\right] \qquad \text{[A-7]}$$

Condition [A-6] requires that

$$b = 0$$

and [A-5] that

$$\sqrt{\frac{\alpha}{D}} = \frac{(n+1/2)\pi}{x_o}$$

Hence, at $t = 0$

$$u(x,o) = \sum_{n=0}^{\infty} a_n \cos\left[(n+1/2)\pi\frac{x}{x_o}\right] \qquad \text{[A-8]}$$

where a_n is given by

$$a_n = \frac{2}{x_o}\int_o^{x_o} u(x,o)\cos\left[\frac{(n+1/2)\pi x}{x_o}\right]dx$$

$$= -\frac{2(-1)^n B' m^2 x_o^2}{\pi(n+1/2)[(n+1/2)^2\pi^2 + m^2x_o^2]} \qquad \text{[A-9]}$$

Combining [A-1, 3, 7, and 9], solution [3] is obtained.

Effect of CdS on the Electroluminescence of ZnS:Cu, Halide Phosphors

Arthur Dreeben

RCA Laboratories, Radio Corporation of America, Princeton, New Jersey

ABSTRACT

The effect of CdS on the electroluminescence of ZnS:Cu phosphors coactivated with Cl, Br, or I has been determined. In each case, brightness is sensitive to the presence of CdS, and there is an apparent relationship between intensity and crystal structure. Maximum brightness is associated with the cubic modification. In iodide coactivated phosphors prepared at 700°C, the cubic phase persists up to 10 mole % CdS, and a decrease in power dissipation leads to improved efficiency. CdS also causes a variation in the amount of retained copper which is explained by postulating the formation of a new phase involving (Cu,Cd) (S,Halide).

Zinc cadmium sulfide solid solutions, activated with copper, are well-known and useful photo- and cathodoluminescent phosphors. It was felt, therefore, that they should also be examined more completely for electroluminescence (hereafter referred to as EL). An earlier finding in this laboratory (1) indicated that the addition of small amounts of cadmium sulfide to EL zinc sulfide phosphors significantly diminished their brightness. Other work describing a similar effect is limited to phosphors coactivated either with chloride (2) or with Group III elements (3). The present study, comparing iodide with chloride and bromide in EL(Zn, Cd)S:Cu, has shown that the effect of cadmium sulfide varies with the particular halide coactivator used.

Unique characteristics of the solid solutions coactivated with iodide and containing up to 10 mole % cadmium sulfide include (*a*) the stabilization of a single cubic phase, whereas the hexagonal modification is usual with as little as 2 or 3 mole % cadmium sulfide in chloride coactivated phosphors fired at 850°-900°C (4, 5); and (*b*) a remarkable decrease in power dissipation with only a slight decrease in brightness.

Experimental

The phosphors were prepared by intimately mixing dried slurries of the component sulfides (RCA Luminescent Grades) containing the activator (as the acetate) and the ammonium salt of the desired coactivator. In the firing process, use was made of the sulfur effect (2, 6, 7) by mixing 10 weight per cent (w/o) of purified sulfur with the unfired mix to facilitate development of EL at a lower firing temperature. For iodide coactivation, some results using this procedure are contrasted with a higher firing temperature in the absence of sulfur.

Firing tubes containing the mixes in covered quartz vials were preflushed with purified, dry nitrogen, but a static atmosphere was maintained during a 1-hr firing time. The gas exit tube was connected through a silicone-oil seal to prevent back diffusion of air. Products were cooled in a stream of the nitrogen.

After cooling, the products were digested in an alkaline solution of sodium cyanide to remove excess, unincorporated copper. In all cases, this treatment lightened the dark body color of the fired products. Finally, samples were washed free of cyanide with water. Brightness of the cells was determined with a McBeth Illuminometer, and power dissipation was measured with a VAW electronic wattmeter.

Results

Analyses confirmed that no copper was lost during synthesis, but that some was dissolved by the cyanide wash. The amount of copper retained in iodide coactivated samples depended on the firing temperature, but not on the proportion of CdS. For example, in phosphors containing up to 20 mole % CdS, and prepared with 0.15 mole % Cu and 10 w/o of ammonium iodide, 39% of the copper was finally retained in samples admixed with sulfur and fired at 700°C, and 28% was retained when the firing was accomplished at 1075°C in the absence of sulfur.[1]

In bromide and chloride coactivated samples, the proportion of CdS influenced the amount of retained copper which first increased and then decreased with greater proportions of CdS as shown in Table I. A progressively darker body color (after the cyanide wash) accompanied this increase in retained

[1] The amount of NH_4I was chosen to compensate for losses through volatilization on firing (9).

Table I. Retention of copper in Cl and Br coactivated (Zn,Cd)S phosphors

Mole % CdS	% Cu retained	
	Cl coactivated	Br coactivated
0	16	47
3	16	49
5	17	—
6	—	56
7	44	—
8	—	61
10	30	67
15	22	64

Mole % Cu originally added: Cl coactivated, 0.62; Br coactivated, 0.51. Both series fired at 950°C.

Table II. Crystal structure of (Zn,Cd)S:Cu, halide phosphors

Mole % CdS	Cl	% Cubic phase Br	I-700°C	I-1075°C
0	100	50	100	50
1	100	—	100	—
2	—	—	—	35
3	90	40	100	—
5	70	—	100	—
6	—	20	—	25
7	25	—	100	—
10	10	0-5	100	5-10
15	0-5	0-5	5	5
20	0-5	—	—	—

* Note: In a predominantly cubic phase, less than 1% hexagonal is detectable, but in a predominantly hexagonal phase, less than 5% cubic cannot be resolved.

copper particularly with chloride coactivation. There was also an increase in the phosphorescence observed after irradiation with 3650Å uv contrary to the typical effect of both increasing Cu and increasing CdS (5). These findings suggested the formation of a new cyanide insoluble phase involving (Cu, Cd) (S, halide). After similar observations, Wachtel (2) prepared a black, hexagonal material thought to be a (Cd,Cu)S compound. Bartels and Wasserman (8) suggested the formation of a copper-rich phase in photoconducting CdS:Cu,Cl powders to account for variations in dark conductivity. The present observation that the formation of such a phase is sensitive to the particular halide used in the phosphor suggests that the halide itself is a part of the complex affecting its stability and equilibrium in the system.

X-ray diffraction examination of representative samples from each of the series showed the presence in some samples of a single phase of either cubic or hexagonal structure, or coexistence of both phases in other phosphors. The proportion of cubic phase is given in Table II. The unit cell of the cubic phase expands linearly with increase in CdS, but the expansion of the hexagonal phase departs from linearity. This is attributed to interference from the cyanide insoluble complex phase described above and is consistent with the observation that the onset of the increase in retained copper, indicative of the formation of the complex phase, coincides approximately with the appearance of the hexagonal phase in chloride and bromide coactivated phosphors. Other effects related to crystal structure will be described later.

Spectral distribution of emission.—Spectral distributions of EL emission for samples with no CdS are shown in Fig. 1. Qualitative features of spectral position and dependence on excitation frequency for the chloride, bromide, and high-temperature iodide coactivated phosphors are in general agreement with similar data reported by Hegyi *et al.* (9). The low-temperature iodide coactivated material, however, has a broader emission band with an apparent peak in the blue at a somewhat longer wavelength than the high-temperature sample.

Representative curves for one (Zn,Cd)S composition from each series are shown in Fig. 2. Samples

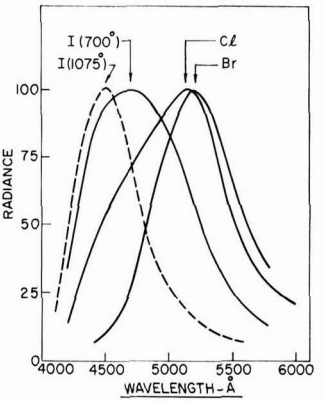

Fig. 1. Spectral distribution of EL emission of ZnS:Cu, halide phosphors, 200v, 200 cps (peaks normalized).

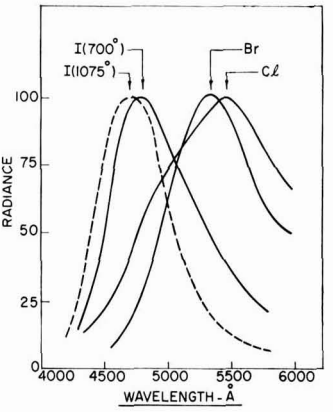

Fig. 2. Spectral distribution of EL emission of (Zn,Cd)S:Cu, halide phosphors; chloride and iodide—7 mole % CdS; bromide—8 mole % CdS; 200v, 200 cps (peaks normalized).

within each series with a given coactivator showed the expected shift to longer wavelengths with increasing proportion of CdS and a shift to shorter wavelengths with increasing excitation frequency. The magnitude of these shifts was somewhat dependent on the particular coactivator.

Brightness, power, and efficiency.—The relative brightness, power dissipation per cell unit area, and efficiency for bromide and chloride coactivation are shown as a function of CdS concentration in Fig. 3a, b, and c respectively.[2] These values all diminish rapidly when CdS is in excess of several mole per cent. Corresponding data for the high-temperature iodide coactivated phosphor are shown in Fig. 4a, b, and c. Here, brightness exhibits an immediate sensitivity to the presence of CdS and begins to decrease at once, but the power dissipation declines at an even faster rate. As a result, maximum efficiency occurs at 6 mole % CdS, but at this point the brightness has suffered a severe loss from its initial value.

2 Changes in EL emission color for the compositions of interest here were slight. Therefore, by considering luminance rather than total quanta, only a small error is introduced without affecting the trends.

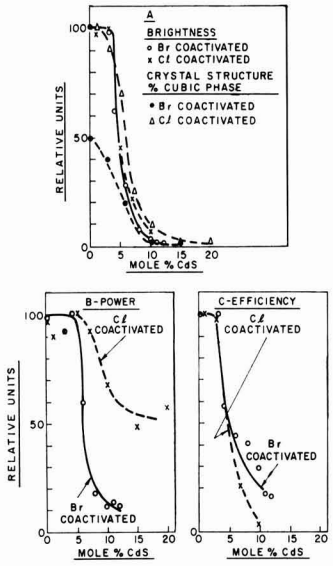

Fig. 3. Crystal structure, relative brightness, power, and efficiency for (Zn,Cd)S:Cu, Br, or Cl as a function of CdS concentration, 200v, 200 cps.

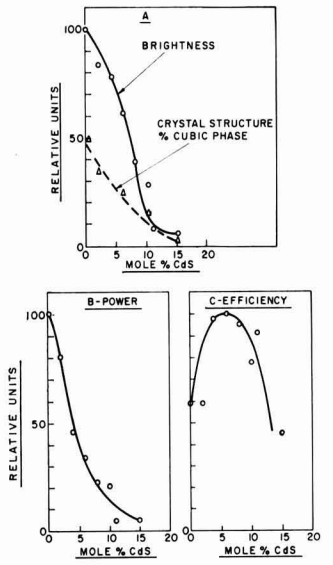

Fig. 4. Crystal structure, relative brightness, power, and efficiency as a function of CdS concentration for (Zn,Cd)S:Cu,I fired at 1075°C, 200v, 200 cps.

The most interesting behavior occurred in the iodide coactivated samples fired at 700°C with sulfur. In this series the phosphor with no CdS was considerably brighter than the corresponding high-temperature preparation, and the brightness of the former, shown in Fig. 5a, was diminished only slightly by the addition of as much as 7 mole % CdS, and even 10 mole % effected only a relatively moderate reduction. The power dissipation (Fig. 5b) was initially the highest in any of the series, but with increasing amount of CdS, a remarkable

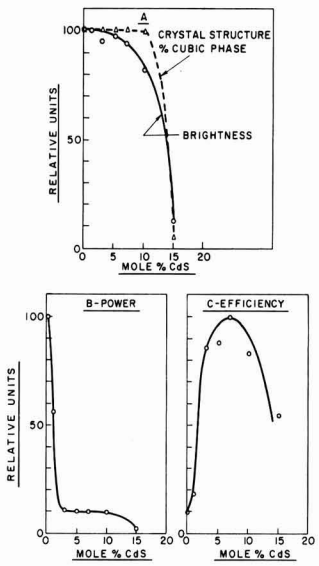

Fig. 5. Crystal structure, relative brightness, power, and efficiency as a function of CdS concentration for (Zn,Cd)S:Cu,I fired at 700°C with sulfur, 200v, 200 cps.

decrease occurred so that with 3 mole % CdS, the power is only 10% of its initial value. Efficiency, shown in Fig. 5c, reaches a maximum with 7 mole % CdS, but in this instance the improvement is not accompanied by the appreciable brightness loss noted with the high-temperature material.

Discussion

In the present study, phosphors with the highest brightness in a given series are associated with cubic or faulted structures. In the low-temperature iodide coactivated samples, the single cubic phase persists with a higher proportion of CdS (10 mole %) than in any of the other series (Fig. 5a). However, a slight decrease in brightness noticeable for the cubic compositions with 7 and 10 mole % CdS may be an indication of the incipient formation of the hexagonal structure. The different firing temperatures for the two iodide coactivated series account for structural differences in samples with equivalent ZnS-CdS ratios (compare Fig. 4a and 5a). The chloride and bromide coactivated samples, however, were fired at the same temperature (950°C) and it is probable that in their case structural differences (Fig. 3a) for equivalent compositions reflect a different influence of the respective coactivators. Similar effects on structure have been described by Shrader and Larach (11).

Conclusions

The data presented support the conclusion of an increasing number of investigators, (2, 3, 11-13) that cubic or complex faulted structures of ZnS are the most suitable for attaining maximum EL. This has been attributed to the absence in the cubic structure of deep traps found in the hexagonal modification (3, 11). The EL properties are simul-

taneously influenced by interrelated effects from phase relationships involving the segregation of copper, crystal structure, and trapping states. The relative importance of each of these separately cannot be decided at present.

Acknowledgment

The problem was suggested by R. E. Shrader with whom the author had valuable discussions. The gracious aid of S. M. Thomsen in making some measurements and his good advice are appreciated. Spectral distributions were recorded by H. E. MacDonald, x-ray diffraction data were obtained by W. C. Roth, and M. C. Gardels performed the chemical analyses for copper.

Manuscript received April 24, 1963. This paper was presented at the Chicago Meeting, May 1-5, 1960.

Any discussion of this paper will appear in a Discussion Section to be published in the June 1964 JOURNAL.

REFERENCES

1. R. E. Shrader and S. Larach, Unpublished data (1958).
2. A. Wachtel, *This Journal*, **107**, 602 (1960).
3. P. Zalm, *Philips Research Repts.*, **11**, 353 (1956).
4. S. Asano, *Science of Light*, **4**, 32 (1955).
5. G. R. Fonda, *Trans. Electrochem. Soc.*, **87**, 339 (1945).
6. S. Larach and R. E. Shrader, Brussels International Conference on Solid State Physics, p. 41, 1958.
7. A. Wachtel, U. S. Pat. 2,874,128 (1959).
8. B. E. Bartels and M. S. Wasserman, New York Meeting, Electrochem. Soc., April 1958, Abstract 31.
9. I. J. Hegyi, S. Larach, and R. E. Shrader, *This Journal*, **104**, 717 (1957).
10. S. Larach and R. E. Shrader, *RCA Review*, **20**, 532 (1959).
11. D. W. G. Ballentyne, *This Journal*, **107**, 807 (1960).
12. A. H. McKeag and E. G. Steward, *ibid.*, **104**, 41 (1957).
13. F. C. Palilla and D. H. Baird, *ibid.*, **109**, 1162 (1962).

An X-Ray Study of Pyrochlore Fluoantimonates of Calcium, Cadmium, and Manganese

M. A. Aia,[1] R. W. Mooney, and C. W. W. Hoffman

Chemical and Metallurgical Division, Sylvania Electric Products Inc., Towanda, Pennsylvania

ABSTRACT

Pyrochlore fluoantimonates of divalent metals have the general formula $M^{II}_{1+a+b/2}Sb_2O_6(O'_a + F_b)$ and can demonstrate both cation and anion defects. Fluoantimonates of Ca, Cd, and Mn having the pyrochlore structure were prepared and indexed as face-centered cubic from x-ray powder patterns. The cell edge of all binary combinations decreased linearly from Ca (10.30Å) to Cd (10.27Å) to Mn (10.14Å) fluoantimonate. Calcium fluoantimonate crystallized as a defect pyrochlore, with both Ca and F deficiencies. The structure of $Ca_{1.56}Sb_2O_{6.37}F_{0.44}$ was determined by the method of least squares from powder patterns. The value of the variable oxygen parameter x was 0.28_7. Fluoride is much less stable in the antimonates of Cd and Mn, but as little as 0.2% fluoride can be sufficient to cause these antimonates to crystallize in the pyrochlore structure.

Cubic compounds of the pyrochlore structure class have been studied with renewed interest since the discovery of ferro-electricity in cadmium niobate, $Cd_2Nb_2O_7$, by Cook and Jaffe (1). Pyrochlores have the idealized formula $A_2B_2O_6X$, where $A^{I,II,III}$ and $B^{IV,V,VI}$ are suitable cations of the proper valences, and X is O, OH, and F. Jona, Shirane, and Pepinsky (2) give an excellent description of the pyrochlore structure in their paper on $Cd_2Nb_2O_7$ and related compounds. Another synthetic compound with the pyrochlore structure, calcium fluoantimonate or fluoromeite, has recently been found to exhibit both fluorescence (3) and phosphorescence (4), thus introducing this structure class to the family of self-activated phosphors.

The first complete structural analysis for antimonate compounds of the type studied herein was given in 1932 by Zedlitz (5). In his study of the mineral romeite, with generalized formula $(Ca,Mn,Na)_2Sb_2O_6$ (O,OH,F), Zedlitz found that fluoride was essential to the formation of the pyrochlore structure, and that a continuous, three-dimensional array of SbO_6 octahedra held the structure together in a framework of composition $(Sb_2O_6)_\infty$. The Ca, F, and excess O ions occupied holes in the framework at special fixed positions. In 1944, Byström (6) reported a complete structural analysis of $Ca_2Sb_2O_7$, $Cd_2Sb_2O_7$, and $Sr_2Sb_2O_7$ and found that they had a structure not like pyrochlore, but instead like weberite, in which all seven oxygen atoms are co-ordinated to antimony atoms resulting in orthorhombic instead of cubic symmetry.

In 1950, Butler and co-workers (7) reported on studies of calcium antimonates as related to the formation of calcium halophosphate phosphors. Some of the x-ray work of Byström (6) and Magnéli (8) was confirmed, as was the contention of Zedlitz that fluoride ion was essential to the forma-

[1] Present address: General Telephone and Electronics Laboratories, Inc., Bayside, New York.

tion of calcium romeite, *i.e.*, calcium antimonate with the pyrochlore structure. However, in an attempt to explain the stoichiometry of calcium fluoantimonate, Butler and co-workers concluded that both trivalent and pentavalent antimony were present. They proposed the formula, $Ca_4Sb_2^{III}Sb_2^{V}O_{11}F_2$, which would invalidate the structure obtained by Zedlitz.

The present work was undertaken to resolve the differences in the literature by means of a structural analysis of cubic calcium fluoantimonate, and to extend the results to cover analogous compounds of manganese and cadmium. Since most calcium halophosphate phosphors now manufactured contain small amounts of cadmium (9), as well as manganese and antimony, the results could also be useful in a study of intermediates formed during the synthesis of such phosphors.

Experimental

Preparation of samples.—The cubic calcium fluoantimonate whose structure was analyzed was prepared by the method of Butler and co-workers (7) from $CaCO_3$, CaF_2, and $(Sb_2O_4)_{0.75}\cdot(Sb_2O_3)_{0.25}$, of luminescent grade purity. The $(Sb_2O_4)_{0.75}\cdot(Sb_2O_3)_{0.25}$ was prepared while attempting to prepare Sb_2O_4 by heating a 1-in. layer of cubic Sb_2O_3 for 10 hr at 400°-650°C in air; about 25% Sb_2O_3 was detected by x-ray diffraction after this treatment. One mole of each ingredient was pebble milled together, fired 1 hr at 980°C in a quartz crucible, ground, refired 1 hr at 1175°C, and reground. The blue-white calcium antimonate was suspended 3 times in 10% HNO_3 to leach out the excess CaF_2. Analysis of the dried product gave 15.0% Ca, 58.5% Sb, and 2.3% F, which corresponds to the formula $Ca_{1.56}Sb_2O_{6.37}F_{0.44}$. The experimental density was 5.02 g-cm^{-3}. If other compounds were present, they could not be found by x-ray diffraction, contrary to the results of Chevalier and co-workers (4) who found $CaSb_2O_6$ and $Ca_2Sb_2O_7$ in a similar preparation.

Cadmium fluoantimonate was best prepared by mixing one mole each of CdO_2 (10), CdF_2, and $(Sb_2O_4)_{0.75}(Sb_2O_3)_{0.25}$. A soft, uniformly reacted material was obtained by firing 1 hr at 845°C in a covered crucible. When CdO or $CdCO_3$ was used in place of CdO_2, the firing product was much less homogeneous. The olive-green cadmium antimonate was leached with 10% HNO_3 to remove the excess cadmium, which was present mostly as CdO after firing. Typical analyses were 38.8% Cd, 42.0% Sb, and 0.2% F, which corresponds to the formula $Cd_{2.0}Sb_2O_{6.9}F_{0.1}$. The experimental density varied from 6.76 to 6.86 g-cm^{-3}. No other compounds were found by x-ray diffraction.

A series was made in which a variable amount of CdF_2 was mixed with CdO and Sb_2O_3, keeping a constant atomic ratio of 2.05 Cd per 2 Sb. Static firing of the mixtures showed that, in the absence of fluoride, the orthorhombic $Cd_2Sb_2O_7$ formed at 430°C after 18 hr, and much faster at higher temperatures. The cubic cadmium fluoantimonate was formed by firing between 480° and 540°C for 75 min, when at least 0.4 atom F per mole Sb_2O_3 was present; samples fired at 720°C showed either the orthorhombic antimonate, or a mixture of this with the cubic fluoantimonate. Presumably, the composition moves across a phase boundary upon the loss of the small quantity of fluoride required to stabilize the pyrochlore structure.

Manganese fluoantimonates, and all the binary mixed antimonates were prepared by combining 2.0 moles of MO (MO was $CaCO_3$, CdO_2, $MnCO_3$, or any binary mixture), 1.0 mole of Sb_2O_3, and 1.2 moles of $NH_4F\cdot HF$. The mixtures were blended by pebble milling overnight in acetone. After drying, the powders were heated in covered porcelain crucibles at 550°C, mortared, reheated from 800° to 1150°C, and reground. The final firing schedule was varied, depending on the composition, to minimize sintering and inhomogeneity; the higher the Mn content, the darker the color, and the lower the firing temperature. Analyses on a manganese fluoantimonate reheated 2 hr at 850°C were 26.8% Mn, 49.7% Sb, and 0.35% F. Impurities (Mn_2O_3 and $MnSb_2O_6$) were found by x-ray diffraction, and it was not meaningful to estimate the stoichiometry of the manganese fluoantimonate prepared. In all samples, metallic impurities detectable by spectrographic analysis were less than 0.1%.

X-ray diffraction methods.—X-ray diffraction patterns were taken on a Philips-Norelco unit, using nickel-filtered CuKα radiation (1.5418Å). Long exposures were made on 114.6 mm Debye-Scherrer cameras to determine impurities. Intensity and 2θ values were taken from diffractometer tracings made at a scanning speed of ¼°/min. The diffractometer was calibrated with Si and checked with W, assuming values given by the National Bureau of Standards. The observed intensities were measured on the diffractometer tracing by graphical integration. The resulting values were corrected for changes in slit width, giving the I_o values, scaled to a maximum value of 1000, shown in Tables I and III. The reflections used to calculate the cubic-cell parameter were 662, 666 (1022), 840, 844, 1062, and 884 (1200). These reflections at high values of 2θ were selected because they were fairly intense and showed less interference from other reflections. Virtually no correction was indicated by calibration.

Chemical analyses.—**Antimony:** The sample was digested overnight with H_2SO_4 and K_2SO_4. Filter paper and more H_2SO_4 were added and the solution heated until clear. Antimony was then determined by titration with $KMnO_4$ (11). **Fluorine:** The sample was fused with Na_2O_2 and Na_2CO_3 then dissolved. Fluorine was distilled off as hydrofluosilicic acid and titrated with thorium nitrate solution (11). **Calcium:** Antimony was fumed off with HBr, then calcium was precipitated and weighed as the oxalate. **Cadmium:** Antimony was fumed off with HBr, then cadmium was precipitated from strongly acid solution and weighed as CdS. **Manganese:** Antimony was fumed off with HBr, then manganese was determined by flame photometry. The presence of calcium or cadmium did not interfere. **Oxygen:** Attempts to determine oxygen as H_2O by heating samples in a stream of hydrogen were unsuccessful, so oxygen was calculated by difference.

Table I. Indexed powder patterns and cell sizes of cubic fluoantimonates of calcium, cadmium, and manganese

hkl	$Ca_{1.56}Sb_2O_{6.37}F_{0.44}$ d (Å)	I_o	$Cd_{2.0}Sb_2O_{6.9}F_{0.1}$ d (Å)	I_o	Mn fluoantimonate (0.35% F) d (Å)	I_o
111	5.94	549	5.92	16	5.85	210
311	3.104	381	3.093	10	3.058	210
222	2.973	1000	2.965	1000	2.927	1000
400	2.573	226	2.567	363	2.536	225
331	2.363	30	2.356	14	—	—
511, 333	1.9819	122	1.9762	20	1.9516	75
440	1.8204	503	1.8149	472	1.7928	385
531	1.7409	98	—	—	1.7142	75
533	1.5706	67	—	—	1.5457	60
622	1.5529	402	1.5478	440	1.5283	375
444	1.4866	95	1.4816	109	1.4636	115
711, 551	1.4422	73	—	—	1.4205	60
731, 553	1.3410	88	—	—	1.3201	100
800	1.2875	55	1.2834	56	1.2680	85
751, 555	1.1895	38	—	—	—	—
662	1.1816	140	1.1779	145	1.1633	150
840	1.1517	119	1.1480	129	1.1335	125
911, 753	1.1307	36	—	—	1.1134	30
931	1.0797	24	—	—	1.0626	35
844	1.0513	108	1.0483	113	1.0348	125
933, 771, 755	1.0352	24	—	—	1.0193	30
951, 773	0.9958	38	—	—	0.9796	35
1022, 666	0.9910	109	0.9883	131	0.9760	145
953	0.9606	20	—	—	0.9459	35
1111, 775	0.9289	23	—	—	0.9140	10
880	0.9105	41	0.9077	48	0.8961	70
1131, 971, 955	0.9000	50	—	—	0.8863	45
1133, 973	0.8737	49	—	—	0.8603	45
1062	0.8706	187	0.8680	200	0.8571	205
1200, 884	0.8585	137	0.8559	146	0.8451	145
1151, 777	0.8496	26	—	—	0.8367	40
1153, 975	0.8274	49	—	—	0.8148	80
1240	0.8144	135	0.8120	145	0.8019	95
1311, 1171, 1155, 993	0.7878	113	—	—		
1066	0.7855	195	0.7831	215		
1244	0.7766	213				
Cell size, a_o (Å)	10.300 ± 0.002		10.269 ± 0.003		10.141 ± 0.003	

X-ray Powder Patterns

X-ray powder patterns, indexed as face-centered cubic, are given in Table I for the fluoantimonates of calcium, cadmium, and manganese described above. Four lines due to Mn_2O_3 and $MnSb_2O_6$ impurities were discounted in the indexing of the manganese fluoantimonate. The cell sizes followed the expected progression and decreased from calcium to cadmium to manganese fluoantimonate. All three compounds were deficient in fluoride, and only the cadmium fluoantimonate contained the expected 2 atoms of divalent metal per two atoms of antimony. The apparent stoichiometry of cubic cadmium fluoantimonate was confirmed by chemical analysis of several other preparations and will be discussed later. However, no special significance need be ascribed to the specific ratios of atoms since they reflect, in part, the particular methods of preparation, the results of chemical analytical procedures, and the peculiarities of the pyrochlore structure.

Structure Determination

The diffraction pattern of $Ca_{1.56}Sb_2O_{6.37}F_{0.44}$, calcium fluoantimonate with the romeite or pyrochlore structure, contained 36 lines, all of which were readily indexed as cubic (Table I). The systematic absence of all hkl reflections for which h + k, k + l, and l + h $\neq$ 2n, and all Okl type reflections for which k + l $\neq$ 4n was consistent with the space group of pyrochlore, Fd3m-O^7_h. The density calculated for 8 molecules of $Ca_{1.56}Sb_2O_{6.37}F_{0.44}$ per unit cell is 5.06, which agrees within 0.8% of the experimental density of 5.02 g-cm^{-3}. The density calculated for $Ca_2Sb_2O_6F$ is 5.33. In 1932, Zedlitz (5) placed the atoms of the mineral romeite in the following special positions of space group Fd3m-O^7_h, with origin at 43m, and 8 molecules of $Ca_2Sb_2O_6(O', F)$, where O′ is the oxygen in excess of 6 atoms per 2 Sb:

16 Sb in 16d: ⅝, ⅝, ⅝; ⅝, ⅞, ⅞; ⅞, ⅝, ⅞; ⅞, ⅞, ⅝.

16 Ca in 16c: ⅛, ⅛, ⅛; ⅛, ⅜, ⅜; ⅜, ⅛, ⅜; ⅜, ⅜, ⅛.

8(O′ + F) in 8a: 0, 0, 0; ¼, ¼, ¼.

48 O in 48f: x, 0, 0; $\bar{x}$, 0, 0; ¼ + x, ¼, ¼; ¼ − x, ¼, ¼; 0, x, 0; 0, $\bar{x}$, 0; ¼, ¼ + x, ¼; ¼, ¼ − x, ¼; 0, 0, x; 0, 0, $\bar{x}$; ¼, ¼, ¼ + x; ¼, ¼, ¼ − x.

Further information is given in the International Tables (12). The only undetermined atomic parameter in the structure was x. As a first approximation, a value of 0.25 was chosen and relative intensities were calculated, with F and O′ atoms in the 8a special positions, from the well-known relation

Table II. Final values of oxygen parameter x for $Ca_{1.56}Sb_2O_{6.37}F_{0.44}$ (x and σ are expressed as fractions of the unit-cell parameter)

F and O′ positions	x	Std. dev., σ	$R = \Sigma\|I_o - I_c\|/\Sigma I_o$
8a	0.287	0.0022	0.101
8b	0.263	0.0051	0.234

$$I_c = k\,p\,|F_{hkl}|^2 \frac{(1+\cos^2 2\theta)}{(\sin^2\theta\cos\theta)}$$

where p is the multiplicity; F_{hkl} is the structure amplitude; f (θ) is the usual Lorentz polarization term; and k is a factor for scaling I_c to I_o by setting $\Sigma I_c = \Sigma I_o$. Values of atomic scattering factors were taken from James and Brindley (13). For the formula $Ca_{1.56}Sb_2O_{6.37}F_{0.44}$, the scattering factor, f, for the (F+O′) sites was taken as the mean between f_O and f_F because of their nearly equal occupancy of these sites (0.44 F + 0.37 O′), and because of their nearly equivalent atomic numbers. Completely randomized location of F and O′ ions in the special positions was thus assumed. The variable parameter x was refined by the method of least squares (14) to minimize $\Sigma w(I_o - I_c)^2$ and determine the probable error in x. The weighting factor, w, was assigned a value of unity throughout. A small temperature correction factor, $B = 0.5\text{Å}^{-2}$, was applied to the total structure during the iteration. This treatment refined the value of x to 0.287 and decreased R $(\Sigma|I_o - I_c|/\Sigma I_o)$ to 0.10. Calculations were then carried out for the F and O′ atoms in special positions 8b, which are also spatially possible. Results are summarized in Table II.

It is obvious that the best fit of calculated to observed intensities is given with the F and excess O atoms in the 8a positions. The 8b positions of F and O′ atoms yield a significantly larger R factor. The large effect of the seemingly small contribution of these atoms to the structure factor, $F^2 = \Sigma A^2 + \Sigma B^2$, occurs because the contribution of these atoms to A and B, the real and imaginary components of the structure factor, undergoes a phase change which reverses sign for all reflections with odd indices. This reversal in sign effects the summed values of A and B, as reflected in Table II. The calculations were not repeated for the formula $Ca_2Sb_2O_6(F,O')$ because the compound with 2Ca per 2Sb atoms would only be a special case of the general family of compounds, $Ca_{1+a+b/2}Sb_2O_6(O'_a + F_b)$, which is suggested by the structure. Furthermore, a formula such as $Ca_2Sb_2O_6F$ is unlikely since it is unbalanced by one electrical unit, and $Ca_2Sb_2O_7$ is not a pyrochlore. Table III gives values of observed intensity and calculated intensity for $x = 0.287$ (8a positions). The observed intensities were scaled so that the strongest reflection (222) had a value of 1000.

Table III. Values of I_o and I_c for the final value $x = 0.287$ for the compound $Ca_{1.56}Sb_2O_{6.37}F_{0.44}$

hkl	d	I_o	I_c	hkl	d	I_o	I_c
111	5.94	549	552	1020	—	—	2
220	—	—	6	862			
311	3.104	381	398	951	0.9958	38	30
222	2.973	1000	1018	773			
400	2.573	226	205	1022	0.9910	109	122
331	2.363	30	41	666			
422	—	—	8	953	0.9606	20	21
511	1.9819	122	110	1042	—	—	1
333				1111			
440	1.8204	503	551	775	0.9289	23	23
531	1.7409	98	101	880	0.9105	41	50
620	—	—	1	1131			
533	1.5706	67	48	971	0.9000	50	40
622	1.5529	402	376	955			
444	1.4866	95	66	1060	—	—	2
711	1.4422	73	61	866			
551				1133	0.8737	49	41
642	—	—	0	973			
731	1.3410	88	87	1062	0.8706	187	190
553				1200			
800	1.2875	55	48	884	0.8585	137	112
733	—	—	3	1151	0.8496	26	21
822	—	—	3	777			
660				1222	—	—	5
				1064			
751	1.1895	38	30	1153	0.8274	49	46
555				975			
662	1.1816	140	136				
840	1.1517	119	91	1240	0.8144	135	149
911	1.1307	36	28	991	—	—	19
753				1082	—	—	0
664	—	—	0	1311			
931	1.0797	24	20	1155	0.7878	113	104
844	1.0513	108	122	1171			
				993			
933	1.0352	24	20	1066	0.7855	195	215
771				1244	0.7766	213	290
755							

It is also spatially possible. Results are summarized in Table II.

The bond distances calculated from the structure are listed in Table IV. The bond distances found

Table IV. Bond distances for compounds related to calcium fluoromeite, and of the general formula $A_xB_2O_yF_z$ (all values in Angstroms)

Bond	Present work, $Ca_{1.56}Sb_2O_{6.37}F_{0.44}$	Zedlitz $(Ca,Mn,Na)_2Sb_2(O,OH,F)_7$	Byström $Cd_2Ta_2O_7$ (pyrochlore)	Byström $Ca_2Sb_2O_7$ (weberite)	Magnéli $PbSb_2O_6$	Pauling (calculated)
A — O	2.47	2.55	2.50 and 2.25	2.32-2.62	2.52	2.39
A — F	2.23	2.23	—	—	—	2.35
B — O	2.04	1.97	2.04	1.95-2.00	2.00	2.02
F — O	2.95	3.08	—	—	—	2.76
O — O	2.63-3.11	2.67-2.90	2.66-?	2.60-?	2.60-?	2.80
O — O (c axis)	4.39	—	—	—	—	—
Error:	±0.02	—	—	—	—	—

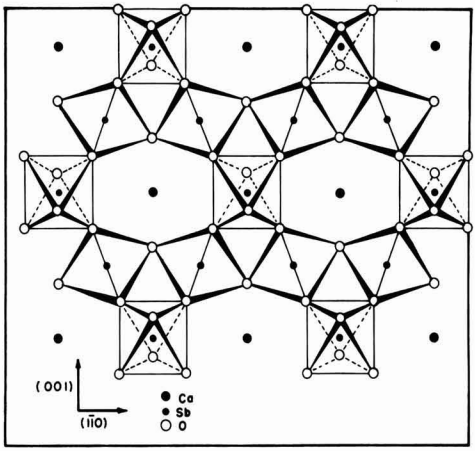

Fig. 1. Configuration of SbO_6 octahedra in calcium fluoantimonate, with pyrochlore structure, projected on (110). Not shown are the Ca ions which overlap the Sb ions at (⅛, ⅛), etc., and the excess oxygens and fluorines, located above and below the Ca ions. Adapted from Jona and co-workers (2).

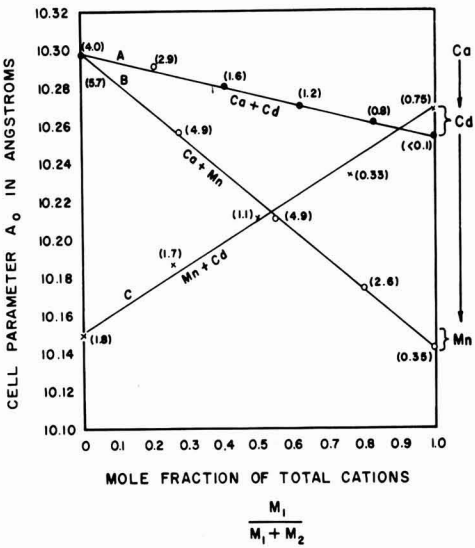

Fig. 2. Cell size *vs.* composition of pyrochlore fluoantimonates of Ca, Cd, and Mn. Weight per cent fluoride found by analysis is given in parentheses. Brackets indicate where cell size varied with fluoride content of antimonates containing only Cd or only Mn.

in $Ca_{1.56}Sb_2O_{6.37}F_{0.44}$ are in good agreement with those found in similar compounds, and with values predicted from Pauling's ionic radii. The agreement is especially good for the B-O, *i.e.*, Sb-O, bond distance. This is expected since the structures of all of the compounds are dependent on a continuous network of BO_6 octahedra for their rigidity.

Figure 1 shows the configuration of SbO_6 octahedra in calcium fluoantimonate, or for that matter, any pyrochlore antimonate. It is easily seen that calcium deficiencies can occur without damaging the integrity of the structure, which is held together by the octahedra, since the calcium ions actually occupy large holes in the network. The same is true of the fluorine and excess oxygen ions, which are located above and below the calcium ions, but are not shown on Fig. 1.

Solid Solution Studies

Binary mixtures of fluoantimonates of Ca, Cd, and Mn were prepared and studied by x-ray diffraction. The compounds showed a linear decrease in cell size as the cation was varied from Ca to Cd to Mn, indicating continuous solid solutions were formed. Variations in cell parameter and fluoride content with composition are shown on Fig. 2. It is evident that fluoride content also varied with composition, and that the cell parameter varied with fluoride content (shown as weight per cent). Much less fluoride than one F per two Sb atoms needs to be incorporated to obtain pyrochlore antimonates of Ca, Cd, or Mn. The fluoride content of five samples of cubic cadmium fluoantimonate ranged from <0.03 to a high of only 0.23 atom F per 2 atoms Sb. The instability of fluoride in cadmium fluoantimonate is discussed further below.

Discussion

Stoichiometry.—The cubic fluoantimonate of cadmium was not cation deficient like that of calcium. This can be explained by the fact that fluoride is not thermally stable in cadmium fluoantimonate, hence cadmium atoms do not have to be removed to compensate for the charge difference between incorporated F and O atoms. The lower thermal stability of fluoride in cadmium fluoantimonate *vs.* the high stability in calcium fluoantimonate is analogous to the relative stabilities of CaF_2 and CdF_2 and can be attributed to the much lower electropositive nature of Cd, which results in lower binding strength with fluorine. A comparison of the estimated partial charges on the atoms in the fluoantimonates and fluorides of calcium and of cadmium is given in Table V. The method of calculation, developed by Sanderson (15), is based on the electronegativities of the elements. The results indicate that the electrostatic attraction between Ca or Cd atoms and F atoms in the fluoride is very similar to the attraction in the fluoantimonates.

As reported above (p. 1050), the calculated and observed densities of $Ca_{1.56}Sb_2O_{6.37}F_{0.44}$ agree within 0.8%. For $Cd_{2.0}Sb_2O_{6.9}F_{0.1}$, the formula suggested by chemical analyses, the density calculated for the same structure is 7.11, which is 3.6% higher than the observed density of 6.86 g-cm^{-3}. The presence of a small amount of impurity such as $Cd_2Sb_2O_7$ cannot be ruled out and may be responsible for the density discrepancy with cadmium fluoantimonate. If all the antimony is assumed to be pentavalent, and the other atoms are assigned their

Table V. Comparison of partial charges on atoms in fluorides and fluoantimonates of calcium or cadmium

Compound	Partial Charge Ca or Cd	F
CaF_2	+0.94	−0.47
$Ca_{1.56}Sb_7O_{6.37}F_{0.44}$	+1.11	−0.38
CdF_2	+0.54	−0.27
$Cd_{2.0}Sb_2O_{6.9}F_{0.1}$	+0.49	−0.30

usual charges, the charges balance to within −0.06 unit in $Ca_{1.56}Sb_2O_{6.37}F_{0.44}$, and to within +0.1 unit in $Cd_{2.0}Sb_2O_{6.9}F_{0.1}$. Thus, it appears that an earlier formulation showing both trivalent and pentavalent antimony in calcium fluoromeite (7) is unnecessarily complicated and does not allow for cation and anion defects. The present structure determination shows that the cation and anion defects in the stoichiometry arise naturally from the peculiarities of the pyrochlore structure and the location of Ca and F ions therein. The general formula for the fluoantimonates studied in this work may be written as $M^{II}_{1+a+b/2}Sb_2O_6(O'_a+F_b)$.

Structure.—The structure found for calcium fluoantimonate agrees well with that found by Zedlitz (5) for the mineral romeite, and may be placed in the general class with pyrochlore. The Ca and F ions occupy holes in an infinite network of SbO_6 octahedra in face-centered cubic symmetry. Cadmium and manganese appear to form analogous fluoantimonates, as would be predicted by the geometric criteria established by Isupov (16) and Aleshin and Roy (17). These criteria and our experimental results indicate that Mn^{2+} is just barely a large enough cation to form a pyrochlore antimonate, and hence it is more difficult to prepare cubic manganese fluoantimonate free of other antimonates, especially $MnSb_2O_6$. While it is well known that fluorine can replace oxygen up to whole atom amounts in pyrochlores (5, 17, 18), it has not been previously reported that quantities of fluoride as low as 0.2% F can be sufficient to stabilize the pyrochlore structure for calcium and cadmium antimonates, which otherwise would have the weberite structure (6). Among the best discussions of the effect of variable oxygen content in pyrochlores is the one by Pyatenko (19).

Importance in calcium halophosphate phosphors.—It was reported in 1950 (7) that at 875°C, during the synthesis of antimony-activated calcium halophosphate phosphors from the usual raw materials, practically all of the original antimony is converted into the cubic calcium fluoantimonate (romeite) before diffusing into the halophosphate lattice. Later work (20) showed that from 875° to 1140°C nearly all the insoluble (pentavalent) antimony was present as the metaantimonate, $CaSb_2O_6$, and not as fluoromeite, but no results at temperatures below 875°C were given. It has recently been found that a small amount of Cd, in partial substitution for Ca, produces brighter halophosphate phosphors under ultraviolet excitation (9). Absorption of 2537Å is increased with about 6 at. % Cd substituted for Ca. Because there is an optimum amount of cadmium substitution in halophosphates, there must be an important interaction with the host lattice, or the activator ions. The nature of the interaction is still unresolved. A large effect on the lattice parameters would not be expected with incorporation of 6 at. % Cd because of the similarity of the ionic radii of Cd^{2+} and Ca^{2+}. The improvement may be due to the formation of $Cd^+ - Mn^{2+}$ pairs, and the resultant resonance exchange, as postulated by Ropp (21) in his study of Mn-activated cadmium pyrophosphate and cadmium chlorophosphate (22) phosphors. In qualitative agreement, we have found that calcium or strontium halophosphates without Mn present are not improved by cadmium. Apple (23) recently reported that Cd substitution in Ca halophosphate reduces color-center formation due to short-wave ultraviolet radiation, and leads to improved maintenance of brightness in Sb-and Mn-activated phosphors exposed to 1850Å radiation. However, Apple's observations do not explain why Mn is also required to obtain improved lamp performance at 0 or 100 hr. Another possibility lies in the phosphor synthesis since the fluoantimonate of cadmium forms at lower temperatures (around 480°C) than that of calcium (around 800°C). During halophosphate synthesis, the pentavalent antimony may be combined with cadmium in preference to calcium. This could reduce the amount of $CaSb_2O_6$ formed and alter the mechanism by which antimony diffuses into the halophosphate lattice. Antimonates of cadmium should be more easily incorporated than antimonates of calcium because of higher vapor pressures and greater possibility of vapor-phase reaction with the matrix at halophosphate firing temperatures. For example, in a furnace used to prepare cadmium-modified calcium halophosphate phosphors, we have found large quantities of cubic cadmium fluoantimonate deposited on the walls of the furnace. A study of the phosphor synthesis indicated that cadmium and antimony were volatilized during phosphor formation, at least in part, as the insoluble pyrochlore fluoantimonate, $Cd_2Sb_2O_7(F)$.

Acknowledgment

The authors wish to thank G. L. Meisenhelter, H. D. Wilcox, and J. E. Mathers who performed the chemical analyses.

Manuscript received March 4, 1963. This paper was presented at the Pittsburgh Meeting, April 15-18, 1963.

Any discussion of this paper will appear in a Discussion Section to be published in the June 1964 JOURNAL.

REFERENCES

1. W. R. Cook, Jr., and H. Jaffe, *Phys. Rev.*, **88**, 1426 (1952).
2. F. Jona, G. Shirane, and R. Pepinsky, *ibid.*, **98**, 903 (1955).
3. F. Gaume, R. Bernard, P. DuPont, and J. Janin, *Compt. rend*, **252**, 544-546 (1961).
4. N. Chevalier, F. Gaume-Mahn, J. Janin, and J. Oviol, *ibid.*, **255**, 1096 (1962).
5. O. Zedlitz, *Z. Krist.*, **81**, 253 (1932).
6. A. Byström, *Arkiv Kemi, Mineral. Geol.*, **18A**, 1 (1944).
7. K. H. Butler, M. J. Bergin, and V. M. B. Hannaford, *This Journal*, **97**, 117 (1950).
8. A. Magnéli, *Arkiv Kemi, Mineral. Geol.*, **15B**, 1 (1941).
9. M. A. Aia and S. M. Poss, U. S. Patent 2,965,786 (1960).
10. C. W. W. Hoffman, R. C. Ropp, and R. W. Mooney, *J. Am. Chem. Soc.*, **81**, 3830 (1959).
11. W. F. Hillebrand, G. E. F. Lundell, "Applied Inorganic Analysis," 2nd Ed., pp. 280 and 742, John Wiley and Sons, Inc., New York (1953).
12. N. F. M. Henry and K. Lonsdale, Editors, "International Tables for X-Ray Crystallography, Vol. I. Symmetry Groups," p. 340, The Kynoch Press, Birmingham, England (1952).

13. R. W. James and G. W. Brindley, *Z. Krist.*, **78**, 470 (1931).
14. D. P. Shoemaker, J. Donohue, V. Schomaker, and R. B. Corey, *J. Am. Chem. Soc.*, **72**, 2328 (1950).
15. R. T. Sanderson, "Chemical Periodicity," pp. 38-44, Reinhold Publishing Corp., New York (1960).
16. V. A. Isupov, *Kristallografiya*, **3**, 96 (1958).
17. E. Aleshin and R. Roy, *J. Am. Ceram. Soc.*, **45**, 18 (1962).
18. R. Mazelsky and R. Ward, *J. Inorg. Nucl. Chem.*, **20**, 39 (1961).
19. Yu. A. Pyatenko, *Kristallografiya*, **4**, 204 (1959).
20. W. L. Wanmaker, A. H. Hoekstra, and M. G. A. Tak, *Philips Research Repts.*, **10**, 11-38 (1955).
21. R. C. Ropp, *This Journal*, **109**, 569 (1962).
22. R. C. Ropp, *ibid.*, **110**, 113 (1963).
23. E. F. Apple, *ibid.*, **110**, 374 (1963).

Behavior of Germanium Electrodes in a Ziegler Electrolyte

R. J. Flannery,[1] J. E. Thomas, Jr.,[2] and Dan Trivich

Department of Chemistry, Wayne State University, Detroit, Michigan

ABSTRACT

The behavior of n- and p-type germanium electrodes, particularly under anodic condition, was studied in a Ziegler electrolyte composed of triethyl aluminum and sodium fluoride in a 2 to 1 mole ratio. Germanium did not dissolve anodically but rather the anode products consisted of principally ethane and ethylene together with some butane and an immiscible liquid. Limiting currents were observed for n-type germanium and silicon but not for the p-type materials. This result, together with the observation that the anodic saturation current increased directly with increase in light intensity on n-type electrodes, indicates that the anode reaction consumes holes. The cathode product, metallic aluminum, formed a rectifying junction on n-Ge or p-Si.

In recent years, studies have been made of the electrochemical behavior of germanium electrodes in relation to their semiconducting properties. Several reviews of this work have appeared (1-3). It has been established for semiconductor electrodes that, in addition to the various current limiting processes which can occur in the electrolyte phase, current-limiting processes can also occur within the electrode and that these can be studied under suitable experimental conditions.

Brattain and Garrett (4) and Turner (5) studied the anodic dissolution of germanium electrodes in aqueous potassium hydroxide solutions. They found that current limitation from within the electrode occurs for n-type germanium but not for p-type germanium. They concluded that holes are consumed in the rate-determining step of the electrochemical process and that the current is controlled by the rate of generation of carriers in the germanium when the supply of holes at the surface becomes depleted by the electrochemical reaction. They demonstrated that when the rate of generation of carriers was increased by illuminating the electrode, the limiting current increased in a predictable manner.

Thus in an anodic process which shows such a preference for reaction with holes, the chemical oxidation occurring on the surface of the electrode involves a transfer of electrons to the valence band of the semiconductor. In an n-type semiconductor, in which holes are the minority carrier, this results in depletion of holes from the surface region of the semiconductor. Application of larger anodic bias does not result in an increase in the concentration of holes at the surface but rather widens the space charge region extending inward from the surface. The anodic process then becomes limited by the rate at which holes are generated by thermal means, light, etc., in the space charge region and in the bulk of the semiconductor within a diffusion length of the edge of the space charge region. Thus all of the holes that diffuse into the space charge region are caught by the field and are driven to the surface.

Gerischer and Beck (6) showed, for many redox couples in aqueous solution at germanium electrodes, that oxidation preferentially occurs by transfer of electrons to the valence band and usually reduction preferentially consumes electrons from the conduction band. Current limitation from within the electrodes occurs for oxidation on n-type germanium or for reduction on p-type germanium.

In the experiments reported in this article it was intended to discern whether the anodic electrochemical process in the chosen nonaqueous electrolyte would be controlled by transfer of electrons to the conduction band or to the valence band as in the aqueous systems. The electrolyte used for these studies is free of oxygen and water, and it is possible that surface oxide films normally present on germanium are removed by electrolytic treatment in this electrolyte. If the preferences for transfer of electrons to the valence or conduction band exhibited by germanium electrodes in aqueous solutions are influenced by the existence of a surface oxide film, the behavior of the electrodes in this medium might be noticeably different from the aqueous case.

The electrolyte used was first reported by Ziegler and Lehmkuhl (7). These workers discovered that two moles of triethyl aluminum react with one mole of sodium fluoride to form a complex,

[1] Present address: Research and Development Department, American Oil Company, P. O. Box 431, Whiting, Indiana.

[2] Present address: IBM Components Division, P. O. Box 110, Poughkeepsie, New York.

$Na(AlEt_3)_2F$, having a high electrolytic conductivity. The complex is liquid at room temperature because it supercools readily. Its melting point is 35°C. It is a clear liquid, slightly more viscous than water. The specific conductivity (8, cf. 7) is 2×10^{-2} $(ohm\text{-}cm)^{-1}$, which is about the same as that of a 5% aqueous solution of sodium sulfate. The electrolyte complex has a high affinity for oxygen. Ethers are stable in its presence but alcohols, water, and oxygen gas react violently with it. For this reason experiments must be conducted in an environment free of active oxygen.

Electrolytic decomposition of the electrolyte produces very pure aluminum at the cathode and products characteristic of ethyl radicals as intermediate products at the anode. This is illustrated by the fact that lead anodes dissolve to produce tetraethyl lead (9). According to Ziegler (9) germanium alkyls can be prepared by anodic dissolution of germanium in this electrolyte. Our results showed that, in contrast to the behavior of lead, and contrary to the reported work of Ziegler, germanium does not dissolve anodically to produce tetraethyl germane, but is inert. The germanium used by Ziegler was probably not single crystal material. Based on the work of Ziegler it was expected that the germanium would etch to produce a truly oxide-free surface. It was found in this study that the germanium electrodes had to be conditioned by alternate heavy anodic and cathodic polarization before reproducible results could be obtained. This result suggests that reduction of the surface oxide occurred at least in part and was perhaps necessary for proper response of the electrodes.

Experimental Details

Electrolyte.—The electrolyte was prepared in an all-glass apparatus under an inert atmosphere of purified nitrogen. The inert atmosphere was required because of the spontaneous flammability in air of both triethyl aluminum and the electrolyte complex. The triethyl aluminum was freed of hydrides by overnight treatment with metallic sodium. The electrolyte was prepared by reacting anhydrous sodium fluoride with an excess of the purified triethyl aluminum at about 80°C. Minor impurities other than hydride in the triethyl aluminum remain in the unused portion. The electrolyte complex is immiscible with triethyl aluminum and more dense. It separates readily to form a layer beneath the unused triethyl aluminum. The spontaneously flammable liquids were moved about through the purification, preparation, storage, and electrolysis system by means of siphons operated by a positive pressure of nitrogen.

Electrodes.—The germanium and silicon electrodes were of single crystal material. They were cut roughly to shape with a diamond saw, polished to size with alundum powders, and etched smooth with CP4 etchant. They were again briefly etched in CP4 just before use. The electrodes were 1 cm wide by 1.5-2.5 cm long with thicknesses up to 2 mm. A collection of other metal electrodes was made for a survey of their properties in this electrolyte. These metal electrodes were cut or cast from the purest materials at hand.

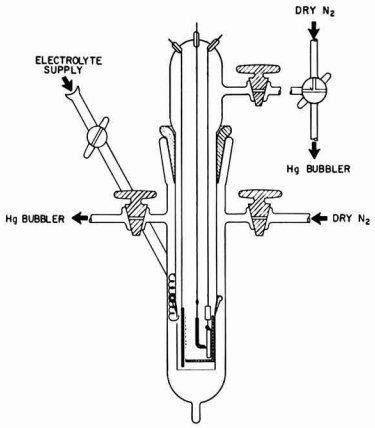

Fig. 1. Electrolysis cell. Flow of N_2 prevents ignition of the electrolyte when the electrodes are removed.

Electrolysis Cell.—A diagram of the cell used for the electrolysis studies is shown in Fig. 1. The cell, made of Pyrex glass, consisted of two parts, an electrolysis vessel containing the electrolyte and an insert carrying the electrodes. The electrolyte was introduced through a tube at the bottom of the vessel.

A N_2 gas-lock was used to prevent access of air to the electrolyte when adjustments or exchanges of electrodes were made. The gas-lock was operated by allowing the nitrogen to flow into the vessel and into the insert simultaneously. When the cell was opened, nitrogen flowed out of the top of the vessel, protecting the electrolyte from the air while, at the same time, nitrogen flowed out of the insert tip, keeping air away from the wet electrodes.

Two different electrode-bearing inserts were used. One insert was used for electrical measurements. The tip of this insert is shown in Fig. 2. The germanium electrodes were shaped to fit exactly at the back wall of a rectangular glass box, which thus served as an anode shield. The box consisted of a Beckman DU spectrophotometer cell (Pyrex), with one window cut off and the frosted sides

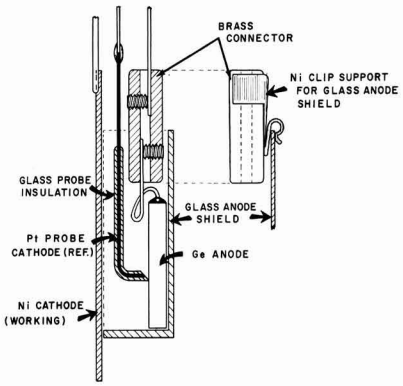

Fig. 2. Details of electrode assembly for germanium anode studies

polished clear. An aluminum-plated nickel counter-electrode was positioned so as to cover the open wall of the cell. A platinum probe electrode, glass coated except at the tip for insulation from the electrolyte, and bevel tipped for constant spacing from the working electrode, was used as a reference electrode for the germanium anode studies. The exploratory studies of other metal electrodes were made without reference electrode or anode shielding.

The other insert was used for collection of products. It contained the germanium electrode under the flared end of a narrow tube. The counter electrode was positioned along the inner surface of the vessel, well away from the flared tube. The opening of the flared tube extended beneath the surface of the electrolyte so that it confined gaseous and floating-liquid products. These were pulled up into the narrow tube and withdrawn from the cell for sampling.

Electrical measurements.—The current for the d-c measurements was supplied from a 22½v dry cell or from a small rectifier in series with a Simpson Model 260 VOM as ammeter and several small potentiometers. Voltage measurements were made with a Heathkit Model V6 vacuum tube voltmeter.

The a-c current-voltage curves were traced on a DuMont Type 250 oscillograph. The current was supplied by a Hewlett-Packard Model 202A low-frequency function generator in series with a 30 ohm resistance. The current signal was taken as a voltage drop across the 30 ohm resistance and was applied to the vertical d-c amplifier. The voltage of the electrode with respect to the platinum reference electrode was applied to the horizontal a-c amplifier. The d-c bias was supplied by a 67½v dry cell in series with 0.3 megohms across the cell.

Illumination of germanium electrodes.—Known multiples of an arbitrary value of light intensity were obtained by means of a small microscope illuminator lamp mounted on a meter-stick track in a horizontal line 45° from the normal to the center of the germanium electrodes. The light thus passed through the walls of the cell and the anode shield and through the electrolyte onto the front face of the electrode. Fixed stops were used to provide 2, 3, 4, and 8 times an arbitrary value of light intensity. A large infrared heat-lamp was used for intense illumination.

Results and Discussion

Results were obtained for: (I) exploratory studies of various metals, (II) detailed studies of germanium and silicon electrodes, and (III) chemical studies of products.

Exploratory studies of metal electrodes.—The current-voltage curves for electrolysis of the Ziegler electrolyte on various metal electrodes are shown in Fig. 3. The d-c anodic behavior of these electrodes was found to be of four characteristic types. Anodic dissolution as the only process was found for Pb, Cd, Bi, Sn, and Sb over the range of current densities studied. Pt, Ni, p-Ge, and p-Si were not etched and the only process observed to occur was the decomposition of the electrolyte. Zn, Al, Ag, and Cu were etched at low current densities but reached

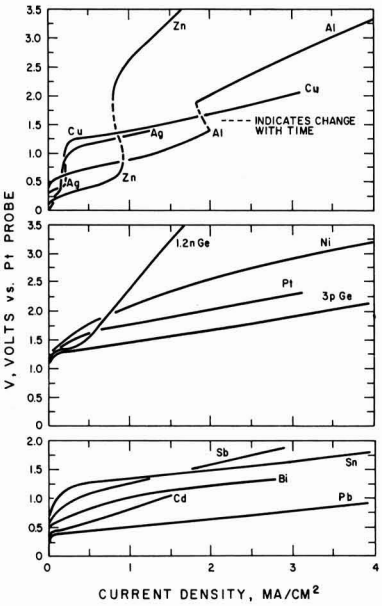

Fig. 3. Current voltage curves showing the anodic behavior of metals in the $Na(AlEt_3)_2F$ electrolyte. Lower block, metal electrode dissolves; middle block, electrolyte decomposes; upper block, metal dissolves at low current density, electrolyte also decomposes at higher current density.

initial limiting current densities at various values less than 2 ma/cm². At the limiting C.D. there was in each case a rapid shift in potential to values near 1.2-1.5v and the generation of gaseous and liquid products commenced. These initial limiting currents apparently correspond to rate controlling processes in the electrolyte or at the electrode surface. The n-Ge and n-Si electrodes also showed limiting current effects. The limiting current occurred at potentials at and above those at which the electrolyte decomposition was known to occur from the other results, including those for p-type Ge and Si. In this case the current-limiting process occurred not in the solution but within the electrodes as discussed below.

Detailed studies of germanium and silicon electrodes.—The preliminary studies of germanium anodes showed a current-limiting process at small current densities for n-type but not for p-type material. Further d-c studies were made with five different germanium electrodes using the anode shield and the insulated platinum probe electrode (cf. Fig. 2). The following germanium electrodes were studied: 0.1, 1, and 10 ohm-cm n-type and 2.5 and 10 ohm-cm p-type. Results are shown in Fig. 4. Current saturation occurs for n- but not for p-type electrodes. The saturation current is smaller for 1 ohm-cm n-type than for 10 ohm-cm n-type. These results indicate that holes are involved in the electrode process and that the limiting current effect exhibited by the n-type electrodes corresponds to diffusion control of the electrode process dependent on the supply of holes within the n-Ge rather than on ions within the solution.

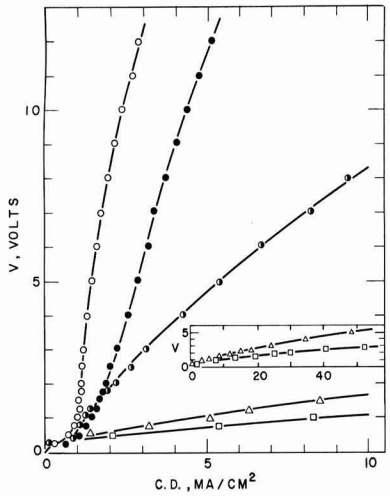

Fig. 4. Current-voltage curves for five different germanium anodes in the $Na(AlEt_3)_2F$ electrolyte. Open circle, 1 ohm-cm n-type; solid circle, 10 ohm-cm n-type; half open circle, 0.1 ohm-cm n-type; triangle, 10 ohm-cm p-type; and open square, 2.5 ohm-cm p-type. The current saturates for the n-type electrodes.

The 0.1 ohm-cm n-type germanium electrode might have been expected to give lower anodic currents than the 1.0 and 10 ohm-cm electrodes, and at low voltage there appeared to be a tendency in that direction, as Fig. 4 shows. However, over most of the voltage range, the currents were highest for the 0.1 ohm-cm sample. This presumably implies that the electric field just inside the semiconductor surface was high enough, in that case, to cause an increase in the supply of holes through some process of impact ionization.

The relatively small shifts in potential with current on the p-type electrodes apparently are due to activation polarization arising from some slow steps in the chemical and electrochemical processes on the surface of the electrode.

The effect of light was investigated to further test whether the current-limiting process on the germanium anodes involved the rate of supply of holes to the electrode surface. Figure 5 shows typical results for the effect of light of various intensities on the d-c anodic behavior of 10 ohm-cm n-type germanium. Similar results were obtained for the 1 and 0.1 ohm-cm electrodes. Light was applied as multiples of an arbitrary amount by moving the light source closer to the electrode through a series of fixed distances from the electrode surface. The saturation current density increased directly with the light intensity. The current density is limited to about 1 ma/cm² in the dark but reaches 50 ma/cm² in intense light. This kind of behavior is characteristic of the generation of holes by light for a hole-limited process. Typical results at 5v and 1v for 10, 1, and 0.1 ohm-cm n-type electrodes for the various light intensities are given in Table I. Additional evidence of the dependence of the anodic rate on the supply of holes to the germanium surface was obtained by means of a-c measurements. Current-voltage oscillograms resulting from application of 1000 cps a-c square-wave voltages, with and without d-c bias showed light-dependent current saturation effects with germanium and silicon electrodes. Without d-c bias and with small anodic bias the results were qualitatively similar to the d-c results.

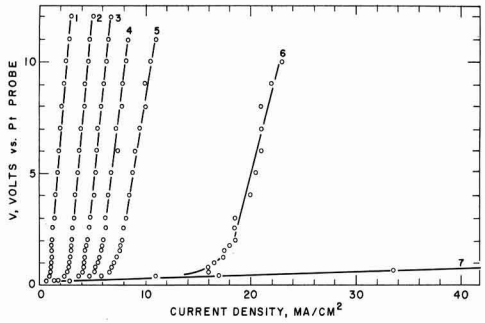

Fig. 5. Current-voltage curves showing the effect of light on the behavior of a 10 ohm-cm n-type germanium anode in the $Na(AlEt_3)_2F$ electrolyte. Curve 1 is the dark curve; curves 2, 3, 4, 5, and 6 result from illumination of the electrode with 1, 2, 3, 4, and 8 times, respectively, an arbitrary value of light intensity; curve 7 results from intense illumination with a heat lamp.

A cathodic bias puts an aluminum film of variable thickness on the electrodes. The effectiveness of light in increasing the saturation current in n-type germanium electrodes was found to decrease as the aluminum film thickness increased. Very thick aluminum films eliminated the light effect as expected. Apparently the aluminum coating formed the familiar metal-to-n-type-germanium rectifier, with the current limiting mechanism still being the supply of holes from the bulk of the semiconductor.

An interesting difference in the behavior of silicon was found. Under anodic bias or no bias, the behavior of silicon in the a-c experiments was similar to germanium. However, when a thin film of aluminum was present on silicon, saturation occurred for p-type but not for n-type material. This is the opposite of the behavior of the germanium electrodes with aluminum coatings. This indicates that aluminum plated onto p-type silicon in this

Table I. Saturation current density at 1v and 5v for various values of light intensity at 10, 1, and 0.1 ohm-cm n-type germanium anodes

Light intensity, multiples of an arbitrary value, L	C.D., ma/cm² at 1v *vs.* Pt probe		
	10 ohm-cm	1 ohm-cm	0.1 ohm-cm
Dark	1.10	0.90	1.20
1 L	2.85	2.45	2.85
2 L	4.20	3.90	4.05
3 L	5.55	5.50	5.25
4 L	7.05	6.80	6.15
8 L	16.5	12.0	12.6
	C.D., ma/cm² at 5v *vs.* Pt probe		
Dark	1.70	1.50	4.05
1 L	3.60	3.40	5.85
2 L	5.30	5.25	7.20
3 L	6.80	7.10	8.40
4 L	8.75	8.80	10.2
8 L	20.5	16.5	21.0

electrolyte forms a rectifying barrier. Rectification by aluminum broad area contacts on p-type silicon has also been reported by Wurst and Borneman (10).

Chemical products.—The products of the electrochemical decomposition of the electrolyte at nonetching electrodes were studied qualitatively. Cathodic treatment produced a coating of metallic aluminum. Anodic treatment at inert germanium electrodes produced gaseous and liquid products. The gaseous anode product was a mixture consisting of ethane, ethylene, and n-butane, as determined by a gas chromatographic method. A 5-ft silica-gel column was used for the separation of ethane and ethylene. A 30-ft tricresyl phosphate on firebrick column was used for butane analyses. Less ethylene than ethane was found. Simple disproportionation of ethyl radicals should produce equal amounts of ethane and ethylene. The smaller than expected yield of ethylene may have occurred because of reaction of some of the product ethylene with triethyl aluminum in the electrolyte to form butyl or longer substituents by Ziegler-type ethylene polymerization catalysis. The liquid product which separated as an immiscible floating layer, consisted mainly of alkyl aluminum compounds. The liquid is believed to be largely triethyl aluminum since the electrolyte was made up to be saturated with $AlEt_3$. The $AlEt_2F$ presumed to be formed may be soluble in the electrolyte. The hydrolysis gas from the liquid product contained ethane, ethylene, and n-butane, but no longer-chained constituents. Diethyl aluminum fluoride was apparently not a prominent constituent of the liquid product since only a small amount of fluoride relative to the aluminum content was found.

Summary and Conclusions

The results show that, for germanium anodes in the $Na(AlEt_3)_2F$ electrolyte, n-type germanium anodes exhibit current-limiting processes which are not obtained for the p-type electrodes. The magnitude of the limiting current is increased by light. This indicates that the mechanism of the anodic electrode process involves a reaction of the electrolyte species with holes from the semiconductor, that is, that the process involves transfer of electrons from some entity in the electrolyte to the valence band of the semiconductor. In the case of the n-type germanium anodes, the rate of supply of holes from the bulk of the semiconductor to the surface of the electrode becomes the rate-controlling step. Product analyses suggest that ethyl radicals are formed as intermediates in the anodic process. The cathodic process involves a reduction of some entity in the electrolyte to form metallic aluminum.

The following proposed mechanism is in conformity with the results obtained:

Anodic reaction:

$(AlEt_3)_2F^- + e^+ \rightarrow Et\cdot$ + aluminum alkyl fluoride compounds (I)

$$2\,Et\cdot \begin{cases} \rightarrow CH_3CH_3 + CH_2 = CH_2 \\ \rightarrow CH_3CH_2CH_2CH_3 \end{cases}$$

Cathodic reaction:

$(AlEt_3)_2F^- + 3e^- \rightarrow Al$ + aluminum alkyl fluoride compounds (II)

For (I), one could postulate the reaction products to be $AlEt_3 + AlEt_2F$. For (II), one could postulate that the reaction products are combined with $3AlEt_3$ to form $AlEt_3F^- + 3AlEt_4^-$. All of these postulated products are known and could exist in this system.

Acknowledgments

The aid of the Kettering Foundation in support of this work, in the form of a fellowship held by one of us (R.J.F.), is gratefully acknowledged. Thanks are due to the Ethyl Corporation which donated the triethyl aluminum used in the work and rendered much assistance in the form of procedures for the purification and handling of the compound. Thanks are also due to the Philco Corporation and to Texas Instruments Company for the donation of the semiconductor materials.

Manuscript received March 7, 1963; revised manuscript received May 6, 1963. This paper was presented at the Columbus Meeting, Oct. 18-22, 1959.

Any discussion of this paper will appear in a Discussion Section to be published in the June 1964 JOURNAL.

REFERENCES

1. J. F. Dewald, in "Semiconductors," N. B. Hannay, Editor, pp. 727-751, Reinhold Publishing Corp., New York (1959).
2. H. Gerischer, in "The Surface Chemistry of Metals and Semiconductors," H. C. Gatos, Editor, pp. 177-202, John Wiley and Sons, Inc., New York (1960).
3. D. R. Turner, in "The Electrochemistry of Semiconductors," P. J. Holmes, Editor, pp. 155-204 Academic Press, New York (1962).
4. W. H. Brattain and C. G. B. Garrett, *Bell System Tech. J.*, **34**, 129 (1955).
5. D. R. Turner, *This Journal*, **103**, 252 (1956).
6. H. Gerischer and F. Beck, *Z. Elektrochem.*, **63**, 943 (1959).
7. K. Ziegler and H. Lehmkuhl, *Z. anorg. allgem. Chem.*, **283**, 414 (1956).
8. G. E. Coates, "Organo-Metallic Compounds," 2nd Edition, p. 138, John Wiley and Sons, Inc., New York (1960).
9. K. Ziegler, Belgium Pat. 543,128, November 26, 1955.
10. E. C. Wurst, Jr., and E. H. Borneman, *J. Appl. Phys.*, **28**, 235 (1957).

Chemical Transport and Epitaxial Deposition of Gallium Arsenide

Frank A. Pizzarello

Semiconductor Division, Development Laboratory,
Hughes Aircraft Company, Newport Beach, California

ABSTRACT

A study of the nature of growth of gallium arsenide on substrates of various crystallographic orientations was conducted in a closed tube system. It is concluded that the dominant growth direction is in the (111) direction. Growth rate studies were conducted at various temperatures and pressures. It was found that the transport of matter is not dependent on a single mechanism, but rather on a combination of diffusion, convective and laminar flow, each contributing to greater or lesser extent depending on the conditions of growth.

The method of chemical mass transport has been used for many years as a method of preparing many materials in a pure state (1). Usually, the materials transported were polycrystalline masses deposited on substrates of no particular relationship to the transported solid. Recently (2, 3) the method of chemical mass transport was combined with the technique of epitaxy to devise the process generally referred to as epitaxial growth. In this method, material difficult to evaporate is transported by means of a chemical equilibrium reaction to a single-crystal substrate of the proper characteristics allowing the deposition of a single-crystal layer. With the advent of this method, a twofold problem arose. One, by what mechanisms is the reaction mass transported to the substrate? Two, what are the relationships of the growth on the substrate to the transport mechanism of material and to the nature of the substrate? In this paper, these questions are studied and some answers are submitted for examination.

Experimental

A schematic view of the apparatus used in these experiments is shown in Fig. 1. The furnace used was constructed with three separate heating elements, each individually controlled. It was found that heating elements arranged in this fashion yield the desired linear thermal gradients. A typical thermal distribution obtained and used for these experiments is shown in Fig. 1. This figure also shows a view of the reaction vessel used in these experiments. The reaction vessel was constructed of quartz tubing, 1.60 cm ID and 15 cm long. Since, as it will be shown later, the geometry of the reaction tube is critical, all dimensions during construction were maintained to a precision of 10%. Also, since temperature fluctuation may cause spurious results during epitaxial growth, temperature control was maintained to 2%.

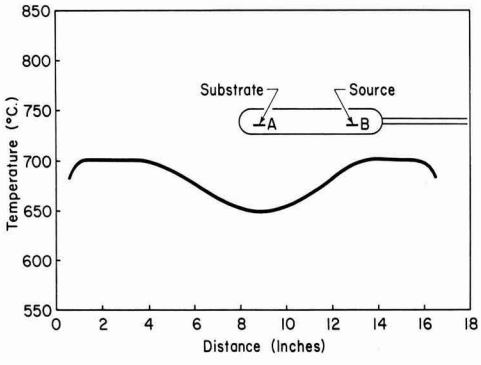

Fig. 1. View of the thermal gradient and the position of the reaction tube during growth.

To maintain optimum experimental control and obtain reproducible results, samples were prepared in the following manner: A wafer of GaAs (usually N-type 10^{17}/cc) was electropolished (4), weighed and placed in the substrate region of the reaction tube. After etching in 1-3-2 solution (1 part HF, 3 parts HNO_3, and 2 parts H_2O) a weighed quantity of polycrystalline GaAs is placed in the source position of the reaction tube. Twenty-five grams of high-purity iodine is placed in the reaction tube. This assembly is sealed on a vacuum system and pumped to 10^{-4} mm Hg. During evacuation the sample region of the reaction tube is kept at liquid N_2 temperature to avoid loss of iodine. After 30 min under vacuum, 20 cm of Hg of pure hydrogen is introduced to the system. The reaction tube is then sealed containing the hydrogen. The tube is placed in the furnace so as to locate the source and the substrate on opposite sides of the temperature dip. In this position, etching of the substrate surface occurs. This step is used to clean the substrate further, and proceed for 10 mins. At the end of this time, the tube is adjusted by means of the attached rod to a position in the thermal gradient where the substrate is located at the low-temperature region of the furnace. In this position growth occurs. The tube is maintained in this position for 24 hr. Using the procedure outlined above, an interface is obtained which has a minimum of structural defects. It was found during the course of experimentation that chemical etching or any mechanical treatment of the surface, such as polishing, leaves sufficient

damage on the surface to yield poor quality interface upon growth of an epitaxial layer.

Growth Habit of Epitaxial Layers

The substrates used in this study were oriented by the Laué back reflection method. Using this method, the orientation of the substrate and its angular relationship with other crystallographic direction was determined. Any growth structure occurring on these oriented surfaces could then be easily transposed to a standard stereographic projection where Miller indices could be assigned. The crystallographic orientation was determined with a precision of one degree.

The growth planes developed were measured by the use of a light figure apparatus with a precision of 1%. Epitaxial growth on substrates oriented in the (100), (110), (111)A, (111)B, (112), and (113) planes were studied. The epitaxial layers studied were grown in a 24-hr period and ranged in thickness from 0.020 to 0.030 in. Figures 2, 3, and 4, show the planes developed on the (100), (110), and (111)A planes, respectively. Note that the angular displacement of the growth figures from the basal plane is greatest for growth on the (100) plane, less for growth on the (110) plane, and least for the

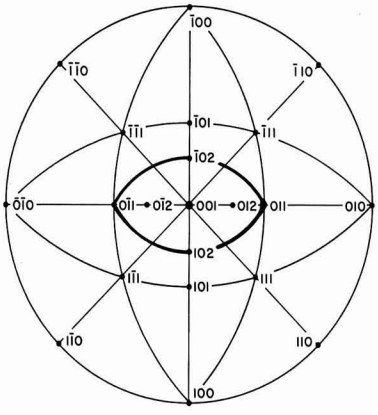

Fig. 2. Stereographic projection of growth occurring on the (001) plane. Series of planes developed during growth lie within region defined by heavy line.

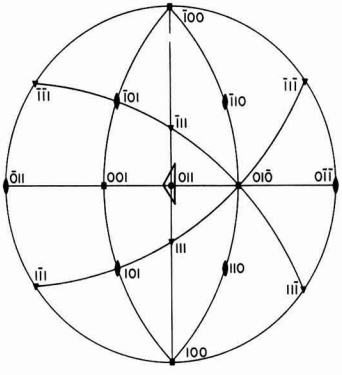

Fig. 3. Stereographic projection of growth occurring on the (011) plane. Series of planes developed during growth lie within region defined by heavy line.

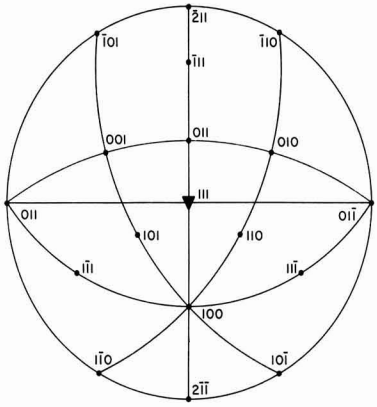

Fig. 4. Stereographic projection of growth occurring on the (111)A plane. Vicinal plane development with maximum angular deviation from the basal plane is 3°.

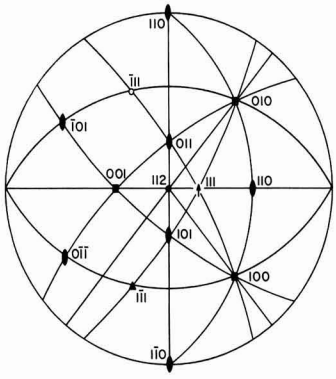

Fig. 5. Stereographic projection of (112) plane. Principal plane developed during growth is the (111)A plane.

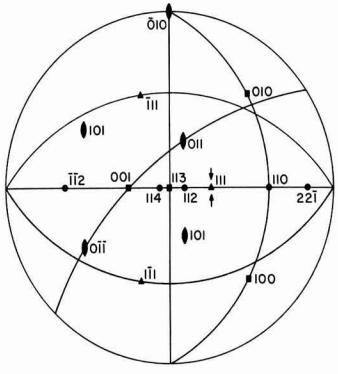

Fig. 6. Stereographic projection of the (113) plane. Principal plane developed during growth is the (111)A plane.

(111) plane. Figures 5 and 6 are stereographic projections of growth on the (112) and (113) planes, respectively. As is shown, only (111) planes are developed.

From the data presented it is seen that the crystallographic planes most readily developed are the (110) and (111) planes. These are planes of high reticular density [where the reticular density of

(100) < (110) < (111) planes]. It is further noted that the range of angular displacement of planes developed decreases with increasing reticular density until only vicinal planes are developed, as on the (111) plane. In the case of the (112) and (113) planes, these are planes of such low reticular density that uninhabited growth can readily occur in the [111] direction forming (111)A faces.

In the case of growth on the (111)A plane a maximum angular displacement of the growth planes is 3°. The vicinal plane developed noted on the (111)A plane is an unexpected result if growth on this plane is conceived to proceed as a sequence of layers forming one on another. It is tempting in view of this data to hypothesize that the vicinal planes developed during growth give rise to a surface containing many corners and edges such as is expounded in the theories of Kossel and Stranski (5) to lower the free energy of a particle on the surface and thus increase the rate of growth. Expanding on this view further, an atomistic model of growth can be developed. Consider a (111)A plane at the beginning of growth; the surface consists predominately of gallium atoms; to this surface an arsenic molecule can readily be absorbed from the gas phase. The arsenic molecule absorbed on this surface provides edges to which additional arsenic molecules may attach, thus forming on the Ga atom surface a small island of arsenic atom which expands in size. Simultaneously with this expansion, molecules of GaI are absorbed on the arsenic island forming a bond with arsenic atoms and liberating GaI_3 to the gas phase. The Ga thus adsorbed expands across the arsenic surface, simultaneously new arsenic molecules absorb on the new Ga surface, and the process repeats itself. With this kind of process occurring, it can readily be seen that in a short time a highly stepped surface will occur if many islands form on the same atomic plane simultaneously and proceed to add layers as described. This theory is verified to some extent by the fact that, when growth proceeds on crystallographic planes not oriented in the (111) direction, a wide angular displacement occurs with a tendency to grow to the (111) plane. An additional fact that also supports these ideas of growth mechanism is that little or no difference in the rate of growth over a 24-hr period seems to exist regardless of the crystallographic orientation used, indicating that growth proceeds in a [111] direction. However, this does not exclude the possibility that the growth rate initially may be drastically different for different crystallographic orientations. Figure 7 shows typical epitaxial growth on the (100), (111), and (113) oriented substrates.

Attempts to grow epitaxially on the $(\bar{1}\bar{1}\bar{1})$B plane resulted in every case in polycrystalline layers when iodine was used as the carrier. On the other hand, when chlorine was used the resultant layer was a single crystalline layer of high quality. An explanation for this effect is possible by noting that the $(\bar{1}\bar{1}\bar{1})$B plane is highly an electronegative (6) surface. Thus the gallium iodide molecule which has a large negative charge distribution on the iodine atom is readily repelled from the $(\bar{1}\bar{1}\bar{1})$B surface.

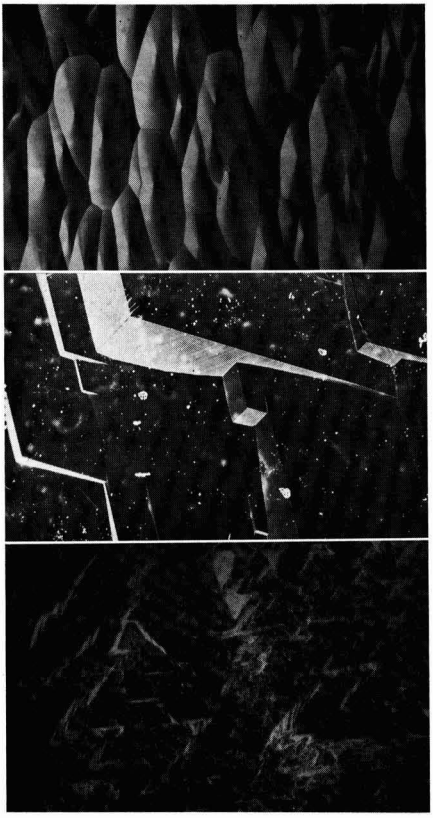

Fig. 7. Photographic views of epitaxial growth on a (top), (100); b (center), (111); and c (bottom), (113) planes. Magnification 45x.

On the other hand, a gallium chloride molecule has smaller negative charge distribution resulting in no significant repulsion from the surface.

Rate of Growth Experiments

To approach the problem of chemical mass transport even on a crude quantitative level the equilibrium reaction taking place and the associated values of free energy must be known. Work by Lyons and Silvestri (7) shows that the predominate equilibrium reaction occurring is

$$2GaI_3(g) + 4GaAs(s) = 6GaI(g) + As_4(g) \quad [1]$$

As the reaction is written the concentration in the gas phase of the products increases with increasing temperature. Consequently, under conditions of a thermal gradient the reaction products transported to the cooler region of the thermal gradient offset the equilibrium partial pressures sufficiently to support the deposition of GaAs. One can visualize this transport as a steady-state process where the GaAs is dissolved by GaI_3 at the higher temperatures to form a gas phase of a specific concentration of the reactants and products. The GaI and As_4 formed are transported through a concentration gradient established in the thermal gradient to the cooler temperature region. At the cooler temperature the

equilibrium concentrations are maintained by the deposition of GaAs and the liberation of GaI_3. The GaI_3 liberated flows back to the higher temperature region through the established concentration gradient and reacts with more GaAs to repeat the cycle. To relate this mechanism into mathematical terms the equilibrium constant

$$K = \frac{P^6_{GaI} P_{As4}}{P^2_{GaI3}}$$

where P_{GaI}, P_{As4}, and P_{GaI3} are the partial pressures of the gaseous constituent of the reaction as noted by the subscripts, must be known. Defining α as the fraction of the products formed (fraction of reaction) the following relations can be derived

$$P_{GaI} = 3\alpha n_{GaI3} \frac{RT}{V} \qquad [2]$$

$$P_{As4} = \frac{\alpha}{2} n_{GaI3} \frac{RT}{V} \qquad [3]$$

$$P_{GaI3} = (1-\alpha) n_{GaI3} \frac{RT}{V} \qquad [4]$$

where V is the volume of the system, n_{GaI3} the number of moles of GaI_3 initially introduced, and T is the absolute temperature. Using these expressions K can be expressed as

$$K = \frac{3^6}{2}\left[n_{GaI3} \frac{RT}{V} \right]^5 \frac{\alpha^7}{(1-\alpha)^2} \qquad [5]$$

Treating the reaction tube lying in the thermal gradient as consisting of three chambers V_1, V_2, and V_3, where V_1 is the volume in the high-temperature region T_1, V_2 is the volume in the low temperature region T_2, and V_3 the region in the thermal gradient, the following expressions for material transport can be used

$$n_{GaI} = D\,\alpha\,t \frac{dC_{GaI}}{dx} + aC_{GaI}\,v\,t \qquad [6]$$

$$n_{GaI3} = D\,\alpha\,t \frac{dC_{GaI3}}{dx} + aC_{GaI3}\,v\,t \qquad [7]$$

The terms in expressions [2] and [3] are defined as: D, diffusion coefficient for the gas, cm^2/sec mixture; a, cross-sectional area of the cm^2 reaction tube; t, time process is continued, sec; dC_{GaI3}/dx, concentration gradient of GaI_3; dC_{GaI}/dx, concentration gradient of GaI; v, mass flow velocity, cm/sec. Assuming $v=0$ in [2] and [3] noting that $3dC_{GaI}/dx = dC_{GaI3}/dx$ and $3n_{GaI} = n_{GaI3}$, the expression

$$n = Dat\, dC_{GaI}/dx \qquad [8]$$

is derived. Assuming a linear concentration gradient $(C_1-C_2)/L$ exists between the volumes V_1 and V_2 expression [8] is reduced to

$$n_{GaI} = \frac{Dat}{L}(C_1-C_2) \qquad [9]$$

where C_1 is the concentration of GaI at T_1, C_2 is the concentration of GaI at T_2, and L is the length of the concentration gradient. Using the expression for the concentration of GaI at T_I and T_2 as

$$\frac{\alpha_1 n_{GaI3}}{V_1}, \frac{\alpha_2 n_{GaI3}}{V_2}$$

respectively, and noting that $V_1 = V_2 = V_{1,2}$ the equation

$$n_{GaI} = \frac{Dat}{LV_{1,2}} n_{GaI3}\,(\alpha_1-\alpha_2) \qquad [10]$$

is obtained. Assuming all the GaI transported reacts to deposit GaAs the equation for the weight of deposition of GaAs in milligrams is given by

$$W = 96.42 \frac{Dat}{V_{1,2}L} n_{GaI3}\,(\alpha_1-\alpha_2) \times 10^3 \qquad [11]$$

Using the free energy data of Silvestri and Lyons (7), values of α were calculated at various temperatures. A plot of this data is given in Fig. 8. Since α is seen to increase with temperature it is predictable from Eq. [11] that the weight transported is temperature dependent and should increase with increasing temperature differences. To verify the degree of applicability of this expression and to obtain an estimate of the diffusion coefficient D, a

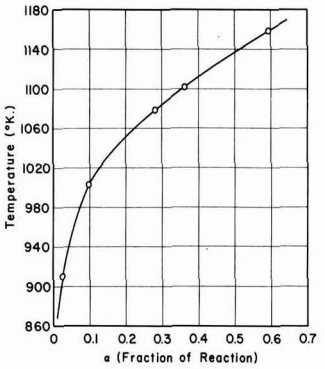

Fig. 8. Temperature of reaction mixture vs. α, the fraction of products GaI and As_4 formed.

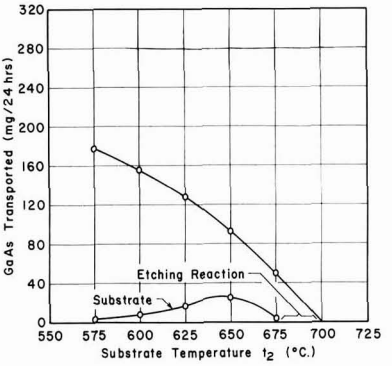

Fig. 9. Weight of GaAs transported in a 24-hr period vs. the temperature of the substrate chamber. The temperature of the source chamber is held fixed at 700°C. The substrate curve is weight gain of the substrate wafer in a 24-hr period. The source curve is the weight lost in a 24-hr period.

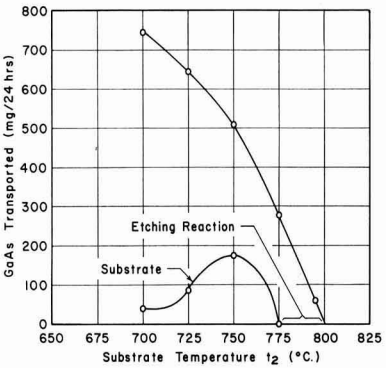

Fig. 10. Weight of GaAs transported in a 24-hr period vs. the temperature of the substrate chamber. The temperature of the source chamber held fixed at 800°C. The substrate curve is the weight gain of the substrate wafer in a 24-hr period. The source is the weight lost in a 24-hr period.

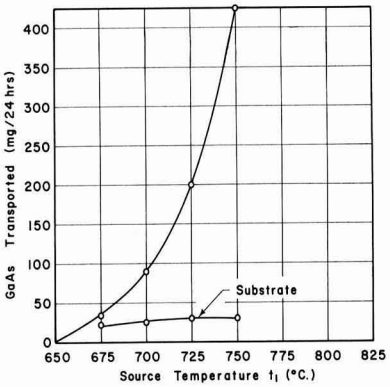

Fig. 11. Weight of GaAs transported in a 24-hr period when the substrate chamber temperature is held fixed at 650°C vs. source chamber temperature.

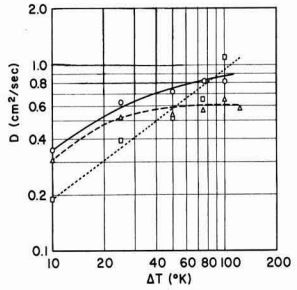

Fig. 12. Gaseous diffusion coefficient vs. the temperature difference between the source and substrate. -○-, source 1073°C, substrate varied; -△-, source 973°C, substrate varied; --□--, substrate 923°C, source varied; curve a, - - - -; curve b, ———; curve c, ...

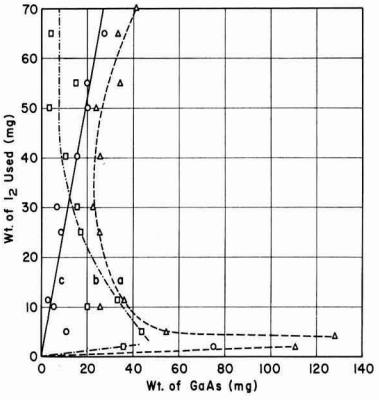

Fig. 13. Rate of growth with source temperature held at 700°C and substrate temperature held at 650°C, while the weight of I_2 used as a transporting media is varied. Curve a is the actual weight loss of the source in a 24-hr period; curve b is the substrate weight gain in a 24-hr period; curve c is the equivalent weight of GaAs in the gas phase.

series of experiments were performed in which in case 1, the source temperature was held fixed at 800°C and the substrate temperature was varied; in case 2, the source temperature was held fixed at 650°C and the source temperature was varied; and in case 3, the substrate temperature was held fixed at 650°C and the source temperature was varied.

The results of these experiments are given in Fig. 9, 10, and 11. Using Eq. [11], D is calculated for a number of points along each curve. In the calculation of D the numerical values $n_{GaI_3} = 1.30 \times 10^{-5}$ moles, $a = 2.01$ cm², $t = 8.65 \times 10^4$ sec, $V_{1,2} = 10.05$ cc, and $L = 5$ cm were used. The results of these calculations are given in Fig. 12 where ΔT, the difference in temperature between the source and the substrate, is plotted against the diffusion coefficient. It is seen in curves a and b that the diffusion coefficient quickly rises to a steady value. Since in these experiments the source is held fixed at 973° and 1073°K, respectively, and the substrate is varied downward to lower temperatures, the average temperature $(T_1 + T_2/2)$ is decreasing, whereas the diffusion coefficient is increasing. This is an anomolous behavior and cannot be explained on the basis of simple gaseous diffusion. An important fact demonstrated by these curves, however, is that the source temperature has a predominate effect on the diffusion coefficient, and the effective temperature in the system is not simply the average temperature. Curve c shows where the substrate temperature is fixed at 923°K, and the source temperature is varied upward. The result in this case is consistent qualitatively with the kinetics theory of gaseous diffusion (8). This theory predicts $D \propto T^n/P$ where n lies in the range of 1 to 2. A value of $n = 20$ was computed from the data of curve c Fig. 12. This value of n precludes the mechanism based on simple gaseous diffusion and indicates the transport process to have perhaps a strong convective flow component (9).

Since the diffusion coefficient is not only temperature dependent, but also pressure dependent, experiments were performed where the total reactant pressure was changed by varying the amount of iodine used initially at a fixed source, substrate temperature difference. Results of these experiments are given in Fig. 13. Curve a of Fig. 13 is the total mass loss of the source material. Curve b is the actual weight gain of GaAs on substrate. Curve c

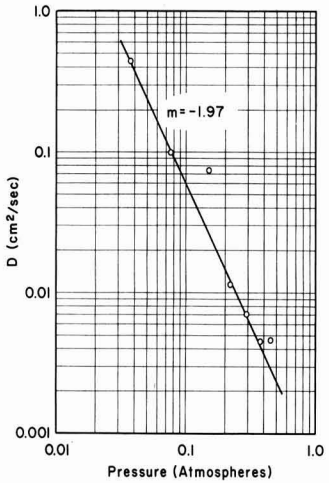

Fig. 14. Gaseous diffusion coefficient *vs.* the average total pressure of the system.

is the quantity of GaAs dissolved in the gas phase determined by assuming the chemical reaction

$$4GaAs(s) = 6I_2(g) = 4GaI_3(g) + As_4(g)$$

is complete and the chemical reaction

$$2GaI_3(g) + 4GaAs(s) = 6GaI(g) + As_4(g)$$

is 0.04% complete. The circular data points shown are obtained by subtracting the weight loss of the source from the weight gain of the substrate. Since these points lie very close to the theoretical curve c, an independent check of the accuracy of α is obtained. These data also show that very small losses of I_2 are encountered by the loading procedure used. At higher iodine weights it was observed that all material transported deposited on the substrate. At low iodine weights, deposition also occurred on the walls adjacent to the substrate. Using Eq. [11], D was calculated at various values of iodine weight used. A plot of D *vs.* total gas pressure is given in Fig. 14. The total gas pressure was calculated by using the equation $P = 2/3\ (1+\alpha_n)\ \frac{Wt_{I_2}}{253.8}\ \frac{RT_{av}}{V}$.

In comparing the slope of the curve 1.9 of Fig. 14 with the expression $D \propto P^{-1}$ a difference is observed which indicates a departure of the transport process from a pure diffusion mechanism.

Substrate Growth

Returning to Fig. 10 and 11, the substrate weight gain is given under the experimental conditions of case I and case II. At small temperature differences an actual weight loss of the substrate occurs (region designated as etching reaction). The etching reaction operating under these circumstances is that given by Eq. [1]. The principal cause for this effect is a combination of slow diffusion of reactant, gases, and small local temperature gradients which act as sites of deposition of GaAs. At larger temperature differences between source and substrate an increase in the quantity depositing takes place until a maximum is obtained. The growth rate on this part of the curve is limited by the competition of the etching reaction rate and mass transport rate. The decreasing rate of deposition at very large temperature differences is attributed to the change in the rate of chemical deposition with temperature. Thus, this part of the growth rate curve is chemical deposition rate limited. To support this view the substrate curve of Fig. 12 is given. Under conditions of growth case III, the substrate temperature is held fixed; consequently, no change in the chemical deposition rate is expected. It is seen under these conditions of growth that the curve moves rapidly from the transport limited process to a saturation value limited by the chemical deposition rate. All the rate studies were performed with wafers of constant area (0.5 cm^2). However, in view of the quantity of GaAs depositing on the walls adjacent to the wafer, it is believed that the wafer area would have little or no effect on the quantity of mass transported.

Conclusion

Through the bulk of this paper an idealized model was applied to the problem of mass transport in a closed tube system. The dependence of the diffusion coefficient on temperature and pressure was given. It was found in both cases that no single mechanism of transport is attributable to results obtained. However, of interest is the marked effect high temperature and an optimum average pressure has on the transport process.

Up to this point very little has been said about the effects of geometry and thermal gradients on the mass transport rate. Preliminary experiments have shown that tubes of larger cross-sectional area and shorter length yield a greater mass transport rate, a result which is at least in qualitative agreement with theory. During the course of experimentation, thermal gradients with a significant radial nonuniformity were formed. As expected, the growth rate was altered drastically, and in some cases GaAs was removed from the substrate and deposited on the cooler walls. Thus it was found to assure uniformally reproducible results in growth rate, great care must be exercised in controlling the uniformity of the thermal gradient used.

Acknowledgments

The author wishes to thank Dr. George Dorosheski for his assistance in the mathematical computations needed, and Mr. Joseph Vuoto and Mr. Alan VanCouvering for the experimental work performed.

Manuscript received Nov. 26, 1962; revised manuscript received May 27, 1963. This paper was presented before the Los Angeles Meeting, May 6-10, 1962.

Any discussion of this paper will appear in a Discussion Section to be published in the June 1964 JOURNAL.

REFERENCES

1. R. I. Rolsten, "Iodide Metals and Metal Iodides," John Wiley & Son, Inc., New York (1961).
2. E. S. Wajda, B. W. Kippenhan, and W. H. White, *I.B.M. Journal*, **4**, 288 (1960).
3. J. C. Marimace, *ibid.*, **4**, 280 (1960).
4. J. G. Harper and M. S. Astor, Enlarged Abstracts,

Electronics Div., Electrochemical Society Philadelphia Meeting, May 1959.
5. H. E. Buckley, "Crystal Growth," John Wiley & Son, Inc., New York (1951).
6. H. C. Gatos and M. C. Lavine, *This Journal*, **107**, 427 (1960).
7. O. J. Lyons and V. J. Silvestri, *ibid.*, **109**, 963 (1962).
8. W. Jost, "Diffusion In Solids, Liquids, Gases," chap. X, p. 425, Academic Press, New York, (1960).
9. R. Nitsche, H. U. Bösterli, and M. Lichtensteiger, *J. Phys. Chem. Solids*, **21** [3/4], 199 (1961).

A Kinetic Theory for Autodoping for Vapor Phase Epitaxial Growth of Germanium

J. J. Grossman[1]

Hughes Research Laboratories, Malibu, California

ABSTRACT

A kinetic theory has been derived for the origin of autodoping in epitaxial vapor grown films based on the transient behavior of a general reaction mechanism. This mechanism is the series combination of an etching and growth reaction. A particular case is solved explicitly in closed form, and the behavior of more general cases is indicated.

Autodoping in epitaxial vapor grown germanium (1) and silicon (2) films was first reported at the October 1961 meeting of the Electrochemical Society by Matovich and Andres (1) and by Kahng, Manz, Atalla, and Thomas (2). The significant experimental observation is that impurities initially present in the substrate redistribute in the growing layer as growth proceeds. They redistribute at an ever decreasing concentration, while the externally added impurity builds up and finally takes control of the grown film doping. Two theoretical approaches are possible for examining autodoping (1, 2).

First, one can be purely phenomenological as were Kahng *et al.* (2, 3) and postulate a countercurrent or distillation type enrichment without regard for the detailed microscopic mechanism. In this theory one postulates three processes, etching, mixing, and growth, which occur repetitiously in that order.

On the other hand, one may derive kinetically an explicit time dependence for the reaction rate and thereby show details of the origin of the redistributed substrate impurity.[2] The observed logarithmic redistribution in the regrowth is then easily found in differential form since the adsorbed, liberated surface impurity C reincorporates into the substrate film in proportion to the growth rate R, the distribution coefficient between the solid and adsorbed phase k, and a loss factor due to impurity diffusion away from the surface A. The net change in adsorbed surface impurity per unit time dC/dt is given by

$$-\frac{dC}{dt}\,dt = AkCR\,dt = akC\,dz \qquad [1]$$

where a is a factor which depends on growth rate R and loss by diffusion. Integration during steady-state growth gives the impurity profile in the grown film with distance z, which is proportional to the adsorbed surface impurity $C(z)$

$$N = N^{\circ}\exp(-akz) \qquad [2]$$

where N° is the initial regrowth concentration of impurity which depends on the distribution coefficient and the total amount of impurity initially liberated from the substrate.

A comparison of the two methods shows that if the repetitive etching-mixing-growth step approaches zero in the Kahng (2)-Thomas (3) treatment, the expression becomes equivalent to Eq. [2]. However, strict adherence to a physical interpretation is no longer feasible. This can be shown in the following way.

In a typical case the substrate concentration is 10^{18} and regrowth starts at 10^{16}, decreasing to 10^{14} in 5μ. If the solid-gas phase distribution coefficient is assumed to be 10^{-2}, then a surface layer $k\overline{\Delta z}$ ($1\mu \cong \overline{\Delta z}$ = the average probable thickness of the autodoped regrowth layer) $10^{-2} \times 1\mu = 100$Å thick of the original solid substrate represents, approximately, the active surface volume from which the impurities are liberated and subsequently redistributed. Since it seems unlikely that at any given time an active surface volume 20 atoms deep is engaged in reaction, it is reasonable to suppose that impurities are first liberated from this volume by etching once, and then reincorporate logarithmically as suggested above.

On the other hand, the mathematical device of repetitive etching, mixing, and growth (3) with a cycle step less than 20 atoms deep is meaningless, since sufficient dopant could not be liberated from the surface. Nevertheless, if taken in perspective, the mathematical form presented by Thomas *et al.* (3) is still very useful.

The purpose of this paper is to demonstrate that the single etch-back mechanism is a natural consequence of the transient behavior involved in initiating a steady-state growth reaction.[3]

[1] Present address: Douglas Aircraft Company, AMT Unit 18, Santa Monica, California.

[2] Here we consider as trivial impurity liberation due to preprocessing the substrate. The combination of diffusion at a rate faster than growth is also ruled out since the two processes, autodoping and diffusion, are differentiated by the excellent capacitive impurity distribution measurements reported by Thomas *et al.* (3).

[3] This mechanism was first reported at The Electrochemical Society meeting by Matovich and Andres (1) with this author's permission.

Prototype Reaction Mechanism

The main assumption made about hydrogen reduction of $GeCl_4$ in an open tube epitaxial growth reactor is that $GeCl_4$ is reduced step-wise to $GeCl_2$ and then by H_2 to Ge. Furthermore, it can be assumed that $GeCl_4$ etches the substrate by means of the well known disproportionation reaction

$$GeCl_4 + Ge \underset{k_1^*}{\overset{k_1}{\rightleftharpoons}} 2GeCl_2 \qquad [3]$$

with

$$GeCl_2 + H_2 \underset{}{\overset{k_2}{\rightleftharpoons}} Ge + 2HCl \qquad [4]$$

acting as the hydrogen reduction step.

These two simplified equations provide a prototype reaction mechanism which contains the two main elements of the reaction, etching and growth, and which is a simplified, representative, mathematically tractable model of the real reaction. After the transient behavior of this simplified reaction mechanism is studied, the modified behavior of more complex mechanisms (more closely approximating the real system) will be examined.

The reaction system is imagined to comprise three phases (Fig. 1): the bulk gas phase, a boundary gas film through which reactants and products diffuse, and the gas-solid interface. The bulk gas phase is composed of hydrogen and germanium tetrachloride with concentrations $[H_2^o]$ and C_4^o respectively. At the gas-solid interface the gas phase concentrations of these two components are $[H_2]$ and C_4 respectively. If the boundary film is idealized to have an effective thickness z^o, the reactants will diffuse to the surface with a rate given by

$$(\text{Diffusion Rate})_i = \frac{\mathcal{D}_i}{z^o} C = \frac{\mathcal{D}_i}{z^o} (C_i^o - C_i) = D_i(C_i^o - C_i) \qquad [5]$$

where $\mathcal{D}_i$ is the diffusion constant of the i^{th} component and $D_i = (\mathcal{D}_i/x)$. Similarly, the reaction products $GeCl_2$ and HCl have gas-solid interface concentrations C_2 and [HCl], respectively, and diffuse out across the boundary film into the bulk gas phase, where their concentrations are assumed to remain zero since the products are carried away by the steady reactant gas stream.

The following simplifying assumptions are made: I, the reaction mechanism is represented by one etching reaction and one growth reaction, Eq. [3] and [4]; II, the reverse reaction of Eq. [4] is considered negligible; III, the concentration of $GeCl_4$ at the interface instantaneously becomes C_4, its steady-state value; IV, the concentration of H_2 at the interface is equal to its gas phase value H_2^o; V, the component adsorption isotherms are linear and rapid.

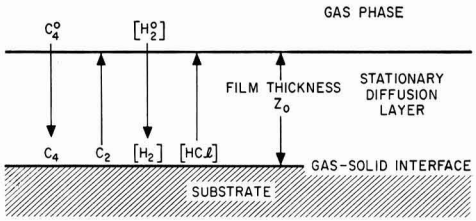

Fig. 1. Schematic representation of epitaxial growth in vapor phase deposition by hydrogen reduction of a gaseous halide.

With these assumptions and the mechanism proposed in Eq. [3] and [4], the time rate of change in concentration of these components C_2 and C_4 is given by the mass action relations at the gas-solid interface

$$-\frac{dC_4}{dt} = 0 = k_1C_4 - k_1^*C_2^2 - D_4(C_4^o - C_4) \qquad [6]$$

$$-\frac{dC_2}{dt} = 2k_1^*C_2^2 - 2k_1C_4 + k_2[H_2^o]C_2 + D_2C_2 \qquad [7]$$

and the germanium growth rate is

$$\frac{d[Ge]}{dt} = k_1^*C_2^2 + k_2[H_2^o]C_2 - k_1C_4 \qquad [8]$$

Since $dC_4/dt = 0$ in Eq. [6] by assumption III

$$C_4 = \frac{D_4C_4^o + k_1^*C_2^2}{D_4 + k_1} \qquad [9]$$

Substitution of C_4 from Eq. [9] converts Eq. [7] into a first order differential equation in the single variable $C_2 = C_2(t)$

$$-\frac{dC_2}{dt} = \left(\frac{2k_1^*D_4}{D_4 + k_1}\right)C_2^2 + (k_2[H_2^o] + D_2)C_2 - \frac{2k_1D_4C_4^o}{k_1 + D_4} \qquad [10]$$

This equation has as its standard solution the form

$$-qt = \ln\left[\frac{2\gamma C_2 + \beta - q}{2\gamma C_2 + \beta + q}\right] \cdot \left[\frac{\beta + q}{\beta - q}\right] \qquad [11]$$

where

$$q^2 = \beta^2 + 4\alpha\gamma$$
$$\alpha = \frac{2k_1D_4C_4^o}{k_1 + D_4}$$
$$\beta = k_2[H_2^o] + D_2$$
$$\gamma = \frac{2k_1^*D_4}{D_4 + k_1} \qquad [12]$$

When $t = \infty$,

$$C_2^\infty = \frac{q - \beta}{2\gamma} \qquad [13]$$

and Eq. [11] can be rearranged to the form

$$C_2 = \frac{C_2^\infty(1 - e^{-qt})}{\left(1 + \left(\frac{q - \beta}{q + \beta}\right)e^{-qt}\right)} \qquad [14]$$

Only two cases of Eq. [14] need be considered. These are the extremes when the $(q - \beta)$ term in the denominator is zero or one.

Case I. $$C_2 = C_2^\infty(1 - e^{-qt}) \qquad [15]$$

Case II. $$C_2 = \frac{C_2^\infty(1 - e^{-qt})}{1 + e^{-qt}} \qquad [16]$$

Normalized plots of these two functions in Fig. 2 show that they do not differ appreciably over the

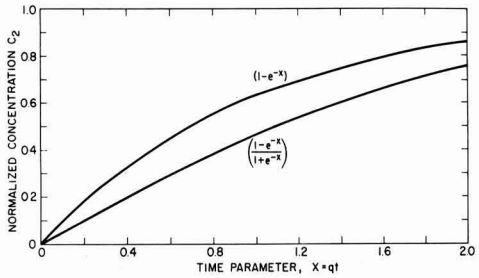

Fig. 2. Normalized plots of the two extremes of the dichloride concentration function variation with time.

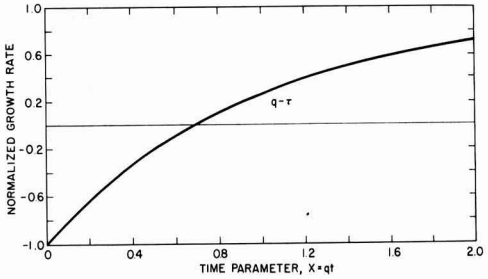

Fig. 3. Normalized growth rate as a function of time showing transient substrate etching during the initiation of the steady-state growth reaction.

entire range of the time parameter x. Therefore we need examine only the simpler case, Case I, to understand the general case as well. The germanium growth rate (Eq. [10]) becomes

$$\frac{d[\mathrm{Ge}]}{dt} = \frac{k_1^{*}\, D_4}{(k_1 + D_4)} C_2^{\infty 2}(1-e^{-qt})^2 + k_2[\mathrm{H_i}]\, C_2^{\infty}(1-e^{-qt}) - \frac{k_1 D_4}{k_1 + D_4} C_4^{o} \qquad [17]$$

A particular case of this function at low C_4^o concentrations, where the assumptions made are most valid, has the form

$$\frac{d[\mathrm{Ge}]}{dt} = R\,[1 - 2(1-e^{-qt})] \qquad [18]$$

and is shown in Fig. 3. The initial etching period followed by growth is in all cases easily understood by referring to Eq. [8] modified by substituting Eq. [9] for C_4

$$\frac{d[\mathrm{Ge}]}{dt} = \frac{k_1^{*} D_4 C_2^2}{(k_1 + D_4)} + k_2[\mathrm{H_2^o}]C_2 - \frac{k_1 D_4}{(k_1 + D_4)} C_4^{o} \qquad [19]$$

Since the last term in C_4^o has a fixed negative value and C_2 builds up from zero to its steady-state value C_2^{∞}, the growth rate is negative until C_2 becomes sufficiently large. The initial time interval, during which the growth rate is negative until it becomes zero, is defined as the induction period. Setting the growth rate $d[\mathrm{Ge}]/dt = 0$, the dichloride concentration $C_2(\tau)$ at a time equal to the induction period τ is given by

$$C_2(\tau) = \frac{k_2(D_4 + k_1)}{2k_1^{*} D_4} \cdot$$

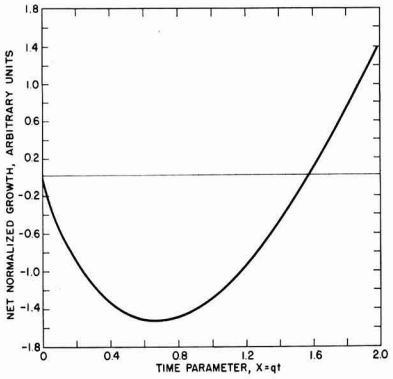

Fig. 4. Substrate growth as a function of time showing the etch-back and subsequent steady-state growth.

$$\left[-1 + \sqrt{1 + \left[\frac{2D_4}{k_1 + D_4}\right]^2 \frac{k_1 k_1^{*} C_4^{o}}{k_2^2[\mathrm{H_2^o}]^2}}\right] \qquad [20]$$

By substituting this value for $C_2(\tau)$ into Eq. [14] one can in principle solve explicitly for the induction period t.

The growth rate can be integrated to give the height of the surface z from its initial position z_o

$$z - z_o = \frac{(MW)}{d}\int_o^t \left(\frac{d[\mathrm{Ge}]}{dt}\right) dt \qquad [21]$$

This function is exemplified by the integral of Eq. [18] shown in Fig. 4.

Discussion

In a real system the tetrachloride concentration C_4 does not start at its equilibrium value but by diffusion builds up to its equilibrium value from zero. Therefore, instead of starting with a finite maximum negative value, the growth rate starts at zero, increases to a maximum negative value, decreases to zero, and then becomes positive. As a result, the etchback distance is not as great as would be expected by the equations derived herein. The differential equation for this case is a second order nonlinear differential equation in the form

$$\frac{d^2C_2}{dt^2} + (\bar{\alpha} + \bar{\beta})\frac{dC_2}{dt} + \alpha\bar{\beta}C_2 + \bar{\gamma} + \delta\left(\frac{dC_2^2}{dt} + \epsilon C_2^2\right) = 0 \qquad [22]$$

which can be solved numerically. One can show that the growth rate at $t = 0$ is zero and that the slope of $d[\mathrm{Ge}]/dt$ *vs.* C_4^o first becomes negative. Qualitatively, C_2 builds up almost as rapidly as C_4, whereas the induction period is comparable. Therefore the difference between the etching and growth rate is always less than in the first case, and the integrated etchback distance is less.

The etching-growth behavior is easily understood in terms of the reaction mechanism proposed. The reduction of the tetrahalide to subhalide C_2 etches the surface until C_2 builds up to a sufficiently high concentration to cause growth. In this reaction, diffusion of C_2 away from the surface limits the growth rate.

When the reverse of the growth reaction Eq. [4], or HCl etching is included, it also inhibits the

growth rate. In fact, it leads to substrate etching as the C_4^o concentration is increased beyond a critical value.[4]

Acknowledgment

The author thanks R. J. Andres, E. Matovich, and C. O. Thomas for fruitful and illuminating discussions on the subject material.

Manuscript received Jan. 21, 1963; revised manuscript received May 9, 1963.

Any discussion of this paper will appear in a Discussion Section to be published in the June 1964 JOURNAL.

REFERENCES

1. E. Matovich and R. J. Andres, Detroit Meeting, Electrochemical Society, October 1961, Abstract No. 137.
2. D. Kahng, R. C. Manz, M. M. Atalla, and C. O. Thomas, *ibid.*, Abstract No. 135.
3. C. O. Thomas, D. Kahng, and R. C. Manz, *This Journal*, **109**, 1055 (1962).

LIST OF SYMBOLS

a,A	loss factor due to impurity diffusing away from the surface defined in Eq. [1].
C	adsorbed impurity as measured by its gas phase concentration next to the solid-gas interface.
C_4	concentration of $GeCl_4$ at solid-gas interface.
C_2	concentration of $GeCl_2$ at solid-gas interface.
$[H_2]$	concentration of H_2 at solid-gas interface.
$[HCl]$	concentration of HCl at solid-gas interface.
C_4^o	concentration of $GeCl_4$ in the bulk gas phase.
$[H_2^o]$	concentration of H_2 in the bulk gas phase.
C_2^∞	see Eq. [13].
$\mathcal{D}_i$	diffusion coefficient of i^{th} species.
D_i	$\mathcal{D}_i/z_o$.
k	impurity distribution coefficient between the solid and gas phases during growth.
k_i	forward rate constant for reaction i.
k_i^*	reverse rate constant for reaction i.
N	impurity concentration in the solid phase.
q^2	$\beta^2 + 4\alpha\gamma$.
R	substrate growth rate.
z	distance measured normal to the surface from time zero.
z_o	effective thickness of stationary gas diffusion layer.
$\overline{\Delta z}$	average probable thickness of autodoped regrowth layer $= \int_0^\infty z\,N(z)\,dz / \int_0^\infty N(z)\,dz$
α,β,γ	see Eq. [12].
$\alpha,\beta,\gamma,\delta,\epsilon$	constants in Eq. [22].
τ	induction period — total time for transient substrate etching.

[4] This question is dealt with in greater detail in a companion paper on steady-state growth rates to be submitted to this Journal.

Vapor Growth of Germanium-Silicon Alloy Films on Germanium Substrates

R. C. Newman[1] and J. Wakefield

Research Laboratory, Associated Electrical Industries, Aldermaston Court, Aldermaston, Berkshire, England

ABSTRACT

Silicon has been transported from a source at 1100°C onto germanium single crystal substrates at 700°-900°C in a sealed system by the disproportionation of the iodide. Deposits thus formed are found to be germanium silicon alloys of variable composition. These structures have been examined by etching techniques, electron microbeam x-ray analysis, and by electron diffraction. During deposition, plastic deformation of the germanium occurs resulting in dislocation densities of up to $5 \times 10^7/cm^2$, and appreciable cavity formation is found in monocrystalline deposits formed at high substrate temperatures.

Epitaxial films of silicon are almost invariably prepared by the decomposition of trichlorosilane (1) or the hydrogen reduction of silicon tetrachloride (2); both these processes require a silicon substrate temperature of about 1200°C. A process less extensively studied is that described by Wajda *et al.* (3), who prepared monocrystalline films on silicon substrates by the disproportionation of silicon di-iodide. Silicon is transported from a source at a high temperature to the substrate at a lower temperature in a sealed tube by the reversible reaction

$$2SiI_2(g) \underset{\text{hot}}{\overset{\text{cold}}{\rightleftharpoons}} Si(S) + SiI_4(g) \qquad [1]$$

Wajda *et al.* gave source and substrate temperatures as 1100° and 900°C, respectively, but did not state the pressures used, which are controlled by the quantity of iodine introduced. The transport of silicon resulting from reactions with iodine has also been studied by Schäfer and Morcher (4), who found that the direction of transport along a temperature gradient depended on the pressure. At low pressures the reaction is

$$Si(S) + 4I(g) \rightleftharpoons SiI_4(g) \qquad [2]$$

and silicon is transported from a low-temperature region to a higher temperature region. At pressures greater than some value between 62-96 mm Hg of silicon tetra-iodide, however, reaction [1] was found to predominate with source and deposition zones at 1150° and 950°C, respectively.

In this paper the above iodide process for silicon deposition is investigated further, and in particular the deposition on germanium substrates has been examined, since it has been shown previously that germanium may be grown epitaxially on silicon using an iodide process (5).

Experimental Technique

The experimental system consisted of a closed quartz tube about 30 cm long and 2.2 cm bore,

[1] Present address: A.E.I. Research Laboratory, Rugby, Warwickshire, England.

similar to that used by Waja *et al.* (3). Slices of silicon or germanium about 1.5 cm diameter and 1 mm thick were hung from hooks on the end of a quartz rod which is sealed into one end of the tube. The silicon source material together with the iodine was also placed in the tube which was then drawn out at the open end and evacuated to a pressure of about 10^{-4} mm Hg. Sublimed iodine was introduced in an evacuated quartz capsule with break-tip seal, enabling the tube to be thoroughly outgassed before it was sealed. The vapor phase reaction was carried out in a vertical furnace with two temperature zones. The source silicon was held in the lower region at a temperature of approximately 1100°C while the temperature in the substrate zone was about 900°C; lower temperatures were however investigated with germanium substrates. Immediately before insertion, the substrates were chemically polished; silicon was etched in a 50/50 mixture of hydrofluoric and nitric acids, and germanium was etched in CP4.

Deposits on Silicon Substrates

The substrate was held at 900°C and the effect of gas pressure on the transport of silicon was investigated by varying the amount of iodine in the tube. When the calculated pressure of silicon tetra-iodide was less than about 100 mm Hg, etching of the substrates occurred indicating the transfer of silicon to the higher temperature end of the tube. At higher pressures, the direction of transport of the silicon was reversed, in qualitative agreement with the findings of Schäfer and Morcher (4). The deposits described in more detail below were obtained with a pressure of about 5 atm, and the growth rate, determined by sectioning, was about 15 μ/hr.

Growths on [111] substrates at 900°C were examined by reflection electron diffraction and found to be monocrystalline. The surfaces of such films were subsequently ground, etched in a mixture of 50% HF and 50% nitric acid and then Dash etched[2] to reveal the crystal structure. The features observed were: (i) a high dislocation density of approximately 2.10^6 cm^{-2}, (ii) a high density of stacking faults lying on <111> planes and up to 100μ in length, in some cases forming closed triangles, and (iii) polycrystalline inclusions about 100-200μ across. To examine the growth in depth and also the interface between the substrate and the film, a vertical section through the film was ground and etched as above. It was found that the interface between the substrate and film etched very rapidly, suggesting that this was a highly strained or dislocated region. The stacking faults could be traced back to the interface, and the regions of polycrystalline growth also appeared to nucleate here but were eventually covered by the surrounding monocrystalline growth. In addition, the dislocation density decreased with increasing distance from the interface.

Although large area single crystal growth was obtained on some [100] surfaces, it was found that randomly oriented particles, again nucleated at the interface, tended to grow preferentially and eventually predominated with increasing film thickness. The dislocation density in single crystal areas was approximately 2×10^5 cm^{-2} and was thus lower than that obtained for films grown on a [111] substrate; in addition, no etching features, characteristic of stacking faults, were observed on the [100] surfaces.

The poor crystal structure was almost certainly a consequence of an oxide or carbide layer (6) being formed on the surface of the substrate prior to the onset of deposition. Attempts to clean the substrate surface in situ by reversing the direction of reaction [1] were not satisfactory due to uneven attack of the substrate by the iodine and the formation of large etch pits. Thus it appears to be more difficult to achieve good crystal perfection in the deposits prepared by this iodide process compared with that obtainable from the chloride processes (1, 2).

Deposits on Germanium Substrates

An oriented overgrowth occurred readily on both [111] and [100] substrates at 900°C (see Fig. 1 and 2) without any special precautions being taken to remove spurious contamination from the reaction tube. The surface layer had the visual appearance of silicon and reflection electron diffraction showed that the lattice spacing of this layer was that of silicon within the experimental error of 0.5%.

Fig. 1. Oriented growth on a (111) germanium surface after 16 hr at 885°C. Magnification approximately 40x.

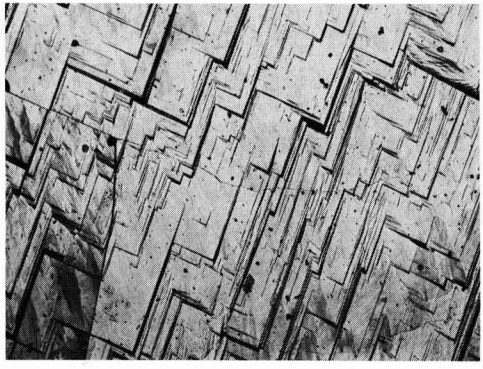

Fig. 2. Oriented growth on a (100) germanium surface after 16 hr at 885°C. Magnification approximately 40x.

[2] HF-HNO_3-acetic acid in ratio 1:3:8.

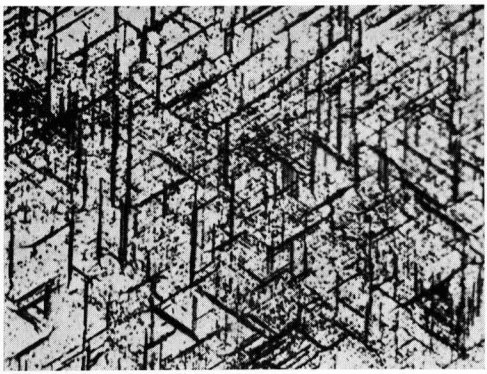

Fig. 3. Etched (111) growth showing a high density of stacking faults and dislocations. Magnification approximately 400x.

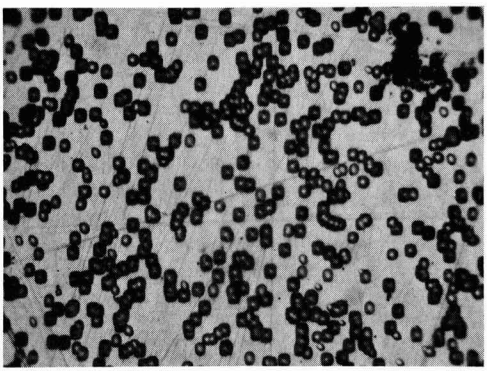

Fig. 4. Etched (100) growth showing only dislocations with a density of 10^7 lines/cm^2. Magnification approximately 1100x.

Chemical etching of these surfaces revealed similar features to those described for deposits on silicon substrates, *i.e.*, stacking faults and slip traces were evident on (111) surfaces but not on (100) surfaces, as shown in Fig. 3 and 4. The samples were then sectioned and polished. The thickness of the surface layer was found to be about 15-30μ, beneath which there was a second layer containing large cavities as shown in Fig. 5. The thickness of this cavitated layer increased with increasing time of reaction, until after 64 hr a germanium substrate originally 1 mm in thickness was no longer identifiable.

To determine the relative concentrations of germanium and silicon in these layers, such sections were scanned in a microbeam x-ray analyzer (7). The germanium content at the surface was about 2-5 a/o, which is consistent with the determination of the lattice parameter of this layer. The germanium concentration increased only slowly with increasing penetration until the interface between the cavitated layer and the germanium was approached; no discontinuity was found between the surface layer and the cavitated layer. The distribution of germanium about the second interface is shown in Fig. 6 for various substrate temperatures. It may be noted that, although this interface appears quite sharp on micrographs of samples reacted at all temperatures, the concentration gradient of the germanium increases with decreasing temperature. The distribution of silicon was likewise determined, but the results could not be interpreted accurately because the absorption coefficient for the characteristic x-rays from the silicon in the germanium-silicon alloy was not known. Qualitatively, however, the results indicated that the sum of the germanium and silicon concentrations was close to unity. Back-reflection Laue photographs showed that the cavitated layers were monocrystalline throughout, and lattice parameters intermediate between germanium and silicon were measured in agreement with the microanalysis.

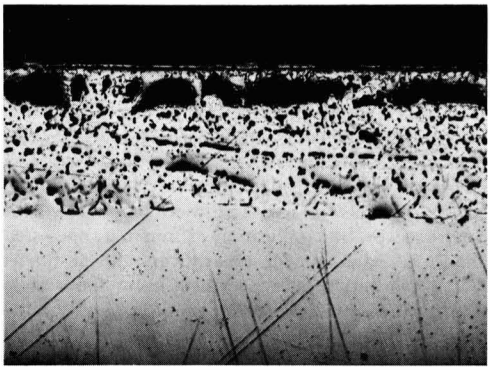

Fig. 5. Sectioned (111) sample showing cavitated layer below the thin coherent surface skin. Treatment 3½ hr at 870°C. Magnification approximately 70x.

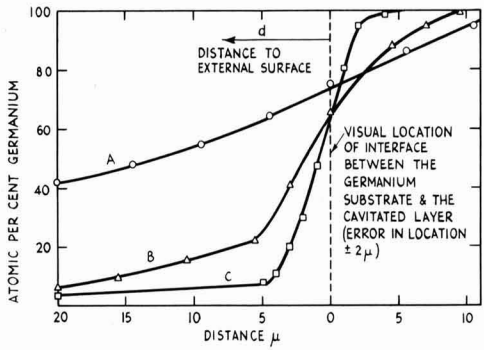

Fig. 6. Concentration of germanium in atomic per cent as a function of distance. The interface between the germanium substrate and the cavitated layer (see Fig. 5) is used as a reference line. Curve A, $T = 885$°C, $d = 410\mu$; curve B, $T = 800$°C, $d = 130\mu$; curve C, $T = 660$°C, $d = 20\mu$. The time of heating in each case was 17 hr and d is the distance from the reference line to the external surface.

The weight of the sample after the reaction was less than the weight of the original germanium substrate, but the thickness was considerably increased. Thus, as silicon is deposited, germanium must be transferred to the gas phase, and in fact, yellow germanous iodide was observed in the reaction tube on removal from the furnace.

This is consistent with the calculated values of the free energy ΔG of -20 kcal/mole and -27 kcal/mole, respectively for the reactions

$$Ge(S) + SiI_2(g) + \Delta G \rightleftharpoons GeI_2(g) + Si(S)$$

and

$$2Ge(S) + SiI_4(g) + \Delta G \rightleftharpoons 2GeI_2(g) + Si(S)$$

at a temperature of 1200°K; values of the free energy for silicon di-iodide and germanium di-iodide were obtained from previously published data (4, 8).

To elucidate the mechanism of the germanium transport through the silicon some further experiments were carried out. A sample was reacted in the usual way for a sufficient time to form a silicon coating on its surface, and then the iodine was condensed by the application of liquid air to a cold finger (at high temperature during the first part of the heating) after which heating of the sample was continued for several hours. Sections of the samples showed a structure appropriate to the short time of deposition, indicating that no appreciable diffusion occurred during the subsequent anneal. In fact, no change in the germanium concentration profile could be detected in a similar sample heated in an evacuated silica tube for 600 hr at 918°C. It therefore appears that the germanium is transported through the pores in the cavitated region (see Fig. 5) by a gas phase reaction involving iodine, although this was not detected by the microanalysis. This is not unexpected, since any condensed germanium or silicon iodides would be hydrolized in the atmosphere, thus allowing the iodine to escape; the concentration of iodine in solid solution is expected to be small in view of the results of Baker and Compton (9).

A possible mechanism for the formation of the cavities is now discussed. There is a continuous charge in lattice parameter from the surface of the deposits to the germanium substrate and dislocations must be generated to accommodate this change. In fact, etching revealed that the dislocation density in the germanium substrate increased during the reaction from about 10^4 cm^{-2} up to 5 x 10^7 cm^{-2}, thus giving positive evidence for the occurrence of plastic deformation. Vacancies generated by the nonconservative motion of jogs on such moving dislocations (10) may subsequently aggregate to form cavities which are likely to be stabilized by the presence of germanium di-iodide gas. The possibility that the pores arise from a Kirkendall effect (11) is thought to be unlikely, due to the observed negligible interdiffusion in the absence of iodine.

Oriented growths were obtained on [111] substrates at temperatures down to 650°C. At the lower temperatures, the rate of silicon deposition on the specimen was much reduced (see Fig. 6) and a film of silicon was deposited on the wall of the reaction tube in a zone at about 800°C. Oriented growths could not be obtained on [100] substrates at temperatures below 800°C. Twinning occurred on all {111} planes as determined by electron diffraction and these twinned crystallites were found to have large planar {111} facets similar to the structure observed on germanium deposits prepared by a similar iodide process (12).

Conclusions

It has been shown that silicon can be deposited onto germanium single crystal substrates to give epitaxial layers consisting of a germanium silicon alloy. The most interesting feature is that a single crystal structure can be maintained throughout the whole range of composition of germanium-silicon alloys in contrast to alloys prepared by the pulling technique (13). These results are thus complementary to those of Millar and Grieco (14) who obtained single crystal germanium-silicon alloy films by means of the chloride process.

Acknowledgments

Thanks are due to J. H. Neave for experimental assistance and to Dr. T. E. Allibone, C.B.E., F.R.S., Director of the Laboratory, for permission to publish this paper.

Manuscript received Feb. 28, 1963; revised manuscript received May 20, 1963. This paper was presented at the Boston Meeting, Sept. 16-20, 1962.

Any discussion of this paper will appear in a Discussion Section to be published in the June 1964 JOURNAL.

REFERENCES

1. R. Glang and E. S. Wajda, "Metallurgy of Semiconductor Materials," (AIME Los Angeles Conf., 1961), J. B. Schroeder, Editor, **15**, 27 (1962), Interscience Publishing Co., New York.
2. H. C. Theuerer, *This Journal*, **108**, 649 (1961).
3. E. S. Wajda, B. W. Kippenham, and W. H. White, *I.B.M. J. Res. Develop.*, **4**, 288 (1960).
4. H. Schäfer and B. Morcher, *Z. anorg. allgem. Chem.*, **290**, 279 (1957).
5. R. P. Ruth, J. C. Marinace, and W. C. Dunlap, Jr., *J. Appl. Phys.*, **31**, 995 (1960).
6. R. C. Newman and J. Wakefield, "Solid State Physics and Telecommunications," Brussels, 1958, Vol. 1, p. 318, Academic Press, New York (1960).
7. T. Mulvey, *J. Sci. Instruments*, **36**, 350 (1959).
8. W. C. Jolly and W. M. Latimer, *J. Am. Chem. Soc.*, **74**, 5752 (1952).
9. W. E. Baker and D. M. J. Compton, *I.B.M. J. Res. Develop.*, **4**, 269 (1960).
10. W. C. Dash, *J. Appl. Phys.*, **29**, 705 (1958).
11. A. D. Smigelskas and E. O. Kirkendall, *Trans. AIME*, **171**, 130 (1947).
12. R. C. Newman and J. Wakefield, "Solid State Physics and Telecommunications," Brussels, 1958, Vol. 1, p. 160, Academic Press, New York (1960).
13. E. R. Johnson and S. M. Christian, *Phys. Rev.*, **95**, 560 (1954).
14. K. J. Miller and M. J. Greico, *This Journal*, **109**, 70 (1962).

The Gettering Properties of Tantalum

E. G. Zubler

Lamp Research Laboratory, General Electric Company, Nela Park, Cleveland, Ohio

ABSTRACT

The reaction of tantalum with the gases, O_2, N_2, CO_2, CO, and H_2 at low pressures (0-200μ) was studied in the range 200°-2000°C. Measurable reaction rates which were independent of pressure were observed for O_2 at 350°-650°C, N_2 at 780°-940°C, CO_2 at 500°-1500°C, and CO at 950°-1500°C. H_2 was reversibly absorbed at 200°-730°C and was the only gas released after sorption below 1600°C.

As part of a general investigation of getters, a study has been made of the kinetics of reactions between tantalum and various gases. Tantalum and other bulk getters have been used in lamps and electron devices to remove detrimental gaseous impurities such as H_2, O_2, CO_2, CO, H_2O, and hydrocarbons. In order to use these getters effectively, a knowledge of sorption and desorption processes as a function of temperature and pressure is necessary.

While a comprehensive survey of gas sorption by metals (1) and recent bibliographies (2, 3) on getters are available, studies of the reactions between tantalum and the gases of interest (4-13, 17, 18) do not cover the low gas pressure (micron) region adequately. Consequently, this investigation of the gettering properties of tantalum as a function of temperature (200°-2000°C) and pressure (0-200μ) was initiated.

Experimental

The tantalum was obtained from Fansteel Metallurgical Corporation in 0.003 x 5/16 in. strips and was specified as 99.9+% purity with C and Fe each at a maximum level of 0.03%. The tantalum was formed into a 1.0 in. diameter ring with an approximate weight of 0.80g. The surface of the tantalum was smooth, and the surface area was calculated from the geometric dimensions.

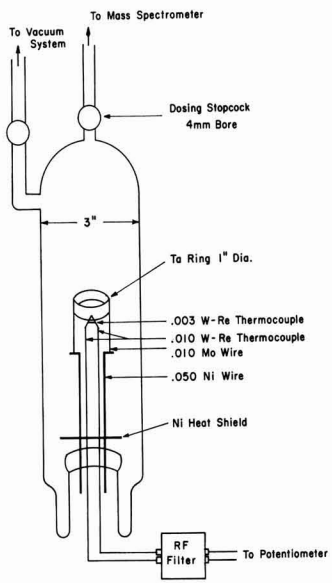

Fig. 1. Getter chamber

The gases with 99.5-99.99% purity were obtained in small cylinders or glass flasks, and further purification was not attempted except when possible the gas was passed slowly through a liquid nitrogen trap packed with glass beads to remove any possible water vapor.

A glass, high vacuum system using a mercury diffusion pump was constructed. The gas pressure for the gettering experiments was measured by a Consolidated Electrodynamics Corporation, Model 23-105, micromanometer. An ion resonance mass spectrometer was used to analyze the gas in the getter chamber.

A diagram of the getter chamber which is similar to one used by other investigators (14) is shown in Fig. 1. The tantalum ring was heated by a radio-frequency induction unit while the temperature was measured by the rhenium-tungsten thermocouple for which a calibration curve to 2100°C was available (15). Tungsten electrodes were used for all spot welding operations. A nickel heat shield was located between the hot and cold junctions of the thermocouple. The bottom section of the getter chamber was immersed in a water bath at room temperature which was taken as the cold junction temperature.

After the getter chamber was sealed to the glass vacuum system and pumped down, the volume of the chamber was determined by a calibrated volume and gas expansion technique. The getter chamber was then baked out at 350°C for 2 hr using heating tape. After bake out, the tantalum ring was slowly heated to 1800°-2000°C and held there until the pressure was less than 10^{-5} mm. Except for the evolution of adsorbed gas and sorbed hydrogen at relatively low temperatures, other gases were evolved only at temperatures greater than 1600°C.

After degassing, the tantalum was allowed to return to room temperature, and the gas under consideration was admitted at a pressure measured by the micromanometer. The tantalum ring was then heated to the desired temperature which was attained in 20-30 sec, and the pressure was then measured at 30 or 60 sec intervals.

As the gas pressure in the system decreased, there was a slight increase in the temperature of the tan-

Table I. Summary of data for the reaction of tantalum with oxygen, nitrogen, and carbon monoxide

Gas	Temp, °C	Time, min	Initial pressure, μ	Rate constant: Parabolic μ·l/cm²·sec^1/2	Rate constant: Linear μ·l/cm²·sec
O_2	360	10	62		1.06×10^{-3}
	390	8	48		1.69×10^{-3}
	410	14	169		2.14×10^{-3}
	430	12	86		2.98×10^{-3}
	460	15	153		5.26×10^{-3}
	460	13	132		5.14×10^{-3}
	485	15	174		9.08×10^{-3}
	500	15	196	0.76	
	515	10	186	0.90	
	535	16	190	0.83	
	550	12	118	0.85	
	555	8	88	0.95	
	590	6	105	1.65	
	635	5	95	2.87	
N_2	780	15	119		7.6×10^{-4}
	810	15	108		1.65×10^{-3}
	860	10	95		3.5×10^{-3}
	940	10	178		1.63×10^{-2}
CO	1200	20	142		7.9×10^{-3}
	1215	10	195		7.4×10^{-3}
	1265	10	170		1.05×10^{-2}
	1315	8	145		1.27×10^{-2}
	1350	10	180		1.70×10^{-2}
	1430	10	130		1.95×10^{-2}
	1535	10	75	0.49	
	1600	8	38	0.52	

talum ring which was corrected manually during the run by using a fine adjustment on the power control of the induction heater. With this technique, the temperature could be held constant to within 5°-10°C during a typical run.

After the run, the getter chamber was pumped down to 10^{-6} mm, and the tantalum ring was degassed at 1600°-2000°C. A new tantalum ring was used for each gas, and the amount of gas sorbed during a series of runs was considerably less than that required for saturation.

Results

The results of the reactions between a degassed tantalum ring and oxygen, nitrogen, and carbon monoxide are summarized in Table I. Below a certain temperature which depended on the gas, the gas pressure above the tantalum decreased linearly with time while above this temperature the pressure decreased linearly with the square root of time. The linear and parabolic relations for these temperature regions persisted even when large quantities of gas had been sorbed.

For oxygen, a linear pressure-time relation was observed at 350°-490°C while a parabolic relation was observed at 520°-650°C as shown in Fig. 2 and 3, respectively. In the linear region, the rate constant for a degassed tantalum sample at constant temperature was independent of initial pressure. Identical slopes were obtained for 3 pressure-time plots with initial pressures in the range 82-169μ. In the transition region, 490°-520°C, a linear rate law was obeyed for a degassed sample, and a parabolic rate law was obeyed if some sorption had occurred previously. The run at 500°C in Fig. 3 shows a linear behavior followed initially by a transition to parabolic behavior.

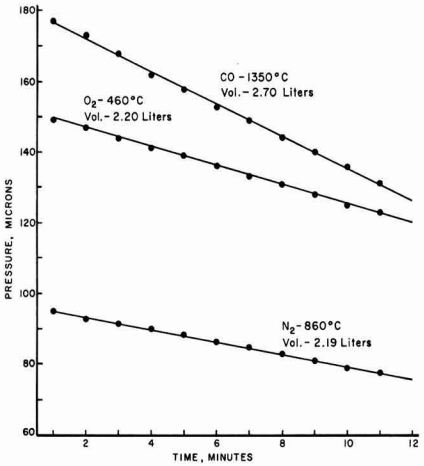

Fig. 2. Linear variation of pressure with time for oxygen, nitrogen, and carbon monoxide.

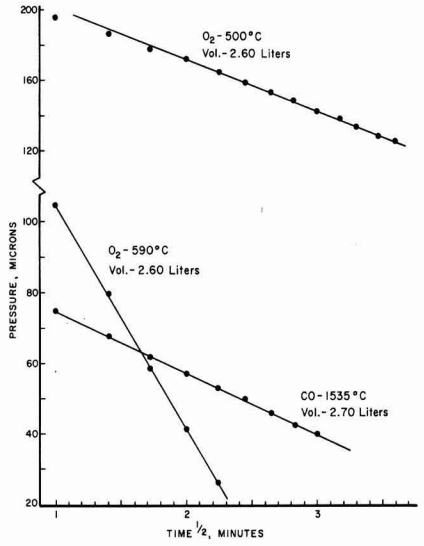

Fig. 3. Parabolic variation of pressure with time for oxygen and carbon monoxide.

Generally, there was no visible change in the tantalum during a run. However, in one experiment, the tantalum sorbed sufficient oxygen at 600°C to result in a visible darkening of the surface. A cross section of the tantalum showed that the product layer was approximately 0.0005 in. thick, and x-ray diffraction analysis identified the layer as β-Ta_2O_5.

For carbon monoxide, a linear rate law was obeyed at 950°-1500°C and a parabolic rate law at 1500°-1600°C for a degassed tantalum sample. However, a run at 1010°C which obeyed a linear rate law for several minutes became parabolic when the temperature was increased to 1180°C. When the tantalum was degassed and the reaction again observed at 1180°C, a linear rate law was obeyed for

14 min. In general for 1000°-1300°C, it was found that, if the temperature during a run was increased more than 70°-80°C, the pressure-time relation changed from linear to parabolic. If the temperature change were less, the reaction continued to follow a linear rate law.

At these low gas pressures and temperatures above 1500°C, there was a tendency for the RF field to produce a discharge in the getter chamber, and this limited the data in this region.

For nitrogen, the pressure-time relation was linear at 780°-940°C. At 940°C, there was a tendency for the pressure-time plot to become parabolic. At higher temperatures the reaction rate was too fast for the techniques employed so that actual parabolic plots were not obtained.

For oxygen, nitrogen, and carbon monoxide, plots of the logarithms of the linear reaction rates *vs.* reciprocal temperature and the activation energies calculated from the Arrhenius equation are shown in Fig. 4. A similar plot for oxygen at 530°-650°C where the reaction follows a parabolic rate law gives E_a = 22 kcal/mole. Insufficient data were available for the parabolic region of carbon monoxide to permit a calculation of E_a.

For carbon dioxide, the decrease in pressure with time was linear at 950°-1200°C and parabolic at 1230°-1440°C. A mass spectrometric analysis of the gas in the getter chamber during a run indicated that a reaction producing carbon monoxide occured at 500°-700°. The decrease of carbon dioxide as indicated by the mass 44 peak was linear with time in this temperature region. At higher temperatures, carbon monoxide was also sorbed, and the system behaved similar to that of pure carbon monoxide except that the transition from linear to parabolic behavior occurred at a lower temperature.

Hydrogen was sorbed reversibly at 200°-730°C. At 200°-500°C the reaction obeyed a parabolic rate law while at higher temperatures the reaction was too rapid to measure. For a degassed tantalum ring, the minimum temperature at which sorption was observed was 370°C. However, if the ring had sorbed some hydrogen at a higher temperature, *e.g.*, 500°-600°C, sorption was observed at 200°C. At any temperature, a plot of the solubility in cubic centimeters at STP per gram of tantalum *vs.* the square root of pressure was a straight line, indicating that atomic hydrogen was involved in the sorption process. The equilibrium pressure at a given temperature and concentration of sorbed gas was the same whether it was obtained by sorption or evolution indicating that the sorption process involved solution rather than compound formation. The temperature dependency of the solubility and the calculated heat of solution per mole of H_2 are given in Fig. 5.

Discussion

The linear and parabolic pressure-time relations observed in different temperature regions for oxygen, carbon monoxide, and indicated for nitrogen suggest different rate-controlling processes. At the lower temperatures where a linear rate law was obeyed, strong adsorption of the gas resulting in nearly complete surface coverage of the tantalum is postulated. Since, for nearly complete surface coverage, the concentration of adsorbed molecules is nearly independent of gas pressure, the reaction rate is pressure independent, and a linear rate law would be observed. At higher temperatures where a parabolic rate law was observed, a rate-controlling diffusion process is indicated. At these temperatures, a fast reaction results in the rapid formation of a product layer, and further reaction involves diffusion through this surface layer, resulting in a parabolic rate law. A product layer has been identified here for oxygen at 600°C. The relation between diffusion constants and parabolic rate constants for similar gas-metal system has been considered (7, 8, 10, 16).

For the gas pressure range considered here, the initial reaction might be expected to follow a linear rate law for degassed tantalum at any temperature. At high temperatures, the product layer is formed rapidly, and the linear region is not observed. At low temperatures, the product layer does not develop sufficiently in the time allowed to become rate controlling. At intermediate temperatures, the linear rate law may be obeyed initially followed by a transition to parabolic behavior. This type of be-

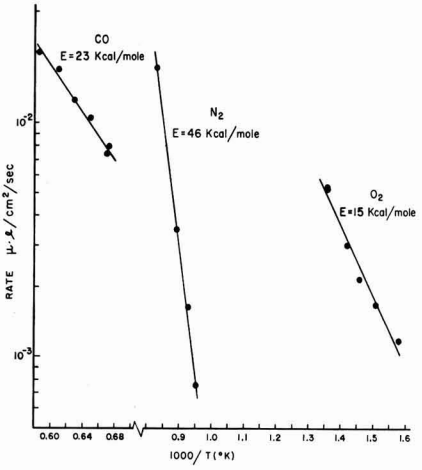

Fig. 4. Temperature dependence of linear sorption rates for oxygen, nitrogen, and carbon monoxide.

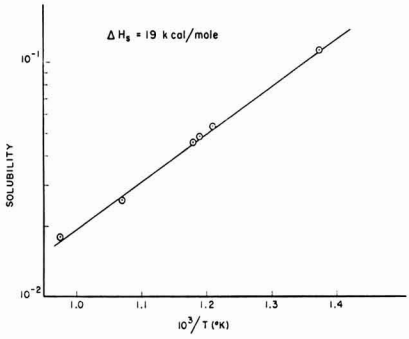

Fig. 5. Temperature dependence of solubility of hydrogen in cubic centimeters at STP per gram of tantalum.

havior was observed for oxygen at 500°C as shown in Fig. 3.

In previous studies, the oxidation reaction has been reported as linear (10, 13), parabolic (7), cubic (17), and logarithmic (9, 11, 12) for comparable temperatures but generally higher pressures and longer times than considered here. The higher pressures and longer reaction times would tend to mask the linear behavior observed in this study. At slightly higher pressures (1.5-16 mm) and longer reaction times (0-120 min), Gulbransen and Andrews reported parabolic behavior for oxygen at 250°-450°C and for nitrogen at 500°-850°C. They calculated E_a = 27.4 kcal/mole for the oxidation reaction compared to the 22 kcal/mole calculated in this study for the parabolic region (520°-650°C). For the diffusion of oxygen through tantalum Ang (19) reported E_a = 27.3 kcal while Albrecht *et al.* reported 22.9 kcal/mole. At much higher pressures (0.2-1.0 atm), Albrecht *et al.* observed linear behavior for oxygen at 400°-600°C with E_a = 60 kcal/mole compared to the 15 kcal/mole found in this study. They also observed that nitrogen obeyed a cubic rate law at 400°-700°C and a parabolic rate law at 800°-1475°C.

Acknowledgments

The assistance of R. Wyland in the laboratory, the x-ray diffraction and microscopy work of Miss J. Cooper, and the valuable suggestions and discussions of Miss A. Easley and Dr. L. V. McCarty are gratefully acknowledged.

Manuscript received Jan. 14, 1963; revised manuscript received May 7, 1963.

Any discussion of this paper will appear in a Discussion Section to be published in the June 1964 JOURNAL.

REFERENCES

1. S. Dushman, "Scientific Foundations of Vacuum Techniques," John Wiley & Sons, Inc., New York (1949).
2. C. J. Wensrich, UCRL-6514, University of California (1961).
3. N. M. Morris, Bell Tel. Lab., Bibl. No. 22, July 1958.
4. D. A. Wright, *Nature*, **142**, 794 (1938).
5. M. R. Andrews, *J. Am. Chem. Soc.*, **54**, 1845 (1932).
6. R. Myers, *Metallurgia*, **41**, 30 (1950).
7. E. Gulbransen and K. Andrews, *Trans. AIME*, **185**, 515 (1949); **185**, 741 (1949); **188**, 586 (1950).
8. E. Gulbransen and K. Andrews, *This Journal*, **96**, 364 (1949).
9. D. A. Vermilyea, *Acta Met.*, **6**, 166 (1958).
10. W. Albrecht, W. Klopp, B. Koehl, and R. Jaffee, *Trans. AIME*, **221**, 110 (1961).
11. H. Basseches, *This Journal*, **109**, 475 (1962).
12. J. T. Waber, G. E. Sturdy, E. Wise, and C. R. Tipton, Jr., *ibid.*, **99**, 121 (1952).
13. R. C. Peterson, W. M. Fassell, and M. E. Wadsworth, *Trans. AIME*, **200**, 1038 (1954).
14. V. Stout and M. Gibbons, *J. Appl. Phys.*, **26**, 1488 (1955).
15. J. C. Lachman, *Instr. & Contr. Syst.*, **32**, 1030 (1959).
16. N. F. Mott, *Trans. Faraday Soc.*, **36**, 472 (1940).
17. J. T. Waber, *J. Chem. Phys.*, **20**, 734 (1952).
18. A. Sieverts and H. Bruning, *Z. phys. chem.*, **A174**, 365 (1935).
19. C. Y. Ang, *Acta. Met.*, **1**, 123 (1953).

The Adsorption of Aromatic Hydrocarbons at the Gold Electrolyte Interface

Harald Dahms[1] and Mino Green[2]

The Electrochemistry Laboratory, The University of Pennsylvania, Philadelphia, Pennsylvania

ABSTRACT

The potential and concentration dependent adsorption of benzene, naphthalene, and phenanthrene at the gold/electrolyte interface has been investigated using a ^{14}C-radio tracer technique. For a fixed concentration of organic material the adsorption peak was found at about +500 mv (NHE) and the potential-adsorption curve was bell shaped, adsorption decreasing with potential on either side of the peak. An analysis of the adsorption isotherms for naphthalene leads to the conclusion that naphthalene lies flat on the electrode surface. Comparison of the extent of adsorption of the aromatic hydrocarbons with cyclohexane, n-octanoic acid, and n-decanoic acid (no detectable adsorption) indicates that aromatic compounds have a higher binding energy with metals than the corresponding aliphatic compounds. The added binding energy for aromatic molecules is attributed to their π-electron systems. Finally a comparison of mercury with gold points to the stronger binding energy of water to gold than to mercury.

Studies of the adsorption of organic molecules at the metal/electrolyte interface have been mainly confined to mercury. Knowledge of the adsorption at solid metals, however, is important to a number of electrochemical problems, *e.g.*, structure of the double layer, corrosion inhibition, and electrochemical oxidation of fuels. Simple aromatic compounds were chosen for this investigation because these substances were expected to give rise to relatively simple systems.

Studies of the adsorption of organic molecules at solid electrodes have been mainly carried out using

[1] Present address: Thomas J. Watson Research Center, International Business Machine Corporation, Yorktown Heights, New York.

[2] Present address: 45 Radley House, Gloucester Place, London, England.

capacity measurements (1), the direct determination of concentration changes in the solution (2), or radioactive tracer techniques. The determination of adsorption from capacity data is, however, not unambiguous because of the implied nonthermodynamic assumptions and the complication of the frequency dependence of the capacity. The direct study of adsorption by determination of the concentration change in the solution is limited to extremely dilute solutions and large area electrodes.

Radiotracer methods have been used by numerous workers. Most of these techniques require a separation of the labelled solution phase from the adsorbed species thereby causing possible sources of error. Various methods have, however, been developed to determine the extent of adsorption without disturbing the equilibrium at the interface. The precursor to the present method was developed by Joliot (3). This technique was modified by several workers: Power and Heyd (4) adopted it for α-emitting species. Kafalos and Gatos (5) presented a technique using hard β- and γ-emitters. Weissmantel (6) determined the adsorption of β-labelled species by measuring their radiation passing through thin films of various metals. Likewise Cook (7) and Blomgren and Bockris (8) measured the β-radiation through thin metal films. The latter workers used a mechanical method to separate the solution background from the total radiation. The mechanical separation in no way interfered with adsorption equilibrium. This last mentioned technique was used by Wroblowa and Green (9) to study the potential dependent adsorption of thiourea on gold.

The work described here was carried out using a similar technique, but with a different method to separate the radiation of the adsorbed species from that of the solution background.

Experimental

Arrangement and procedure.—A schematic diagram of the cell and counting arrangement is shown in Fig. 1. The cell is essentially the same as that described by Wroblowa and Green (9) modified only to permit continuous electromagnetical stirring.

The gold electrode, a foil of 2.10^4Å thickness, was fixed on the window of a gas-flow proportional counter. The electrode potential of the gold electrode was controlled by means of a potentiostat. The compartments for the reference electrode (saturated calomel electrode) and the working electrode were separated by stopcocks. Purified hydrogen or nitrogen (cleaned by passing the gas over heated platinum-asbestos, charcoal, and through liquid nitrogen cooled traps) was passed through the cell. The cell was isolated from the atmosphere by means of a water-seal. The labelled organic solution was added from a calibrated burette. The cell was placed on a microscopic drive to adjust it vertically in its position to the counter. The whole arrangement was operated in an air-thermostat.

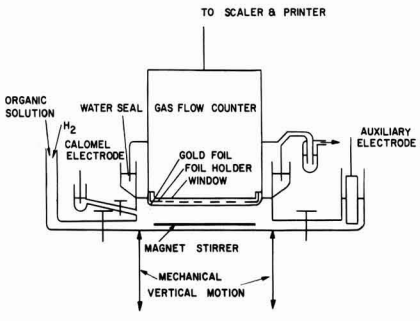

Fig. 1. Diagram of the experimental arrangement

The gold foil (purity 99.99% as given by the manufacturer) was first cleaned by extraction in ethanol and acetone. The foil holder was then covered with a thin layer of a high vacuum grease, and one side of the foil was fixed onto it. The gold electrode covered the foil holder and the lower part of the counter so that any contact of the grease with the outer side of the gold foil or with the solution was strictly avoided. Finally the gold electrode was cleaned by alternate anodic-cathodic pulsing in $1N$ H_2SO_4 (going from oxygen evolution to hydrogen evolution), terminating on cathodic polarization (hydrogen evolution for 1 min). The evolved hydrogen and oxygen were removed from solution by sweeping with nitrogen. After this treatment the electrode was perfectly wetted by water. Different cleaning procedures of the gold electrode (heating to about 300°C) did not influence the adsorption behavior.

The electrolyte in the cell was $1N$ H_2SO_4 prepared from pure concentrated sulfuric acid and conductivity water. After the dissolved gases had been swept out, the labelled organic solution was added. Then only a minimum amount of purified nitrogen was passed through the adsorption compartment to maintain a controlled atmosphere and yet minimize evaporation. The electrolysis current never exceeded 10^{-5} amp/cm^{-2} over the entire range of potential investigated and dropped during the experiment to values of 10^{-7} amp/cm^{-2}. Variation in current between had no apparent influence on the extent of adsorption. The count rate of the radiation counter was recorded automatically as a function of time and electrical potential.

Determination of the amount adsorbed.—Without any adsorption a certain amount of the radiation from the labelled solution will reach the counter, the resulting count rate will be given by

$$\mathrm{cps_{sol}} = k\ 3.7\ 10^{10}\ Ac\ \alpha \int_0^\infty e^{-\mu x}\, dx = k\ 3.7\ 10^{10}\ Ac\ \alpha \frac{1}{\mu} \qquad [1]$$

where $\mathrm{cps_{sol}}$ is the count rate from solution (sec^{-1}); k is the counting efficiency; A, the area of the electrode exposed to the counter (cm^2); c, the concentration of the organic material in solution (mole cm^{-3}); α, the specific activity of the organic material (curie mole^{-1}); μ, absorption coefficient of ^{14}C radiation in water [314 cm^{-1} (11)].

If adsorption occurs, the additional count rate is given by

$$\mathrm{cps_{ads}} = k\ 3.7\ 10^{10} \Gamma\ A\alpha \qquad [2]$$

where $\mathrm{cps_{ads}}$ is counts from the adsorbed material (sec^{-1}); and Γ is the amount of adsorbed material (mole cm^{-2}).

The total recorded count rate from [1] and [2] above is

$$cps_{sol} + cps_{ads} = k\ 3.7\ 10^{10}\ A\alpha\left(\frac{c}{\mu} + \Gamma\right) \quad [3]$$

In order to determine Γ from Eq. [3] we have to count under identical experimental conditions a solution of known specific activity in which adsorption is negligible ($\Gamma << c/\mu$). A 10^{-2}M $Na_2{}^{14}CO_3$ solution was used for this calibration after every experiment. Adsorption of CO_3'' does not influence this calibration technique, since the condition $\Gamma << c/\mu$ would still be fulfilled in a 10^{-2}M solution.

The specific activities of the $Na_2{}^{14}CO_3$ solution and the solutions of the organic compounds were determined in a liquid-scintillation counter with a standard deviation of several runs less than ±2%. The labelled organic material was supplied by Chemtrac Corporation, Boston. It was purified and analyzed by gas chromatography directly before delivery. The carbonate solution (Nuclear Chicago) was checked against a NBS standard solution.

The reproducibility of determinations of the adsorbed amount was found to be from 5 to 10% in the concentration range 2.10^{-7} to 10^{-4}M. The reproducibility was checked for every compound at all concentrations and potentials.

Results

Aromatic compounds.—

(*A*) The surface coverage as a function of potential at constant solution concentration is given in Fig. 2 to 4. The surface coverage θ is given by

$$\theta = \frac{\Gamma}{\Gamma_{max} \cdot R} \quad [4]$$

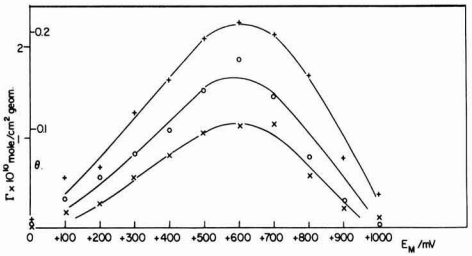

Fig. 2. Adsorption of benzene on gold from aqueous solution as a function of potential. C_{H2SO4} = 0.5M. —×—, 2.10^{-4}M benzene; —O—, 5.10^{-4}M benzene; —+—, 10^{-3}M benzene.

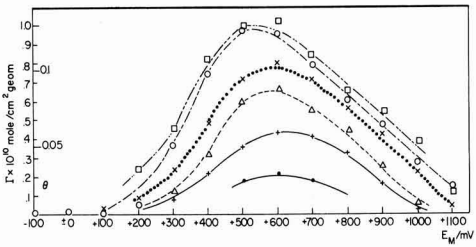

Fig. 3. Adsorption of naphthalene on gold from aqueous solution as a function of potential. C_{H2SO4} = 0.5M, temperature, 25°C. —●—, 1.10^{-7}M naphthalene; —+—, 2.10^{-7}M naphthalene; —△—, 5.10^{-7}M naphthalene; ●●●×●●●, 10^{-6}M naphthalene; —·—O—·—, 5.10^{-5}M naphthalene; —·—□—·—, 10^{-4}M naphthalene.

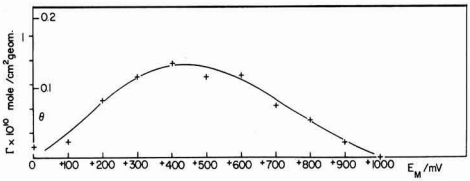

Fig. 4. Adsorption of phenanthrene on gold from aqueous solution as a function of potential. C_{H2SO4} = 0.5M; $C_{phen.}$ = 10^{-6}M.

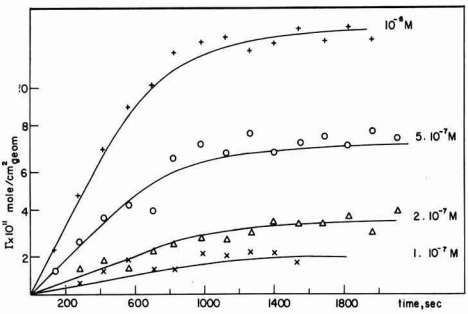

Fig. 5. Time dependence of naphthalene adsorption at +500 mv (NHE) for various concentrations of naphthalene (solution stirred at 60 rp).

where Γ is the amount adsorbed per apparent unit area; Γ_{max} is the maximal adsorbed amount in 1 monolayer (calculation as shown below); and *R* is the roughness factor of the electrode, determined by the BET method to be 2.2 ± 0.2.

(*B*) Time effects. The adsorption in more dilute solutions showed a considerable time-dependence (Fig. 5). The solution was stirred at 60 rpm. The equilibrium value at each potential was constant for hours after equilibrium had been established.

(*C*) Temperature effects. The temperature-dependence of adsorption was checked for the adsorption of naphthalene at 25° and 5°C. The change of the maximal adsorption at *E* = +500 mv was less than 5%.

(*D*) The surface coverage for naphthalene as a function of the solution concentration is plotted in Fig. 6 over the concentration range 10^{-7} to 10^{-6}M. For the other aromatic compounds (benzene

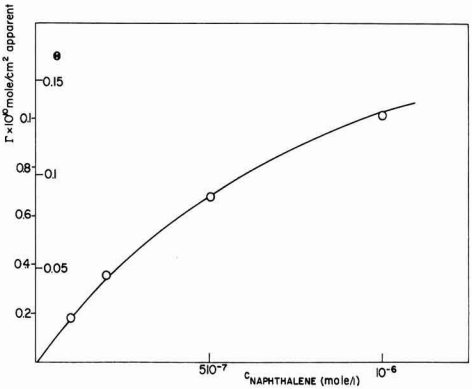

Fig. 6. Adsorption isotherm for naphthalene at +500 mv (NHE)

Table I. Limit of detectible adsorption of cyclohexane n-octanoic acid and n-decanoic acid

Compound	Solution concentration, mole/l	Sensitivity (adsorption must be lower than)
Cyclohexane	5.10^{-5}	θ^* <0.02
	10^{-5}	<0.01
	10^{-6}	<0.01
n-octanoic acid	10^{-5}	<0.005
n-decanoic acid	2.10^{-5}	<0.03
	10^{-4}	<0.06

* θ calculated using Eq. [4] [$\Gamma_{max} = 2.10^{-10}$ mole/cm² for cyclohexane; $\Gamma_{max} = 8.10^{-10}$ mole/cm² for the aliphatic chains as experimentally observed by Blomgren, Bockris, and Jesch (10) and Hansen *et al.* (1)].

and phenanthrene) the concentration dependence could not be studied over a sufficient concentration range because the specific activity available for benzene was too small and the solubility of the phenanthrene is too low.

Aliphatic compounds.—There was no measurable adsorption of the aliphatic compounds, cyclohexane, n-octanoic acid, and n-decanoic acid. Table I gives the sensitivity of the experimental arrangement. The sensitivity depends on the background of the solution and the available specific activity of the labelled compound.

Discussion

Adsorption Isotherm

The competitive adsorption of two species from a liquid phase has been treated by numerous authors, *e.g.*, (12-15), by means of the Langmuir isotherm. Recently, a Temkin isotherm was applied to the adsorption of neutral molecules on electrodes (16).

The isotherms, however, have to be modified if the two species in competition do not cover an equal molecular area at the surface. For the general case of different size of the species a relation based on the Langmuir isotherm will be given here. The competitive adsorption of species with different size has been treated recently for adsorption from the gas phase (17) and from nonelectrolyte solutions (18). The adsorption on electrodes will be derived here in terms of surface coverage.

The reaction leading to adsorption can be formulated as

$$n[\text{Water}_{ads}] + [\text{Organ}_{sol}] = n[\text{Water}_{sol}] + [\text{Organ}_{ad}] \qquad [5]$$

n is the number of molecules of water which occupy the same surface area as one molecule of the organic compound. n is given by

$$n = \frac{\Gamma_{max,\ water}}{\Gamma_{max,\ organic}} \qquad [6]$$

where Γ_{max} (mole/cm²) is the amount forming a monolayer of water and organic species, respectively.

Under ideal conditions (negligible interaction between the adsorbed particles, activity coefficients = 1) the electrochemical potential of the adsorbed organic entity in Eq. [5] may be written

$$\bar{\mu}_{org,ad} = \bar{\mu}^{o}_{org,ad} + RT \ln \theta \qquad [7]$$

where $\bar{\mu}_{org,ad}$ is the electrochemical potential of the adsorbed organic species, $\bar{\mu}^{o}_{org,ad}$ is the standard electrochemical potential referred to the standard state of complete coverage with the organic compound. θ is the surface fraction covered by the organic species as defined by

$$\theta = \frac{\Gamma_{org}}{\Gamma_{max,org}} \qquad [8]$$

For the adsorbed water the electrochemical potential is given by

$$\bar{\mu}_{w,ad} = \bar{\mu}^{o}_{w,ad} + RT \ln (1-\theta) \qquad [9]$$

The electrochemical potentials of the species in solution are written in the usual way, *viz.*

$$\bar{\mu}_{org,s} = \bar{\mu}^{o}_{org,s} + RT \ln X_{org,s} \qquad [10]$$

and

$$\bar{\mu}_{w,s} = \bar{\mu}^{o}_{w,s} + RT \ln X_{w,s} \qquad [11]$$

where $X_{org,s}$ and $X_{w,s}$ are the mole fractions of organic and water, respectively.

For equilibrium according to Eq. [5]

$$\bar{\mu}_{org,s} + n\bar{\mu}_{w,ad} = \bar{\mu}_{org,ad} + n\bar{\mu}_{w,s} \qquad [12]$$

Taking Eq. [7] and [9]-[11] for the electrochemical potentials and expressing the difference in standard free energy as

$$\Delta\bar{G}^{o} = \bar{\mu}^{o}_{org,ads} - \bar{\mu}^{o}_{org,s} - n(\bar{\mu}^{o}_{w,ads} - \bar{\mu}^{o}_{w,s}) \qquad [13]$$

the isotherm is given by,

$$\frac{\theta \cdot X_{w,s}^{\,n}}{(1-\theta)^n \cdot X_{org,s}} = e^{-\frac{\Delta\bar{G}^{o}}{RT}} \qquad [14]$$

In dilute solutions of the organic species in water $X_{w,s}$ becomes constant = 1 and [14] is then

$$\frac{\theta}{(1-\theta)^n} = e^{-\frac{\Delta\bar{G}^{o}}{RT}} \cdot X_{org,s} = K_a \cdot X_{org,s} \qquad [15]$$

Equation [15] differs from the Langmuir equation by the power factor n.

The change of the ideal isotherms with n is plotted in Fig. 7 against an arbitrary concentration scale. For better comparison the concentration scale is chosen so that θ values of 0.25 coincide. It is evident that the value of n has a strong influence on the isotherm. For higher n-values the gradient of the curve decreases significantly even at low coverages.

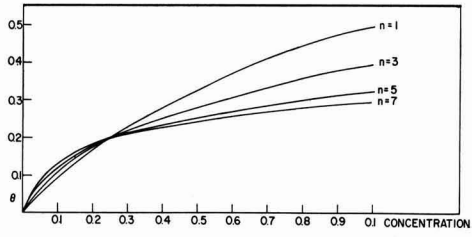

Fig. 7. Theoretical adsorption isotherms for competitive adsorption for molecules of various size ratios (n).

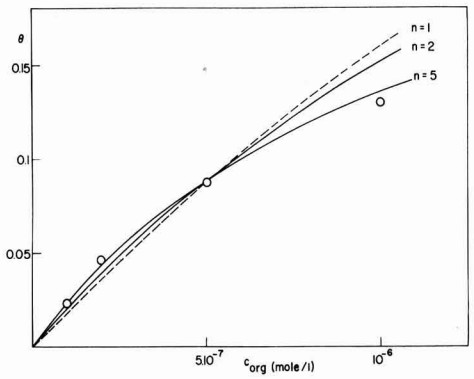

Fig. 8. Experimental values (○) of naphthalene adsorption at +500 mv (NHE) and calculated isotherms (Eq. [15]) for a planar position of naphthalene on the electrode ($n = 5$), a perpendicular position ($n = 2$), and equal size of the adsorbing species ($n = 1$).

This behavior is in good agreement with our experimental data for naphthalene (Fig. 8) for which $n = 5$ in planar configuration (Table III).

Free Energy of Adsorption of Aromatic and Aliphatic Compounds

The fact that only the aromatic compounds are adsorbed while the aliphatic compounds showed no detectable adsorption indicates the interaction of the aromatic π-electrons with the metal.

The solubilities of the investigated aliphatic compounds in aqueous solutions are similar to those of the aromatic entities (Table II).

For quantitative considerations the free energy of adsorption can be calculated from Eq. [15] for the more intensively studied systems (Table II). The adsorption values are taken at a potential near the maximum of adsorption, *i.e.*, $E_H = +500$ mv.

Table II. Adsorption and solubility of various organic compounds at the gold electrolyte interface

Compound	Solubility, mole/l	Adsorption at solution concentration $\frac{1}{10}$ saturated
Benzene	$1.1\ 10^{-2}$	$\theta = 0.2$
Naphthalene	$2\ 10^{-4}$	$\theta = 0.12$
Phenanthrene	$\sim 4\ 10^{-6}$	$\theta = 0.1$
Cyclohexane	$2.\ 10^{-4}$	Not detectable ($\theta < 0.01$)
n-Octanoic acid	$5.\ 10^{-3}$	Not detectable ($\theta < 0.005$)
n-Decanoic acid	$1.7\ 10^{-4}$	Not detectable ($\theta < 0.003$)

Table III. Geometrical areas of various molecules adsorbed on gold

Compound	Molecular area calculated from Fisher-Taylor-Hirshfelder models		Monolayer calculated $\times 10^{10}$ mole cm^{-2}		Experimental observed maximum adsorption $\times 10^{10}$ mole cm^{-2}
	Planar	Perpendicular	Planar	Perpendicular	
Benzene	34Å^2	18Å^2	5.0	9.5	2.3
Naphthalene	49Å^2	22Å^2	3.5	7.7	1.0
Phenanthrene	65Å^2	30Å^2	2.6	5.7	0.8
Cyclohexane	36Å^2	20Å^2	4.6	8.3	<0.05
(Water)	10Å^2		~17		

The free energy of adsorption as calculated from Eq. [15] and defined by Eq. [13] still contains contributions from organic compound-solvent interactions and the organic compound in its pure form. In order to compare the adsorption energy of the different compounds these contributions have to be excluded. This is done by replacing the mole fraction of the organic compound in the solution $X_{org,sol}$ in Eq. [15] by the activity and referring the activities of the organic compound in solution to a standard state in the gas phase.

In a saturated solution the vapor pressure of the organic is the same over the saturated solution and over the pure organic compound. So we can write

$$a_{org,sol} = p\frac{X_{org}}{X_{org\ sat}} \qquad [16]$$

where p is the vapor pressure of the organic compound at 25°C, X_{org} the mole fraction of the organic in solution, and $X_{org\ sat}$ is the mole fraction of the organic compound in the saturated solution.

In order to compare different compounds expression [16] has to be employed for both, so that the difference in their energy of interaction with the solution is then given by

$$\Delta\mu_{interaction} = RT \ln \frac{a_{1,org\ sol}}{a_{2,org\ sol}} = RT \ln \frac{p_1 \cdot X_{1\ org} \cdot X_{2,org\ sat}}{p_2 \cdot X_{2\ org} \cdot X_{1,org\ sat}} \qquad [17]$$

Adding this $\Delta\mu$ term to the free energy of adsorption $\Delta\bar{G}^{\circ}$ (Eq. [14]) we obtain free energies which are comparable (Table IV).

It can be seen from the last column in Table IV that there is a considerable difference in the free energy (more than 3 kcal mole^{-1}) between comparable aliphatic compounds and aromatic compounds. This difference is attributed to π-bond/metal interaction. This comparison is possible because cyclohexane has about equal size and vapor pressure as benzene and has a solubility similar to that of naphthalene. The same comparison holds qualitatively for the other aliphatic compounds, n-octanoic acid and n-decanoic acid.

On the mercury-electrolyte interface aromatic and aliphatic compounds are adsorbed (10), while on the gold-electrolyte interface no detectable adsorption of aliphatics was found from solutions of equivalent concentration. This result can be interpreted that the bonding between gold and water is stronger than between mercury and water. Hence only the bonding aromatic compound-gold can overcome the increased bonding gold-water while the

Table IV. Comparison of free energies of adsorption of organic compounds at the gold electrolyte interface

	$\Delta\bar{G}^{\circ}$ (Eq. [14]), kcal mole^{-1}	$P_{25°C}$, atm	Solubility, $X_{org\ sat}$	$\Delta\bar{G}^{\circ} - \Delta\mu_{interaction}$, kcal mole^{-1}
Benzene	−6.1	0.125	$4.1\ 10^{-4}$	−6.1
Naphthalene	−0.7	$0.40.10^{-4}$	$4.8.10^{-6}$	−8.0
Cyclohexane	<−5.8	0.130	$3.6.10^{-6}$	<−2.8

Vapor pressures and solubilities were taken from ref. (19-21).

aliphatic compounds do not have the necessary energies. Unfortunately, no reliable data on the adsorption energy of water on gold are available.

Orientation of the Adsorbed Species

The experimentally observed maximum adsorption is considerably smaller than the calculated maximum values for a monolayer either in planar or in perpendicular orientation to the surface (Table III). Therefore no conclusion on the question of orientation can be drawn from the observed upper limit of coverage.

Evidence for the planar position (which would seem to favor π-bond interaction) is provided by the shape of the adsorption isotherm (Fig. 8).

It can be seen from Fig. 8 that the experimental values are fitted best by an isotherm calculated with Eq. [15] assuming a planar position of naphthalene on the electrode ($n = 5$). The isotherms calculated under the assumption of a perpendicular position ($n = 2$) or of equal size ($n = 1$) do not fit the results.

Influence of Electrical Field on Adsorption

The potential dependence of the adsorption of neutral molecules on electrodes can be due to one or more of the following factors:

1. The coverage of the electrode with hydrogen or oxide layers at cathodic or anodic potentials, respectively.

2. The specific adsorption of ions of the electrolyte solution and the adsorption of counter ions at the charged electrode.

3. The change of the free energy of adsorption of the water and the organic compound with the electrical potential.

In the case of gold in $1N$ H_2SO_4 the coverage with hydrogen or oxygen is negligible in the investigated potential region [hydrogen coverage less than 4% at $E_H = 0$ mv (22); oxygen coverage less than 10% at $E_H = +1100$ mv (23)].

The specific adsorption of ions seems not to play an important role in this system since the effects of the potential in the Gouy layer could be interpreted only under the assumption of no specific adsorption (28). The change in the free energy of adsorption of water and an organic species with the applied electrical field was treated by Frumkin (24), Butler (25), and Bockris, Devanathan, and Müller (26). These electrical contributions to the free energy of adsorption are different for water and the organic species. If the dipole moment of the organic species in the double layer (in our case = 0) is negligible compared with the effective dipole moment of water, the water plays the dominant role. [Differences in the polarizabilities between the organic and the water have no significant influence (26).] The theory (24-26) predicts, in this case, a maximum of adsorption near the point of zero charge of the metal with monotonically decreasing adsorption to negative and positive potentials.

This general picture is in agreement with our observations on gold. The point of zero charge of gold was determined by Pfuetzenreuther and Masing (27) to be at $E_H = +300$ to $+400$ mv. Our recent determination of the zero charge point (28) is in agreement with these data ($E_H = +300 \pm 50$ mv). The maximum of adsorption (Fig. 2-4) was observed to be at potentials of $E_H = +500$ to $+600$ mv. This fact has to be considered as a partial confirmation of the predominant role of water in determining the shape of the adsorption *vs.* potential curves on gold.

Acknowledgments

The authors are grateful to Professor J. O'M Bockris for the encouragement of this work. They wish to thank Mr. D. A. Swinkels of this laboratory for carrying out BET measurements on our gold electrodes and also for numerous stimulating discussions of this work. It is also a pleasure to thank the United States Steel Corporation for generous support of this research.

Manuscript received Nov. 27, 1962; revised manuscript received April 22, 1963. This paper was presented at the Pittsburgh Meeting, April 15-18, 1963.

Any discussion of this paper will appear in a Discussion Section to be published in the June 1964 JOURNAL.

REFERENCES

1. *E.g.*, R. Hansen and B. Clampitt, *J. Phys. Chem.*, **58**, 908 (1954); R. Hansen, R. Minturn, and D. Hickson, *ibid.*, **60**, 1185 (1956).
2. B. E. Conway and R. G. Barradas, Transact. Phila. Symp. Electrode Proc., Philadelphia 1959, p. 299, John Wiley & Son, Inc., New York (1961); B. E. Conway, R. G. Barradas, and T. Zawidski, *J. Phys. Chem.*, **62**, 676 (1958).
3. F. Joliot, *J. Chem. Phys.*, **27**, 119 (1930).
4. W. H. Power and J. W. Heyd, *Anal. Chem.*, **28**, 523 (1956).
5. I. A. Kafalas and H. C. Gatos, *Rev. Sci. Instr.*, **29**, 47 (1958).
6. Ch. Weissmantel, Thesis, Dresden, Germany (1958).
7. H. D. Cook, *Rev. Sci. Instr.*, **27**, 1081 (1956).
8. E. Blomgren and J. O'M. Bockris, *Nature*, **186**, 305 (1960).
9. H. Wroblowa and M. Green, To be published.
10. E. Blomgren, J. O'M. Bockris, and C. Jesch, *J. Phys. Chem.*, **65**, 2000 (1961).
11. W. F. Libby, *Phys. Rev.*, **103**, 1900 (1956).
12. A. Frumkin, *Z. physik. Chem.*, **116**, 466 (1925).
13. For comprehensive bibliography see J. J. Kipling, *Quart. Rev.*, **5**, 60 (1951).
14. E. Blomgren and J. O'M. Bockris, *J. Phys. Chem.*, **63**, 1425 (1959).
15. R. G. Barradas and B. E. Conway, *Electrochim. Acta*, **5**, 349 (1961).
16. P. Delahay and D. M. Mohilner, *J. Am. Chem. Soc.*, **84**, 4247 (1962).
17. S. Yu. Elovich and O. G. Larionow, *Izvest. Akad. Nauk USSR, Otdel. khim. Nauk*, **1962**, 531.
18. S. Yu. Elovich and O. G. Larionow, *ibid.*, **1962**, 209.
19. R. L. Bohen and W. F. Claussen, *J. Am. Chem. Soc.*, **73**, 1572 (1951).
20. "Handbook of Chemistry and Physics" The Chemical Rubber Publishing Co., Cleveland, Ohio, 1960.
21. A. Timmermanns, " Physico Chemical Constants," Elsevier Publishing Co., New York (1950).
22. M. Breiter, C. A. Knorr, and W. Völkl, *Z. Elektrochem.*, **59**, 681 (1955).
23. H. Dahms, J. O'M. Bockris, To be published.
24. A. Frumkin, *Z. Physik*, **35**, 792 (1926).
25. J. Butler, *Proc. Roy. Soc. (London)*, **A122**, 399 (1929).
26. J. O'M. Bockris, M. Devanathan, and K. Müller, Paper presented at CITCE Meeting Rome, 1962.
27. A. Pfuetzenreuther and G. Masing, *Z. Metallk.*, **42**, 361 (1951).
28. M. Green and H. Dahms, *This Journal*, **110**, 466 (1963).

Technical Notes

The Semiconducting Nature of Stannic Oxide

L. D. Loch

Research Branch, Research and Development Division, The Carborundum Company, Niagara Falls, New York

The research reported here is part of a broad study of SnO_2-based compositions as semiconductors. The electronic configurations of the outer shells of the Sn and O atoms are $5s^25p^2$ and $2s^22p^4$, respectively. Therefore, in forming solid SnO_2 the 5s and 5p electrons of the Sn atom are transferred to O atoms. Each O atom can accept two electrons in its 2p orbital to form a stable octet. On this basis a simple picture of the band structure of SnO_2 consists of a 5s conduction band and a 2p valence band, separated by a forbidden gap. As the 5s band is a broad band, we expect broad-band semiconduction.

The purpose of this particular phase of research was to determine whether SnO_2 actually does show broad-band behavior.

The literature contains many references to the properties of SnO_2 films and coatings as these have been commercial products for many years. Very few detailed studies can be found, however, on polycrystalline bodies or single crystals. Marley (1) and Reed (2) both have grown single crystals, but have not reported on their properties as yet.

A recent paper by Kohnke (3) on the electrical and optical properties of natural SnO_2 crystals is of interest. Kohnke found a value of 0.72 ev for the conductivity activation energy, compared to 0.77 ev calculated from the data of Foex (4) on polycrystalline specimens. Two of Kohnke's crystals were fairly pure, with indicated carrier densities of only 4×10^{14} and 8×10^{14} cm^{-3}, respectively. These crystals had Hall mobilities of approximately 50 cm^2-v^{-1}-sec^{-1} at 200°C. Above 150°C, the variation of Hall mobility with temperature was not far different from the $T^{-1,5}$ dependence for simple lattice scattering. On the basis of his observed mobilities and activation energy and of an effective mass less than one, Kohnke concludes that SnO_2 behaves as a normal broad-band semiconductor in the extrinsic conductivity region above room temperature.

In our experiments σ and S were measured for four different values of the electron concentration which spanned nearly three decades of concentration. The electron concentration was controlled by adding Sb to the lattice. The outer electron configuration of Sb is $5s^25p^3$ so that each atom of Sb adds one electron to the conduction band of SnO_2.

Experimental

The measurements of σ and S were made simultaneously at temperatures between 100° and 900°C in vacuum and in air. Specimens were polycrystalline bars 0.5 x 0.5 x 5 cm. They were held in a lava jig placed inside a Vycor tube, which could be evacuated to 10^{-6} mm Hg. All contacts were spring loaded pressure contacts. They consisted of Pt sheet for the current leads at either end and of two Pt-Pt 100 Rh thermocouples mounted on one side and spaced approximately 2 cm apart. The thermocouples served as potential probes for a four-terminal measurement of σ and to measure the temperature drop ΔT.

All of the conductivity measurements were, in effect, made with d.c. However, the direction of current flow was reversed at a frequency of 12 cpm, producing square wave patterns for the voltage drops across the specimen and across a standard resistor. The furnace was moved by small increments along the axis of the specimen to vary ΔT between 5° and 20°C. The resistive voltage drop V_{IR} across the specimen was obtained from the amplitude of the square wave, while the thermoelectric voltage V_T was obtained from the position of the square wave with respect to zero. The current was calculated, of course, from the voltage drop through the standard resistor.

Specimens were prepared from "Certified" reagent grade SnO_2 and Sb_2O_3 obtained from Fisher Scientific Company. The chief impurities in the SnO_2, as determined by spectrographic and wet analysis, were 0.10% Cu and 0.07% Pb. Neither of these impurities seemed to be electronically active. The ingredients were mixed in an acetone slurry and mixing was continued while the acetone evaporated. The essentially dry powder then was cold pressed at 8000 psi and sintered at 1400°C in air.

Results and Discussion

At the outset of this research the electronic measurements were made in air and in vacuum. It was found that the measurements in air were not very reproducible, while those in vacuum were. Also, the specimens behaved in air as though the Sb were coming out of solution at the lower temperatures. This is shown in Fig. 1, where the conductivities of highly doped (0.1 mole % Sb_2O_3) specimens in air and in vacuum are compared. It was not possible to prove conclusively our suspicion that the Sb was coming out of solution by means of x-ray diffraction. The shift in the x-ray lines as a result of solution of Sb in the SnO_2 lattice is too small to detect with assurance. However, in order to

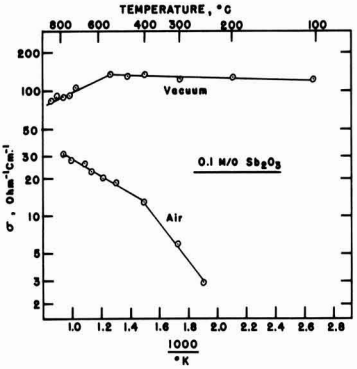

Fig. 1. σ for heavily doped SnO_2 in vacuum and in air

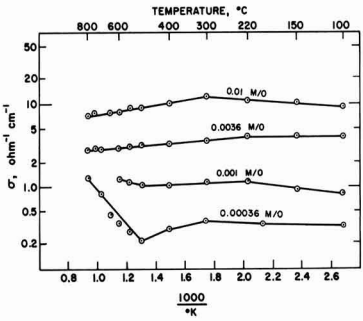

Fig. 2. σ vs. temperature for four doping levels

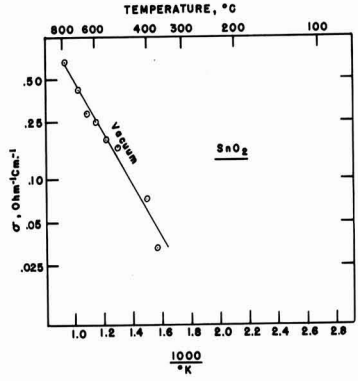

Fig. 3. σ for undoped SnO_2 in vacuum

obtain reproducible results and to insure that the Sb remained in solution, most of the experiments were conducted in vacuum.

Values of σ *vs.* temperature for four doping levels are shown in Fig. 2. These curves are typical of saturated extrinsic conduction as they show very little dependence on temperature; that is, the donors are completely ionized at and above room temperature. This agrees with the observation by Imai (5) that the donor levels in Sb-doped SnO_2 are already fully ionized at liquid nitrogen temperature.

To be certain that the majority of the conduction electrons were supplied by the Sb dopant and not by defects, σ of the undoped Fisher SnO_2 was measured in vacuum at temperatures up to 800°C. Comparison of the resulting data, shown in Fig. 3, with those in Fig. 2 suggests that the number of free electrons arising from defects is negligible compared to those supplied by the Sb donor levels, except at the very highest temperatures and the lowest Sb concentrations. The steeply rising conductivity of the 0.00036 mole % Sb specimen above 500°C in Fig. 2 is evidence that defect carriers are becoming important in this instance.

Plots of σ *vs.* N_d at constant temperature, where N_d is the concentration of Sb donor atoms, are quite linear. By means of the usual equation: $\mu = \sigma/ne$, and our observation that ionization of donors is complete, so that $n = N_d$, values for the electron mobility μ of 10.9 to 12.0 cm^2-v^{-1}-sec^{-1} were calculated for the temperature range 100°-500°C. Although at any one temperature the maximum deviation of μ from the average is 10% or less, there is no perceptible dependence of mobility on temperature.

One would expect to have contributions to electron scattering from both lattice vibrations and ionized impurities. As lattice scattering would cause a decrease in μ with increasing temperature while impurity scattering would have the opposite effect, the two types of scattering might tend to compensate each other over the temperature range of interest, thus accounting for the small change with temperature. However, final conclusions about the variation of μ with temperature should not be attempted on the basis of data obtained on polycrystalline semiconductors where the influence of particle size and chemical changes can be appreciable. The good agreement obtained here among the mobilities calculated for four different doping levels is about the most one can expect when working with polycrystalline materials.

The above range for μ compares favorably with the Hall mobilities of 17-32 cm^2-v^{-1}-sec^{-1} measured on SnO_2 films by Ishiguro *et al.* (6). Finally, Kohnke's value of 50 cm^2-v^{-1}-sec^{-1} is in reasonable agreement with our data, as one expects higher values of μ in single crystals than in polycrystalline compacts.

Comparison of the above values for μ with those for other oxides, both broad-band and narrow-band, shows rather conclusively that SnO_2 is a broad-band semiconductor. For example, room temperature Hall mobilities for the known broad-band oxide ZnO have been reported to be 60 cm^2-v^{-1}-sec^{-1} for sintered material (7) and 200 cm^2-v^{-1}-sec^{-1} for single crystals (8). On the other hand, two oxides of Ti, which almost certainly exhibit 3d narrow-band conduction have shown mobilities of 0.1-1.0 cm^2-v^{-1}-sec^{-1} for TiO_2 single crystals (9) and 0.36 cm^2-v^{-1}-sec^{-1} for polycrystalline TiO (10, 11). These values for μ are one to two orders of magnitude lower than those for SnO_2.

Our values of S up to about 900°C for the four doping levels are shown in Fig. 4. All of the values are negative, and they become numerically smaller as n increases. At the lower temperatures, there is a rapid increase in S with increasing temperature.

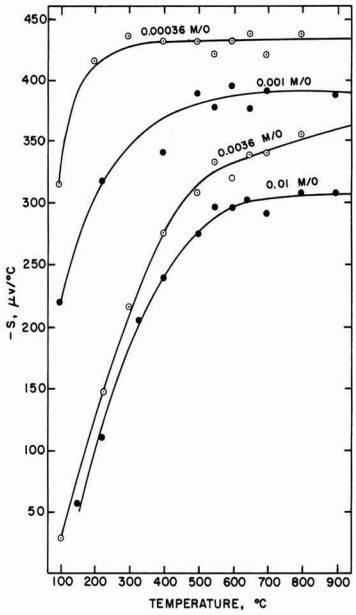

Fig. 4. S vs. temperature for four doping levels

The data of Fig. 4 were analyzed using the customary equations from classical statistics for nondegenerate broad-band semiconductors: $n = N_c \exp(E_F/kT)$ and $eST = E_F - 2kT$, where N_c is the effective density of states in the conduction band and E_F is the Fermi energy level with respect to the conduction band edge, *i.e.*, $E_F = \epsilon_F - \epsilon_c$. On combining these equations one obtains $eS/k = 2.303 \log (n/N_c) - 2$. As N_c is constant at a given temperature, the quantity eS/k should be a linear function of $\log n$. That this is the case is shown in Fig. 5, in which eS/k is plotted against $\log n$ at four different temperatures. This agreement is further evidence that SnO_2 is a broad-band semiconductor.

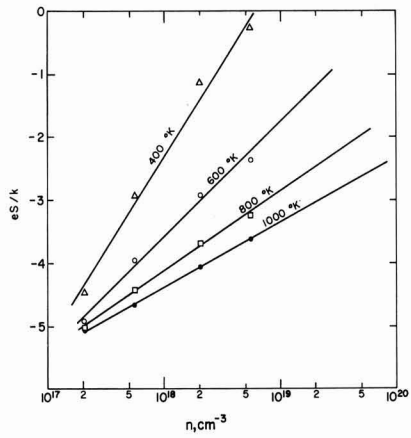

Fig. 5. eS/K vs. n for four temperatures

Summary

On the basis of electron mobilities calculated from the conductivities of Sb-doped polycrystalline specimens and the behavior of the Seebeck coefficient of such specimens, it is concluded that SnO_2 is a broad-band semiconductor. This agrees with Kohnke's conclusion, which was based on the Hall mobility and donor activation energy in natural single crystals. SnO_2 showed n-type behavior throughout.

Acknowledgment

The author wishes to acknowledge the fine assistance of Mr. W. H. Kaufmann in the experimental portion of this research.

Manuscript received April 2, 1963; revised manuscript received June 25, 1963. This paper was presented at the Boston Meeting, Sept. 16-20, 1963.

Any discussion of this paper will appear in a Discussion Section to be published in the June 1964 JOURNAL.

REFERENCES

1. J. A. Marley and T. C. MacAvoy, *J. Appl. Phys.*, **32**, 2504 (1961).
2. T. B. Reed, J. T. Roddy, and A. N. Mariano, *ibid.*, **33**, 1014 (1962).
3. E. E. Kohnke, *J. Phys. Chem. Solids*, **23**, 1557 (1962).
4. M. Foex, *Bull. soc. chim. France*, **11**, 6 (1944).
5. I. Imai, *J. Phys. Soc. Japan*, **15**, 937 (1960).
6. K. Ishiguro, T. Sasaki, T. Arai, and I. Imai, *ibid.*, **13**, 296 (1958).
7. S. E. Harrison, *Phys. Rev.*, **93**, 52 (1954).
8. A. R. Hutson, *ibid.*, **108**, 222 (1957).
9. R. G. Breckenridge and W. R. Hosler, *ibid.*, **91**, 793 (1953).
10. A. D. Pearson, *J. Phys. Chem. Solids*, **5**, 316 (1958).
11. F. J. Morin, "Semiconductors," Chap. 14, N. E. Hannay, Editor, Reinhold Publishing Corp., New York (1959).

X-Ray Diffraction Study of Evaporated CdS Films

Arthur J. Behringer and Lester Corrsin

Fundamental and Applied Research Laboratories, Xerox Corporation, Rochester, New York

An x-ray diffraction study was made of the structure of CdS films deposited on amorphous substrates as a function of substrate temperature. A marked decrease in condensate was observed with increase in substrate temperature. Modifications of the films' crystallinity and preferred orientation with changing deposition temperature were observed. Pyrolytic treatment of films in contact with $CdCl_2$ containing CdS powder resulted in modifying the orientation from preferred to random.

Optical and electrical measurements on evaporated cadmium sulfide films have been reported extensively in the literature (1-9). However, only a few publications describe the structure of such

films (10, 11). In one of these, Gilles and Van Cakenberghe (11), using x-ray diffraction studies, conclude that cadmium sulfide evaporated on heated amorphous glass substrates forms principally hexagonal crystallites with the C-axis normal to the substrate surface.

Film Preparation

General Electric EL grade CdS pellets were evaporated from molybdenum source, 800° ± 10°C, on preheated tin oxide coated borosilicate glass substrates at a pressure of about 4 x 10^{-5} Torr. The deposition temperatures ranged between 70° and 445°C. For the same quantity of starting material, the film thicknesses, measured with a profilometer, varied markedly according to deposition temperature. Thicknesses ranged from less than 1μ to 15μ at deposition temperatures of 445° and 250°C, respectively; thicknesses recorded for films deposited at 350° and 400°C were about 3μ.

Analysis of Films

Film crystallinity was examined with nickel-filtered copper radiation, using a General Electric XRD-5 Diffractometer Unit. In agreement with the findings of Gilles and Van Cakenberghe, the OOOL series of reflections appeared in all the diffractometer patterns, indicating preferred orientation with the C-axis normal to the substrate. In addition, the crystallites in the films were frequently found to be oriented with either or both the $10\bar{1}3$ and $10\bar{1}5$ lattice planes positioned parallel to the substrate. Considerable broadness in these later reflections was observed in patterns for films deposited at substrate temperatures between 70° and 250°C; this is presumably due to stacking faults, a condition described in some detail for cobalt by Edwards and Lipson (12). In the diffractometer patterns of the films deposited at the higher substrate temperatures, the reflections appeared sharp, indicating an enhancement of crystalline perfection attributable to the higher deposition temperatures. The presence of well-formed hexagonal crystallites in these films was confirmed on inspection of x-ray photograms of evaporated films stripped from their substrates and reduced to a fine powder.

Two methods used to enhance the photoconductivity in evaporated CdS films were studied to determine their effects on the crystallinity of films deposited on a substrate preheated to 350°C. One method, direct air-baking of film at 480°C for 1 hr, was found to have virtually no effect in altering the preferred orientation (Fig. 1a). This result is in agreement with the findings of Gilles and Van Cakenberghe (11). In the other method a similar film was heat-treated for the same duration at 480°C in contact with a copper-chlorine-doped cadmium sulfide powder containing an estimated 0.5% $CdCl_2$; the orientation of the crystallites was altered from preferred to random (Fig. 1b). The powder used in this heat treatment is hexagonal, as indicated in Fig. 1c. A random orientation also results if the film is similarly heat-treated in contact with a chlorine-doped CdS powder containing approximately 0.5% $CdCl_2$ and essentially free of copper; however, unactivated, $CdCl_2$-free CdS powder has virtually no effect on altering the orientation. These results indicate that the trace amount of $CdCl_2$ in the CdS powder is the influential factor. The presence of the chloride at the film surface probably initiates recrystallization at the surface by chemical exchange, resulting in crystal growth with the crystallites randomly oriented.

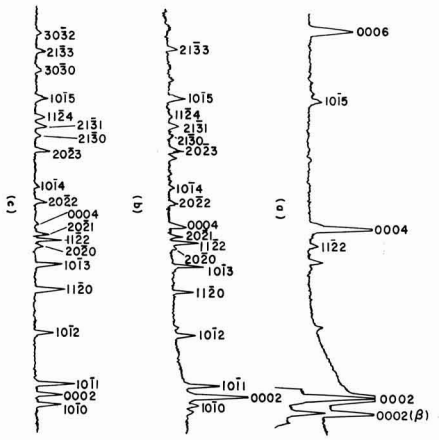

Fig. 1. X-ray diffractometer patterns, demonstrating the effect of heating evaporated CdS films previously deposited at 350°C: (a) at a temperature of 480°C for 1 hr in air; (b) in contact with Cu-Cl doped hexagonal CdS powder containing 0.5% $CdCl_2$; (c) pattern for the cadmium sulfide powder referred to in (b). The ordinate scale in each pattern is logarithmic.

Remarks

The details of the observed relationship between the quantity of condensate and the deposition temperature are not understood at this time; presumably a thorough investigation of the vapor phase composition will solve this problem. The aforementioned technique to obtain random orientation in evaporated CdS films may well be extended to evaporated films of other materials.

Acknowledgments

Appreciation is expressed to Drs. John C. Schottmiller, Paul Cherin, and Michael Smith for their helpful discussions and suggestions, to Keith Johnson for obtaining the x-ray diffraction data and to R. Moore who prepared the evaporated films. This work was supported by the Department of the Navy, Bureau of Naval Weapons under Contract No. NOas 59-6166-c.

Manuscript received March 27, 1963; revised manuscript received July 8, 1963.

Any discussion of this paper will appear in a Discussion Section to be published in the June 1964 JOURNAL.

REFERENCES

1. K. Weiss, German Pat. 837,424 (Apr. 28, 1952).
2. J. Gottesman and W. F. C. Ferguson, *J. Opt. Soc. Am.*, **44**, 368 (1954).
3. J. F. Hall and W. F. C. Ferguson, *ibid.*, **45**, 714 (1955).
4. A. B. Bramley, *Phys. Rev.*, **98**, 246 (1955).

5. A. Carlson, WADC Tech. Rept. 56-62, ASTIA 132274.
6. R. Lawrence, *Brit. J. Appl. Phys.*, **10**, 298 (1959).
7. H. I. Moss, *RCA Rev. XXII*, No. 1, 29 (1961).
8. K. V. Shalimova, T. S. Travina, and L. L. Golik, *Soviet Phys. Doklady*, **6** [5], 396 (1961).
9. K. V. Shalimova, T. S. Travina, and R. R. Rezby, *ibid.*, **6** [5], 404 (1961).
10. J. Dresner and F. V. Shallcross, *Solid State Electronics*, **5**, 205 (1962).
11. J. M. Gilles and J. Van Cakenberghe, "Solid State Physics in Electronics and Telecommunications," Vol. 2, Part 2, 900-906, Academic Press, Inc., New York (1960).
12. O. S. Edwards and H. Lipson, *Proc. Roy. Soc. (London)*, **A180**, 268 (1942).

Polarography of π-Complexes of Cobalt, Chromium, and Titanium in Formamide and Dimethylformamide

Hsiao-shu Hsiung[1] and Glenn H. Brown[2]

Department of Chemistry, University of Cincinnati, Cincinnati, Ohio

Few polarographic measurements appear to have been made on π-complexes. The work of Page and Wilkinson (1) showed the polarographic behavior of ferricinium, cobalticinium, and ruthenicinium ions in water. Pauson and Wilkinson (2) determined the half-wave potential for the solution of bis-indenylcobalt (III) ion while Wilkinson and Birmingham (3) reported polarographic data for the bis-cyclopentadienyl complexes of titanium (IV), vanadium (IV), and niobium (V) ions. With the exception of the niobium (V) complex all of these ions were found to give well-defined and reversible waves. The rhodicinium ion (4) shows a cathodic wave corresponding to the formation of neutral $Rh(C_5H_5)_2$. Kuwana *et al.* (5) studied the chronopotentiometric oxidation of a number of metal cyclopentadienyls and their derivatives in acetonitrile. They found ferrocene and its derivatives undergo a one-electron change, ruthenocene and its derivatives a two-electron change, while osmocene and its derivatives show a two-stage oxidation, involving one electron each in each stage.

Polarographic measurements have been made on a few π-complexes formed with compounds containing six-membered rings. Furlani and Fisher (6) were the first to investigate the $Cr(C_6H_6)_2$-$Cr(C_6H_6)_2^+$ transition. Furlani and Sartori (7) made polarographic measurements on compounds of the type $Ar_2Cr^+I^-$, where Ar is benzene, toluene, mesitylene, or pseudocumene; also, bis-cyclohexylphenylchromium iodide has been studied polarographically (8).

This paper reports the polarographic behavior of some aromatic complexes of cobalt, chromium, and titanium in two nonaqueous solvents, formamide and dimethylformamide.

Experimental

Formamide was purified as described previously (9) and N,N'-dimethylformamide obtained from the Matheson Company was purified by a method similar to that used by Wawzonek *et al.* (10). All polarographic measurements were made at a temperature of 25.0° ± 0.5°C and were taken in the same manner as reported in previous papers (9, 11).

[1] Present address: Department of Chemistry, Alton Center, Southern Illinois University, Alton, Illinois.

[2] Present address: Department of Chemistry, Kent State University, Kent, Ohio.

Cobalticinium triiodide, $(C_5H_5)_2CoI_3$, bis-indenylcobalt (III) perchlorate, $(C_9H_7)_2CoClO_4$, and bis-cyclopentadienyltitanium (IV) bromide, $(C_5H_5)_2TiBr_2$ were prepared according to Wilkinson (12), Pauson and Wilkinson (2), and Wilkinson and Birmingham (3), respectively. Bis-diphenylchromium (I) iodide, $(C_6H_5 \cdot C_6H_5)_2CrI$ and bis-benzenechromium (I) iodide, $(C_6H_6)_2CrI$, were contributed by H. H. Zeiss of the Monsanto Chemical Company.

Anhydrous sodium perchlorate was used as the supporting electrolyte for the study of the π-complexes of cobalt and chromium in both solvents. It was of "reagent grade" quality and was purchased from the G. Frederick Smith Chemical Company; it was used without further purification. Tetraethylammonium perchlorate, prepared according to the directions of Kolthoff and Coetzee (13), was used as the supporting electrolyte in formamide for the π-complex salt of titanium.

Results and Discussion

Of the π-complexes studied only the bis-cyclopentadienyltitanium (IV) bromide did not give a well-defined reduction wave. The polarographic characteristics of five different π-complexes are recorded in Table I. Our value of −0.81v *vs.* S.C.E. for the bis-benzenechromium cation in dimethylformamide compares favorably with the value obtained by Furlani and Fischer (6) who investigated its behavior in the mixture, 80% methanol-20%

Table I. Polarographic characteristics of some π-complexes of cobalt, chromium, and titanium
(supporting electrolyte 0.2M $NaClO_4$)

Compound	Conc. mM/l	$-(E1/2)$, v *vs.* S.C.E.	I_d	D $cm^2 \times 10^5$, sec	$0.059/n$
Formamide as the solvent					
$(C_6H_6)_2CrI$	2.0	1.04	0.85	0.194	0.062
$(C_6H_5 \cdot C_6H_5)_2CrI$	2.0	0.89	0.85	0.194	0.057
$(C_5H_5)_2CoI_3$	4.0	1.11	0.30	0.025	0.059
$(C_9H_7)_2CoClO_4$	2.0	0.71	0.81	0.177	0.072
$(C_5H_5)_2TiBr_2$*	2.0	0.62	0.57	0.088	—
N,N'-dimethylformamide as the solvent					
$(C_6H_6)_2CrI$	2.0	0.81	0.88	0.200	0.063
$(C_6H_5 \cdot C_6H_5)CrI$	2.0	0.75	0.57	0.088	0.063
$(C_9H_7)_2CoClO_4$	0.74	0.53	1.18	0.375	0.071

* Supporting electrolyte is Et_4NClO_4.

benzene (by volume). From the data presented it can be seen that bis-diphenylchromium (I) iodide reduces more readily than bis-benzenechromium (I) iodide in both solvents.

The value of n established from diffusion current data and results of others (6-8) show that the reduction of the π-complexes of chromium is a one-electron step and that the complexes have a rather high stability to reduction. Even though bis-indenylcobalt (III) perchlorate gives well-defined reduction waves in formamide and dimethylformamide, the reduction is not reversible if one electron is involved in the process. As expected the diffusion current constants for the π-complexes reported here are smaller than those of the simple metal ions in the same solvent (9) and in water (14).

The composition of the ligand has an influence on the half-wave potential of π-complexes. Considering polarographic data on π-complexes published by others (1-3, 6-9) along with those obtained in this study, one finds that the bonding of a ring-type compound to a metal ion generally causes a marked decrease in the reduction potential of the ion when compared to the simple metal ion in the same solvent. Increased aromaticity around the metal ion increases the ease of reduction [*e.g.*, compare $(C_6H_6)_2CrI$ and $(C_6H_5 \cdot C_6H_5)_2CrI$ in the two solvents used]. A trend is noted in that substitution of a group on the parent compound (*e.g.*, cyclopentadiene) compared to indene causes the half-wave potential to shift, the direction of the shift depending on whether the substituent is an electron donating group or an electron withdrawing group. It is observed from this study and others (5, 7, 8) that the electron donating group causes the potential to shift to a more negative value than that of the parent compound, and an electron withdrawing group causes the potential to shift in a more positive direction.

Acknowledgment

The authors wish to express their thanks to Dr. H. H. Zeiss of the Monsanto Chemical Company for supplying samples of bis-diphenylchromium (I) iodide and bis-benzenechromium (I) iodide.

Manuscript received Feb. 18, 1963; revised manuscript received June 18, 1963.

Any discussion of this paper will appear in a Discussion Section to be published in the June 1964 JOURNAL.

REFERENCES

1. J. A. Page and G. Wilkinson, *J. Am. Chem. Soc.*, **74**, 6149 (1952).
2. P. L. Pauson and G. Wilkinson, *ibid.*, **76**, 2024 (1954).
3. G. Wilkinson and J. M. Birmingham, *ibid.*, **76**, 4281 (1954).
4. F. A. Cotton. R. O. Whipple, and G. Wilkinson, *ibid.*, **75**, 3586 (1953).
5. D. E. Bublitz, G. Hoh, and T. Kuwana, *Chem. and Ind. (London)*, **1959**, 635.
6. C. Furlani and E. V. Fischer, *Z. Elektrochem.*, **61**, 481 (1957).
7. C. Furlani and G. Sartori, *Ricerca Sci.*, **28**, 973 (1958); *C.A.*, **52**, 19606 (1958).
8. I. A. Korshunov, L. N. Vertylina, G. A. Razuvaev, Y. A. Sorokin, and G. A. Domrachev, *Doklady, Akad. Nauk. (USSR)*, **122**, 1029 (1958); *C.A.* **53**, 1959 (1959).
9. G. H. Brown and H. S. Hsiung, *This Journal*, **107**, 57 (1960).
10. S. Wawzonek, E. Blaha, R. Berkey, and M. E. Runner, *ibid.*, **102**, 235 (1955).
11. G. H. Brown and R. Al-urfali, *J. Am. Chem. Soc.*, **80**, 2113 (1958).
12. G. Wilkinson, *ibid.*, **74**, 6148 (1952).
13. I. M. Kolthoff and J. F. Coetzee, *ibid.*, **79**, 870 (1957).
14. L. Meites, "Polarographic Techniques," p. 247 ff, Interscience Publishers, Inc., New York (1955).

Brief Communications

A High Performance Saturated Hydrocarbon Fuel Cell

W. T. Grubb and L. W. Niedrach

Research Laboratory, General Electric Company, Schenectady, New York

A key technical problem in fuel cells is the achievement of high electrochemical oxidation rates using cheap fuels. Among such fuels the saturated hydrocarbons represent a class of major importance. Heretofore the saturated hydrocarbons have not displayed significantly high rates of electrochemical oxidation directly at fuel cell anodes below the fused salt temperature region or about 500°C.

It has now been found that propane can be oxidized rapidly at a platinum catalyzed fuel cell anode at 150°C. A polarization curve (voltage *vs.* current density curve) obtained from a propane-oxygen fuel cell containing platinum catalyzed electrodes and 14.6M phosphoric acid electrolyte is shown in Fig. 1. A cross-section diagram of the cell

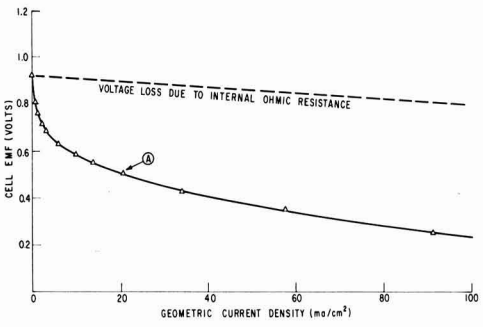

Fig. 1. Polarization curve for propane-oxygen fuel cell at 150°C; electrodes-platinum; electrolyte 14.6M phosphoric acid.

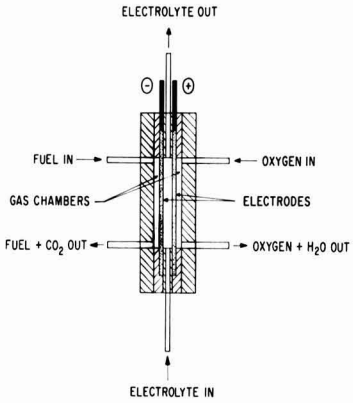

Fig. 2. Test cell cross section

used in the experimental work appears in Fig. 2. Two key features of this cell are (i) the employment of a new porous, gas electrode structure due to Niedrach and Alford (1) which preserves the catalytic (electrocatalytic) properties of platinum, and (ii) the employment of phosphoric acid electrolyte at a suitable temperature and concentration.

Practical implications of the results depend not only on obtaining high performance, but also on achieving complete oxidation of the fuel. The yield of CO_2 from the cell operating at point A of Fig. 1 was measured by a gas chromatographic method and found to be 98% ± 4% of that required by the reaction for complete anodic oxidation of propane

$$C_3H_8 + 6H_2O \rightarrow 3CO_2 + 20H^+ + 20e^-$$

The absence of a limiting current in the polarization curve is also of importance. This results from the thin structure of the new electrodes. Eight to ten mils thick, they are free from the long pores which tend to limit mass transport at relatively low current densities when the thicker "gas diffusion" electrodes of the literature are operated in the presence of inert gases (the CO_2 product in the present case). Similar freedom from limiting currents is seen when the new electrodes are operated on air to current densities of several hundred milliamperes per square centimeter.

Details of this work and further experiments up to 200°C will be reported later.

Acknowledgment

It is a pleasure to thank Miss Carol J. Michalske for carrying out the experimental work. This work was supported in part by the Advanced Research Projects Agency through the United States Army Engineer Research and Development Laboratories, Fort Belvoir, Virginia under Contract No. DA-44-009-ENG-4909.

Manuscript received April 15, 1963. Detailed paper was presented at the New York Meeting, Sept. 29-Oct. 3, 1963.

Any discussion of this paper will appear in a Discussion Section to be published in the June 1964 JOURNAL.

REFERENCE

1. L. W. Niedrach and H. R. Alford, To be published.

The Relative Corrosion Rates of Nickel Electrodeposits Having Different Textures

A. K. N. Reddy

The Electrochemistry Laboratory, University of Pennsylvania, Philadelphia, Pennsylvania

The author recently proposed (1, 2) a mechanism for the development of preferred orientations, with special reference to nickel electrodeposits. It was argued that textures result from two growth processes: (i) the preferential formation of facets of a particular crystallographic type, and (ii) the alignment of these facets normal to the substrate surface. The zone-axis of these "Wilman" facets becomes the texture axis.

The theory is applied, in this short communication, to some recent work (3) wherein it was observed that nickel electrodeposits having different preferred orientations confer different extents of protection against corrosion in dilute hydrochloric acid. Deposits with <210> orientation provide the best corrosion protection, and those with <110> orientation give less protection.

From the standpoint of the theory, deposits acquire a <210> texture by the formation of {211} facets on the free surface, and deposits with a <110> texture have octahedral facets. When {211} facets (in contrast to {111} facets) are exposed to the solution, not only can we consider the heat of hydrogen adsorption to be higher (4), and hence also the hydrogen overpotential (4, 5), but the dissolution of {211} facets can also be considered to be smaller [due to the reciprocity of growth and dissolution (6)].

The anodic dissolution reaction and the cathodic hydrogen evolution reaction are both hindered more on {211} facets than on {111} facets. Hence, the corrosion of deposits with {211} facets (*i.e.*, <210> texture) should be less than those with {111} facets (*i.e.*, <110> texture). This conclusion is in agreement with experiment.

Manuscript received Jan. 28, 1963; revised manuscript received June 24, 1963.

Any discussion of this paper will appear in a Discussion Section to be published in the June 1964 JOURNAL.

REFERENCES

1. A. K. N. Reddy, *J. Electroanal. Chem.*, **5** (1963).
2. A. K. N. Reddy and S. R. Rajagopalan, *ibid.*, **5** (1963).
3. B. C. Banerjee, *This Journal*, **107**, 80 (1960).
4. G. Okamoto, J. Horiuti, and K. Hirota, *Sci. Papers Inst. Phys. Chem. Res. Tokyo*, **29**, 223 (1936).
5. L. P. Bicelli and A. La Vecchia, *WADD Technical Note 60-270*, February 1961.
6. H. E. Buckley, "Crystal Growth," p. 304, John Wiley & Sons, Inc., New York (1951).

The Adsorption of Iron during Etching of Lithium Fluoride Crystals

G. Rosenblatt and M. B. Ives

Department of Metallurgy and Metallurgical Engineering, McMaster University, Hamilton, Ontario, Canada

The action of cation inhibitors in aqueous solutions on the etch morphology of cleavage surfaces of lithium fluoride has been exhaustively studied by Gilman, Johnston, and Sears (1). Of some thirty cations investigated only two, iron and aluminum, produced etchants that would form regular square dislocation etch pits. Gilman *et al.* concluded that the inhibitor ions, which need only be present in concentrations of the order of one part in 10^6, must be (*a*) within 25% of the size of the Li^+ ion, (*b*) have a stable fluoride salt with low solubility, and (*c*) form a stable fluoride complex. These criteria suggest that such ions will adsorb readily at cation sites on the crystal surfaces and thereby modify the dissolution conditions. That so few ions are necessary in solution to modify the etch morphologies profoundly suggests that they adsorb preferentially at the primary dissolution sources, *viz.*, kinks in crystal ledges (1, 2).

The present experiments were undertaken to investigate this possibility by relating the spatial distribution of adsorbed ferric ions to the etch morphologies. Etching of freshly cleaved {100} surfaces of lithium fluoride was carried out in dilute aqueous solutions of ferric chloride containing radioisotope Fe^{59} of known activity. After washing, the etched surfaces were placed on nuclear photographic emulsions and the distribution of radioactivity deduced by track-autoradiography. Preliminary experiments established that the washing procedures after etching produced a reproducible activity independent of washing time.

An early observation demonstrated that there is no (detectable) dependence of ferric ion adsorption on dislocation etch pit density, manifest as a constant track density over the whole of a given crystal surface. (Exceptions include large adsorption at gross defects, such as high cleavage steps, etc.) Any variations in track density with location of surface area measured are included in the statistical deviations of the mean results of track-counting fifteen areas per surface.

Using a ferric chloride stock solution of known specific activity of iron, a series of etchants was prepared of varying iron content and two lithium fluoride samples etched for 2 min in each. There is no observable change in adsorption for etching time greater than 3 sec. The ferric ion adsorption, measured as track densities (corrected for background) and converted to ions per square centimeter, is represented by the adsorption isotherm of Fig. 1. The isotherm is seen to exhibit a definite inflection corresponding to a mean iron coverage of about 3.5 x 10^{13} ions/cm^2, and occurring in the range of iron concentration in the bulk solution of from 0.2 to 2.0 x 10^{-6} parts by weight.

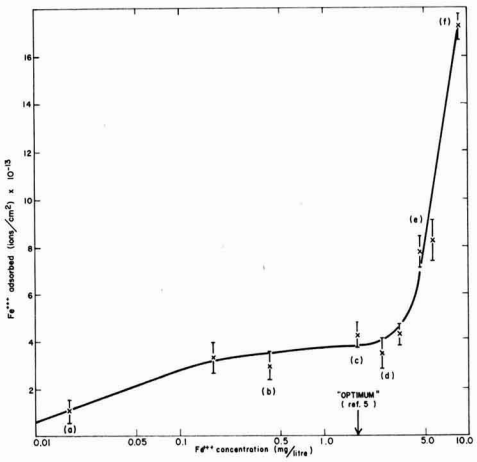

Fig. 1. Adsorption isotherm for ferric ions on a {100} cleavage surface of lithium fluoride at 22°C. (a), (b), (c), etc., refer to the bulk iron concentrations to which the micrographs of Fig. 2 correspond.

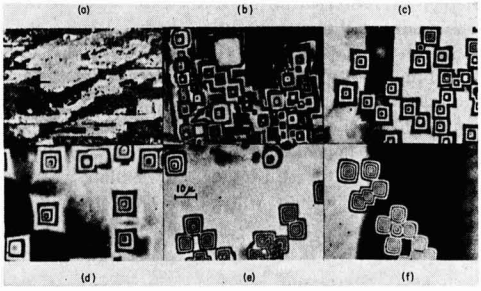

Fig. 2. Interference micrographs of dislocation etch pits on lithium fluoride surfaces etched in aqueous solutions of ferric chloride containing (a) 0.017; (b) 0.42; (c) 1.7; (d) 2.5; (e) 4.6; (f) 8.4 mg Fe^{+++}/liter.

Observation of dislocation etch pit morphology as a function of iron concentration followed the form first pointed out by Gilman *et al.* (1) and is demonstrated by the interference micrographs of Fig. 2. Correlation with the isotherm shows that the optimum etchant concentration (to produce square-based dislocation etch pits) corresponds closely to the point of inflection of the isotherm. At larger ferric ion concentrations, when adsorption increases, rounded pits are observed. At lower concentrations, terraced shallow pits correspond to less iron adsorption. These results are consistent with recent theoretical ideas on the effect of inhibitor on kink motion (2).

It should be realized that the whole surface of an ionic crystal is not available to an adsorbing cation (3). Assuming such an adsorbate to form a monolayer when all cation surface sites are filled, it is found that for the {100} surfaces of lithium fluoride, monolayer adsorption exists at 1.23×10^{15} ions/cm^2. On this scale, the adsorption inflection of Fig. 1 occurs at 1/35 of a monolayer of ferric ions.

Employing the established concepts of adsorption theory, this inflection may correspond to the complete filling of a particularly favorable type of adsorption site on a heterogeneous surface. It is attractive to suppose that these more favorable sites for the ferric ions are the kink-sites proposed by Gilman *et al.* (1). The inflection then corresponds to "monokink" adsorption. This suggests that in the ranges of optimum etchant concentration of iron, there will be, on the average, only three kinks in every hundred possible surface sites, the remainder comprising close-packed surface and straight ledges. This low density of kinks will cause the crystal surface to appear macroscopically composed of only ledge-surface {Okl} (2). This is observed in the form of flat-faced {Okl} pyramidal etch pits at points of dislocation emergence. Furthermore, for a uniform coverage of 1/35 of a monolayer, the absorbed ions will be about six sites apart in a square array, and this is approximately the spacing between monomolecular ledges on etch pit sides. This correlation suggests that dissolution morphologies are subject to part-poison, part-diffusion control (4) wherein the latter exists by the interaction of hemispherical diffusion fields centered on the dissolving kink-sites. The hemispheres can then interact both between kinks in the same ledge and between kinks in adjacent ledges. Also, since uniform iron coverage is observed, it is proposed that the whole crystal surface is composed, during dissolution, of {Okl} facets inclined to the close packed {100} plane at the same angle as the faces of etch pits. These other "surface" facets are not resolvable, however, since they are never able to attain sufficient size, due to the lack of a constant dissolution source. In many instances there is a suggestion of a surface mottle which could represent such facets.

Application of the Gibbs adsorption isotherm equation (5) to the results of this investigation allows for an estimate of the mean kink free energy, as follows. One form of the Gibbs equation may be written as

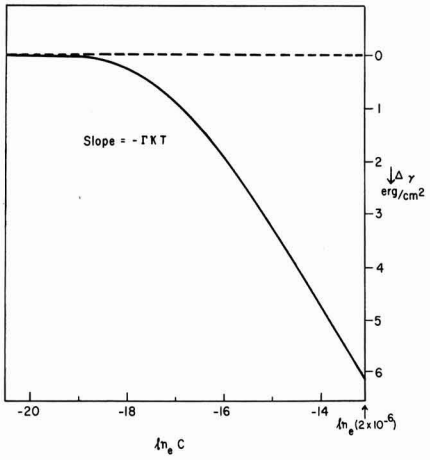

Fig. 3. Surface free energy of lithium fluoride surface as a function of the natural logarithm of the bulk solution concentration of ferric ions. Constructed geometrically.

$$\frac{d\gamma}{d(\ln c)} = -\Gamma kT$$

relating the rate of change of surface free energy γ with the natural logarithm of the bulk concentration of adsorbate, c, to the surface excess, Γ. Thus a curve of surface energy plotted against (ln c) will have instantaneous slope $-\Gamma kT$. Since we know Γ as a function of c, from the isotherm, we can therefore construct such a curve. This was done geometrically, and the result is reproduced in Fig. 3. Arbitrarily taking a bulk concentration of 2×10^{-6} for monokink adsorption, we obtain a measure of $\Delta\gamma$, the change in surface free energy due to the adsorption, as 6.1 erg/cm^2. Although the surface energy of a kink is not reduced completely to zero when it is filled with adsorbate, it can be assumed that a large fraction of its energy is reduced in this process, and the value obtained can be taken as a lower limit to the energy of kink-site in a lithium fluoride surface. These results give such a kink energy as 1.56×10^{-13} erg/kink, which appears to be of the correct order of magnitude, since it predicts a surface energy of a high index surface (maximum kink density) of approximately 200 ergs/cm^2. This compares favorably with the value of interfacial free energy of a {100} lithium fluoride surface in water of $\gamma_{LiF\text{-}H_2O} = 177$ erg/cm^2, used in a previous study (4).

In order to delineate further the kinetics of inhibitor adsorption in this system, it is necessary to deduce isotherms at other temperatures and undersaturations, and this work is in preparation. A complication feature of the system is its dynamic nature, in that the surface is continuously dissolving at a rate which, on the atomic scale, is considerable.

Acknowledgment

This work was performed under the sponsorship of the National Research Council of Canada and the U. S. Office of Naval Research.

Manuscript received March 25, 1963. This paper was presented at the Pittsburgh Meeting, April 15-18, 1963.

Any discussion of this paper will appear in a Discussion Section to be published in the June 1964 JOURNAL.

REFERENCES

1. J. J. Gilman, W. G. Johnston, and G. W. Sears, *J. Appl. Phys.*, **29**, 747 (1958).
2. M. B. Ives, *J. Phys. Chem. Solids*, **24**, 275 (1963).
3. W. C. Walker and A. C. Zettlemoyer, *J. Phys. Chem.*, **57**, 182 (1953).
4. M. B. Ives and J. P. Hirth, *J. Chem. Phys.*, **33**, 517 (1960).
5. See, for example, S. Brunauer, "The Adsorption of Gases and Vapors," Vol. 1, Princeton University Press, Princeton, N. J. (1945).

FUTURE MEETINGS OF
The Electrochemical Society

★ ★ ★

New York, N. Y., September 29, 30, and October 1, 2, and 3, 1963

Headquarters at the Hotel New Yorker

Sessions will be scheduled on Batteries (including Electrochemistry of Sealed Secondary Batteries and Recent Developments in Battery Testing), Corrosion (including Electron and Optical Microscopy Studies of Corrosion Processes and possibly, Reactions of Metals with Steam), Electrodeposition (including Electrodeposition from Nonaqueous Media and Physical Properties and Structure of Electrodeposits), Electronics (including Semiconductors), Electronics and Electrothermics and Metallurgy—Joint Symposium on Refractory Materials for Electron Devices, Electro-Organics (including Symposia on Biochemical Energy Conversion Processes and Radical Formation in Electro-Organic Reactions), Electrothermics and Metallurgy

★ ★ ★

Toronto, Ont., Canada, May 3, 4, 5, 6, and 7, 1964

Headquarters at the Royal York Hotel

Sessions probably will be scheduled on Electric Insulation, Electronics (including Luminescence and Semiconductors), Electrothermics and Metallurgy (E&M Div. will sponsor jointly with The Metallurgical Society of AIME, a Symposium on Electron and Ion Beam Science and Technology.)

★ ★ ★

Washington, D. C., October 11, 12, 13, 14, and 15, 1964

Headquarters at the Sheraton-Park Hotel

★ ★ ★

San Francisco, Calif., May 9, 10, 11, 12, 13, and 14, 1965

Sheraton Palace, Sir Francis Drake, and St. Francis Hotels

★ ★ ★

Buffalo, N. Y., October 10, 11, 12, 13, and 14, 1965

Headquarters at the Statler-Hilton Hotel

★ ★ ★

Cleveland, Ohio, May 1, 2, 3, 4, and 5, 1966

Headquarters at the Sheraton-Cleveland Hotel

★ ★ ★

Philadelphia, Pa., October 9, 10, 11, 12, 13, and 14, 1966

Headquarters at the Sheraton Hotel

Papers are now being solicited for the meeting to be held in Toronto, Ont., Canada, May 3, 4, 5, 6, and 7, 1964. **Triplicate copies of the usual 75-word abstract, as well as of an extended abstract of 500-1000 words** (see notice on following page), are due at Society Headquarters, 30 East 42 St., Rm. 1806, New York, N. Y., 10017, *not later than December 13, 1963* in order to be included in the program. *Please indicate on abstract for which Division's symposium the paper is to be scheduled, and underline the name of the author who will present the paper.* No paper will be placed on the program unless one of the authors, or a qualified person designated by the authors, has agreed to present it in person. Clearance for presentation of a paper at the meeting should be obtained before the abstract is submitted. An author who wishes his paper considered for publication in the JOURNAL or in ELECTROCHEMICAL TECHNOLOGY should send triplicate copies of the manuscript to the Managing Editor of the appropriate publication, 30 East 42 St., Rm., 1806, New York, N. Y., 10017.

Presentation of a paper at a technical meeting of the Society does not guarantee publication in the JOURNAL or in ELECTROCHEMICAL TECHNOLOGY. However, all papers so presented become the property of The Electrochemical Society, and may not be published elsewhere, either in whole or in part, unless permission for release is requested of and granted by the Editor. Papers already published elsewhere, or submitted for publication elsewhere, are not acceptable for oral presentation except on invitation by a Divisional program Chairman.

Extended Abstract Book Publication Program for the Society's 1964 Spring Meeting in Toronto

The Board of Directors has provided that the National Office shall assist Divisions with the mechanics of publishing Extended Abstracts for sessions involving 15 or more papers at our National Meetings.

The Divisions will handle the technical editing of the abstracts following which the Society Office will arrange for the printing and distribution of the books, thus relieving Division representatives of this responsibility. Each Division program will be the subject of a separate Extended Abstract Book.

This means that each author who submits a paper for presentation at our meeting should do three things:

1—Submit *three* **copies of the usual 75-word abstract of the paper for publication in the printed program of the meeting;**

2—Simultaneously submit *three* **copies of an extended abstract of the paper of 500-1000 words; and**

3—Send the 75-word abstract and the 500-1000-word extended abstract to Society Headquarters, 30 East 42 St., New York 17, N. Y., *not later than December 13, 1963.*

The Extended Abstract Books will be published by photo-offset reproduction *from typewritten copy submitted by the author.* Special care should therefore be given to the following typing instructions so as to establish uniformity in printing:

1—Abstracts are to be 500-1000 words in length.

2—Use white bond paper, size 8½ x 11 inches.

3—Abstracts should be typed SINGLE space.

4—Use 1¼ inch margins at the top and bottom and at the sides of each page.

5—All copy, including figure and corrections, should be in black ink.

6—Figures should be pasted in within the typing dimensions indicated. Captions should be typed not wider than figure dimensions and pasted in proper place in the abstract. Figure captions should appear at bottom of figure. Table titles should appear at top of tables.

7—Wherever possible, avoid use of halftones.

8—Title of paper should be in capital letters. Author(s) name and affiliation should be typed immediately below.

9—Mail to Society Headquarters *unfolded.*

Members and JOURNAL subscribers will receive notice of Extended Abstracts Books to be scheduled for publication. The notices will be accompanied by order blanks for the copies desired. Orders should be submitted with remittance. The advance orders will be necessary for estimating numbers of books to be printed and will be mailed to purchasers prior to the Toronto meeting. Some extra copies will be available at the meeting but the advance-paid order is the only way to be assured of getting copies.

Officers of Local Sections of The Electrochemical Society

(In cases where current information has not been available, the most recent officers have been listed.)

Council of Local Sections (1962-1963)
S. W. Scott, Chairman
1097 98 St., Niagara Falls, N. Y.
H. C. Gatos, Vice-Chairman
Morris Feinleib, Secretary
R. F. Bechtold † (1963-1965)
J. C. White † (1962-1964)

Boston (Spring 1963-1964)
E. H. Newton, Chairman
Arthur D. Little, Inc., 15 Acorn Park, Cambridge, Mass.
Walter W. Harvey, Secretary
John L. Sienczyk, Treasurer
H. C. Gatos* (1963-1965)
Paul T. Woodberry* (1963-1964)

Chicago (Spring 1963-1964)
John J. Daly, Jr., Chairman
Continental Can Co.,
1350 W. 76th St., Chicago 20, Ill.
George Timmings, Vice-Chairman
Arthur Haskell, Secretary
Herman Kerfman, Treasurer
Ernest Koehler* (1963-1965)

Cleveland (Fall 1963-1964)
L. F. Urry, Chairman
Union Carbide Consumers Products, Co., P.O. Box 6056, Cleveland 1, Ohio
L. V. McCarthy, Vice-Chairman
G. R. Gillooly, Secretary
J. Booker, Treasurer
R. A. Powers* (1963-1964)
D. E. Kinney* (1963-1964)

Columbus (Fall 1963-1964)
John McCallum, Chairman
Battelle Memorial Institute, 505 King Ave., Columbus 1, Ohio
Charles S. Peet, Jr., Vice-Chairman
Wilbur J. Wilson, Secretary-Treasurer
E. M. Sherwood* (1963-1964)
C. A. Snavely* (1963-1965)

Detroit (Spring 1963-1964)
Leland M. Morse, Chairman
3289 Interlaken, Rt. 2, Orchard Lake, Mich.
John L. Griffin, Vice-Chairman
Sam H. Dreisbach, Vice-Chairman
H. Chessin, Secretary-Treasurer
J. P. Hoare* (1962-1964)
A. E. Remick* (1963-1965)

India (Fall 1960 to Present)
M. S. Thacker, Chairman
Council of Scientific & Industrial Research, Old Mill Rd., New Delhi 2, India
A. Joga Rao, Vice-Chairman
S. Ramaswamy, Vice-Chairman
S. Krishnamurthy, Secretary-Treasurer
H. V. K. Vdupa*
J. Balachandra*

Indianapolis (Spring 1963-1964)
T. C. O'Nan, Chairman
4720 E. New York, Indianapolis 1, Ind.
M. L. Whitehurst, Vice-Chairman
Ambrose Smith, Secretary-Treasurer
George Fitzgibbons*

Midland (Spring 1963-1964)
J. L. Robinson, Chairman
Dow Chemical Co., Metallurgical Lab., Bldg. 241, Midland, Mich.
James L. Kroon, Vice-Chairman
Joseph H. Sullivan, Secretary-Treasurer

Mohawk-Hudson (Spring 1963-1964)
John H. Westbrook, Chairman
Ceramics Study Section, Res. Lab., General Electric Co., P.O. Box 1088, Schenectady, N. Y.
R. P. Hamlen, Vice-Chairman
E. J. Cairns, Secretary-Treasurer
M. W. Breiter*

New York Metropolitan (Spring 1963-1964)
Cecil V. King, Chairman
American Gas & Chemicals, Inc., Box 101, Gracie Station, New York 28, N. Y.
A. J. Salkind, Vice-Chairman
Carl J. Lang, Secretary-Treasurer
John Everhart*

Niagara Falls (Spring 1963-1964)
Walter Trainor, Chairman
611 Ferry Ave., Niagara Falls, N. Y.
Peter P. Beno, Vice-Chairman
Luther Vaaler, Secretary-Treasurer
S. Scott* (1963-1964)
J. Peterson* (1963-1965)

Ontario-Quebec (Spring 1963-1964)
André Hone, Chairman
Ecole Polytechnique, Montreal, Canada
T. R. Pezzack, Vice-Chairman (Program)
W. C. Cooper, Vice-Chairman (Membership)
A. J. Charez, Secretary-Treasurer
R. A. Campbell* (1963-1964)

Pacific Northwest (Spring 1963-1964)
Henry J. Wittrock, Chairman
Dept. of Met. Res., Kaiser Aluminum & Chemical Corp., Spokane 69, Wash.
Glen C. Ware, Vice-Chairman
John A. Ayres, Secretary-Treasurer

Philadelphia (Spring 1963-1964)
E. C. Evers, Chairman
University of Pennsylvania, Philadelphia 4, Pa.
H. C. Miller, Vice-Chairman
F. X. McGarvey, Secretary
A. A. Ware, Treasurer
G. F. Temple* (1963-1964)
G. Schnable* (1963-1965)

Pittsburgh (Spring 1963-1964)
R. P. Frankenthal, Chairman
U. S. Steel Research, Monroeville, Pa.
H. A. Johansen, Vice-Chairman
George Economy,
Secretary-Treasurer
W. Haupin* (1962-1964)
J. W. Faust, Jr.,* (1962-1963)

San Francisco (Spring 1963-1964)
H. F. Bauman, Chairman
1164 Danbury Dr., San Jose, Calif.
E. F. Duffek, Vice-Chairman
B. Deal, Secretary
D. C. Gernes, Treasurer
G. W. Waring*

Southern California-Nevada (Spring 1963-1964)
Lee J. Droege, Chairman
1514 W. Olympic Blvd., Los Angeles 15, Calif.
Anthony J. Kolk, Jr., Vice-Chairman
Nelson P. Nies, Secretary-Treasurer
W. M. Hetherington, Jr.* (1962-1964)
P. E. Friebertshauser* (1963-1965)

Texas (Spring 1963-1964)
Oliver Osborn, Chairman
Dow Chemical Co., Freeport, Texas
Isaac Trachtenberg, Vice-Chairman
Earl S. Snavely, Jr., Secretary-Treasurer
R. M. Hurd*

Washington-Baltimore (Spring 1963-1964)
Blanton C. Duncan, Chairman
13 Center St., Washington Grove, Md.
Gilbert W. Castellan, Vice-Chairman
Frederic M. Bowers, Secretary
Charles B. Kenahan, Treasurer
David Schlain* (1962-1964)
Joseph C. White* (1963-1965)

† Council Representative on Board of Directors.

* Representative on Council of Local Sections.

Officers of Divisions of The Electrochemical Society

Battery (Fall 1962-1964)
Arthur D. Fleischer, Chairman
466 S. Center St., Orange, N. J.
Thedford P. Dirkse, Vice-Chairman
Howard R. Karas, Secretary-Treasurer

Corrosion (Fall 1962-1964)
Harry C. Gatos, Chairman
Dept. of Metallurgy, Massachusetts Institute of Technology, Cambridge 39, Mass.
E. L. Koehler, Vice-Chairman
H. Leidheiser, Jr., Secretary-Treasurer

Electric Insulation (Spring 1963-1965)
C. C. Houtz, Chairman
Bell Telephone Laboratories, Inc., Murray Hill, N. J.
Barlane R. Eichbaum, Vice-Chairman
James R. Black, Secretary-Treasurer

Electrodeposition (Fall 1962-1964)
D. R. Turner, Chairman
Chem. Res. Dept., Bell Telephone Laboratories, Inc., Murray Hill, N. J.
Dan Trivich, Vice-Chairman
Edwin J. Smith, Secretary-Treasurer

Electronics (Spring 1963-1965)
Austin E. Hardy, Chairman
Chemical & Physical Lab., Radio Corporation of America, New Holland Pike, Lancaster, Pa.
Horace Homer, Vice-Chairman (General)
Eugene F. Apple, Vice-Chairman (Luminescence)
N. Bruce Hannay, Vice-Chairman (Semiconductors)
F. Hubbard Horn, Secretary-Treasurer

Electro-Organic (Fall 1960-1963)
M. J. Allen, Chairman
Melpar, Inc., 3000 Arlington Blvd., Falls Church, Va.
R. A. Day, Jr., Vice-Chairman
E. C. Olson, Secretary-Treasurer

Electrothermics & Metallurgy (Spring 1963-1965)
William E. Kuhn, Chairman
Spindletop Research Center, 975 Liberty Rd., Lexington, Ky.
Lawrence M. Litz, Vice-Chairman
T. D. McKinley, Vice-Chairman
Stanley T. Wlodek, Secretary-Treasurer

Industrial Electrolytic (Spring 1962-1964)
R. F. Bechtold, Chairman
4405 James Dr., Midland, Mich.
J. R. Currey, Vice-Chairman
Clifford Hampel, Secretary-Treasurer

Theoretical Electrochemistry (Spring 1963-1965)
Sidney Barnartt, Chairman
Westinghouse Research Labs., Beulah Rd., Churchill Boro, Pittsburgh 35, Pa.
Sigmund Schuldiner, Vice-Chairman
David A. Vermilyea, Secretary-Treasurer

Section News

San Francisco Section

At a recent meeting of the San Francisco Section of the Society the following officers were elected to office for the 1963-1964 season:

Chairman—H. F. Bauman, 1164 Danbury Dr., San Jose 29, Calif.

Vice-Chairman—E. F. Duffek, Fairchild Semiconductor Co., 4001 Junipera Serra Blvd., Palo Alto Calif.

Secretary—Bruce Deal, Fairchild Semiconductor Co., 4001 Junipera Serra Blvd., Palo Alto, Calif.

Treasurer—D. C. Gernes, P. O. Box 870, Los Gatos, Calif.

Councillor—Worden Waring, Fairchild Semiconductor Co., 4001 Junipera Serra Blvd., Palo Alto, Calif.

H. F. Bauman,
Chairman

Calendar of Events

Other Organizations

Conference on Electrical Insulation of the National Academy of Sciences-National Research Council, Greenbrier Hotel, White Sulphur Springs, W. Va. Nov. 3-6, 1963.

The Pittsburgh Conference, Penn-Sheraton Hotel, Pittsburgh, Pa. March 2-6, 1964.

Fourth Rare Earth Research Conference, Camelback Inn, Phoenix, Ariz. April 22-25, 1964.

Fourth Informal Conference on Vacuum Microbalance Techniques, Mellon Institute Auditorium, Pittsburgh, Pa. May 7-8, 1964.

Personal

Walter A. Koehler retired from West Virginia University at the end of June, 1963. Dr. Koehler was Director of the Engineering Experiment Station, Associate Dean of the College of Engineering, and Professor of Chemical Engineering. The Koehlers now reside in Sister Bay, Wis.

Letter to the Editor

Dear Sir:

I would be grateful if you would draw the attention of the readers of your JOURNAL to the fact that high enrichments of both stable isotopes of oxygen have recently been achieved. Up to 99 atom % Oxygen-18 has been available for some time in various chemical forms and has already been widely used in chemistry and biology as a tracer and as both target and projectile in nuclear studies. Oxygen-18 labelled compounds also have great potentialities in studies of isotope effects and spectral isotopic shifts.

Oxygen-17 with a spin of 5/2 is the only isotope of oxygen which can be used for NMR and ESR studies. Enrichments of over 10 atom % O^{17} in water and 50 atom % O^{17} in oxygen gas have recently been reached on a production scale in the Isotope Separation Plant of the Weizmann Institute of Science. These concentrations represent a 250 fold enrichment of O^{17} in water and 1350 fold enrichment in oxygen gas.

These materials are now available through YEDA Research and Development Co., Rehovoth, Israel. Under separate cover, I am sending you a booklet containing some pertinent references and a catalogue of O^{18} and O^{17}-enriched materials.

Further copies of this booklet are available on request.

A. Ravia
The Weizmann Institute
of Science

Notice to Members and Subscribers

(Re Changes of Address)

To insure receipt of each issue of the JOURNAL, please be sure to give us your old address, as well as your new one, when you move. Our records are filed by states and cities, not by individual names. The Post Office does not forward magazines.

We should have this information *by the 16th of the month* to avoid delays in receipt of the next issue.

Obituaries

Thomas D. Callinan

The Society and many friends and business associates have suffered a grievous loss in the death of Thomas D. Callinan in an air lines crash near Rochester, N. Y., on July 2, 1963.

He was a native of New York and was educated in New Jersey, received a B.S. degree from St. Peter's College in Jersey City in 1939. He began his career in dielectrics at the Ellis Laboratories in Montclair, N. J., where he spent two years in the development of polyester resins for component encapsulation. During the next six years he worked successively at the General Electric Co. in Pittsfield, the Industrial Condenser Corp., in Chicago, the Western Electric Co. in Hawthorne near Chicago, and the Johns-Manville Research Center in Manville, N. J. In these positions, he invented and developed asbestos fiber capacitor papers and contributed to the development of oil-impregnated capacitors for military applications. In 1947, he joined the U.S. Naval Research Laboratory in Washington, D. C., as a consultant. Here he spent ten years in the study of capacitor materials, inventing and improving such materials as glass fiber, glass flake, silica fiber and ceramic fiber papers for capacitor dielectrics; liquid and elastomeric impregnants; and additives to inhibit radiation deterioration of dielectrics. He returned to private industry in 1956 as the manager of the paper and ink research section at the Watson Research Center of International Business Machines Corp. in Yorktown Heights, N. Y. Here he was concerned with practically all aspects of cellulosic materials, drawing on his background of experience in dielectric sheet materials and expanding his interest in their physical and chemical properties.

Joining The Electrochemical Society shortly after beginning his professional career, he affiliated with the Electric Insulation Division and became one of its outstanding members in service to the Society. He was twice Chairman of the Division and a member of the Board of Directors of the Society, in 1951 and in 1961-1962. He was the Electric Insulation Division Editor of the JOURNAL from 1958 until his death. Among other positions, he had also been Chairman of the Steering Committee for the National Convention in Washington in 1957 and for three years was on the Society's Membership Committee.

He also held membership in a number of other technical societies, including the Conference on Electrical Insulation of the National Research Council, where he was editor in 1961 and a member of various committees; the American Chemical Society; the Institute of Radio Engineers and the American Institute of Electrical Engineers (now combined); the Technical Association of the Pulp and Paper Industry; and the National Conference on the Application of Electrical Insulation, where he served as program vice-chairman in 1961 and session chairman in 1958.

The loss to science by this untimely death is brought to focus by consideration of his accomplishments in what in terms of years would be about half of a usual life-time career, in that he was the holder of several patents, the author of some 40 papers of both original and review material and a speaker before a wide variety of audiences. His loss leaves a void in the affairs of The Electrochemical Society and the Electric Insulation Division in particular which will take several lesser men to fill, as his combination of unfailing good humor, ability to come to grips with problems and unflagging effort is not often found in one individual. Many of us will miss him greatly as a personal friend, while the Society and the scientific world have lost a highly valued member from whom many more years of constructive effort had been anticipated. Our sincerest sympathy goes to his wife, who has suffered the greatest loss of all.

Charles C. Houtz, *Chairman*
Electric Insulation Division

Leo Cavallaro

Leo Cavallaro, Dean of the Faculty of Sciences in the University

of Ferrara, died on June 29, 1963 in Farrara, Italy. He was 58 years old. Professor Cavallaro was Director of the Chemical Institute, Director of the Corrosion Center, Aldo Dacco, Past-President of the Accademia Della Scienze Di Ferrara, and winner of the Golden Medal for Science and Culture.

Milo W. Krejce

Milo W. Krejce, 87, of Newark, Dela., died in his home on Monday, June 24, 1963.

Mr. Krejce graduated from the Case School of Applied Science in Cleveland, Ohio, in 1898. He worked for many firms, including the Boston and Montana Consolidated Copper and Silver Mining Co., Great Falls, Mont., from 1900-1910; and the Anaconda Copper Mining Co. in Great Falls from 1910-1920. In 1923 he started a private practice as a consultant metallurgical engineer.

From 1930-1932 he was a consultant for the USSR and from 1941-1953 worked for the Reconstruction Finance Corp. and was on the U.S. Metals Reserve Government Board.

He was a member of The Electrochemical Society, the American Institute of Mining Engineers and Metallurgists, and was a member of the Worcester First Presbyterian Church, Masonic Order, and the Worcester Rotary Club.

Book Reviews

"Thermodynamische Elektrochemie," by E. Lange and H. Göhr, Alfred Hüthig Verlag Heidelberg, 1962, 429 pp., DM 39.00.

The book describes in 22 chapters the fundamental electrochemical aspects of single- and multiple-phase systems in the presence and absence of electric current and temperature differences. Typical subjects covered are: single electrodes in electrochemical equilibrium (11 pp.), the electrochemical double layer (14 pp.), galvanic cells (48 pp.), polarized electrodes (30 pp.), electrodes with surface layers (13 pp.), and their relation to corrosion (26 pp.), and passivation of iron (30 pp.). An appendix (30 pp.) deals essentially with systematics of terminology. The presentation is elementary and clear and requires from the reader an only moderate knowledge of German and thermodynamics and virtually none of mathematics.

The authors' preface claims that significant progress has been made in the last two decades, particularly in the use of chemical and electrochemical potentials, and that the properties of complex *multiphase systems* can now be deduced quantitatively from those of *single phases* (italics are the authors'). In the reviewer's opinion, most of the recent progress has been in kinetics while little has been added to thermodynamics since Guggenheim, about 30 years ago. Indeed, the book does not really break new ground but, rather, translates conventional electrochemical thermodynamics into a different formalism, characterized by the authors' building-block approach as stressed in the preface. This mechanistic approach is carried through with consistent clarity and precision and has great didactical merit. Cause and effect in many phenomena as well as distinctions such as that between Galvani and Volta potential differences become readily apparent and are easily understood and remembered. On the other hand, this approach lets the authors embark into thermodynamics from single-ion potentials and activities (p. 29), chemical potentials of electrons and silver ions in metallic silver (p. 30), single phase-boundary potentials (p. 63), and other such quantities which are thermodynamically ill-defined and whose physical significance has been questioned by thermodynamic purists. The results, of course, conform with rigorous thermodynamics as far as measurable quantities (emf of a cell, *etc.*) are concerned, so that the end largely justifies the means. Nevertheless, it is unfortunate that this thermodynamics text fails to explain and defend its essentially nonthermodynamic starting point.

A temptation inherent in the mechanistic approach is to include kinetic aspects. To this the authors have succumbed but have met with the impossibility of providing an adequate basis in a moderate-size thermodynamics text. The kinetic derivations are based on tacit oversimplifications (cf., derivation of the Nernst-Einstein relation, Sec. 3-10; limiting current, Sec. 14-6) and deal almost exclusively with the often less interesting steady state.

Great and commendable care has been taken to use a rigorous and consistent notation. This reflects Dr. Lange's leading work in terminology

June 1964 Discussion Section

A Discussion Section, covering papers published in the June-December 1963 JOURNALS, is scheduled for publication in the June 1964 issue. Any discussion which did not reach the Editor in time for the December 1963 Discussion Section will be included in the June 1964 issue.

Those who plan to contribute remarks for this Discussion Section should submit their comments or questions in triplicate to the Managing Editor of the JOURNAL, 30 East 42 St., Rm. 1806, New York, N. Y., 10017, *not later than March 2, 1964.* All discussion will be forwarded to the author(s) for reply before being printed in the JOURNAL.

Notice to Members
Re Voting Ballot

You soon will receive your official voting ballot from Society Headquarters. Please return it by *December 15* so that your vote can be included in the final election count.

commissions. But may be the authors have overshot their goal. The book starts with a 5-page list of symbols (including entries such as "B, a constant" and "f, symbol for function of") followed by a 7-page treatise defining and classifying the branches of natural sciences in terms of their concern with the various forms of matter, their transformations, and quantities observed. Later, the attempt at ultimate rigor in notation often leads to accumulation of subscripts, subscripted subscripts, and superscripts with the result that even some simple equations are difficult to read. The 30-page appendix includes definitions of terms such as "unit" and "quantity", discusses mass as defined in terms of inertia or gravity, *etc.* The reader gains the impression that the authors' main concern was not so much with the how and why but, rather, with defining exhaustively (and exhaustingly) phenomena and quantities and giving each its logical name and symbol, to be filed for future reference.

These criticisms should not detract from the otherwise high quality of the book. To give so wide and balanced a coverage in a text of modest length is an achievement. The reviewer has seen few books prepared with so much care and attention to detail.

Although not for use as a text, the book can be recommended to those interested in the field and its didactic aspects.

F. Helfferich,
Shell Development Co.

"The Collected Works of Irving Langmuir," Edited by Guy Suits, Pergamon Press Ltd., New York, 1961. Vol. I, 481 pp.; Vol. II, 415 pp.; Vol. III, 481 pp.; Vol. IV, 409 pp.; Vol. V, 261 pp.; Vol. VI, 304 pp.; Vol. VII, 227 pp.; Vol. VIII, 251 pp.; Vol. IX, 521, pp.; Vol. X, 451 pp.; Vol. XI, 597 pp.; and Vol. XII, 473 pp. $15.00 per volume.

The two hundred and twenty nine articles and reports in these twelve volumes are the complete scientific output of the late great Irving Langmuir. The first paper was published in 1906, the last in 1955, two years before his death.

Much of this material is primarily of historical interest. At the time of publication, most of the articles were outstanding contributions in their particular field and a surprising number were of fundamental importance. However, over a fifty year period, many of Langmuir's theories have become commonplace and axiomatic to those now standing on his scientific shoulders. Why then should this set of books be recommended to the libraries of all universities and research institutions?

For the graduate student, each volume serves as an excellent introduction to its field. The grouping of papers by topic and subtopic and their arrangement in chronological order show the development of Langmuir's ideas, which were usually basic to the field. Also in each volume, the introductory article, written by a scientist of the stature of Bridgeman or Roginski, discusses currently accepted theories and Langmuir's contributions. For the teacher and the nonspecialist, each volume is an excellent review of classical work in a broad field of fundamental importance, such as surface chemistry. For the specialist,

Notice to ECT Subscribers

Nonmember subscriptions to ELECTROCHEMICAL TECHNOLOGY will expire on *December 31, 1963.*

Avoid missing any issue. Send us your remittance now in the amount of $15.00 for your 1964 subscription. (Subscribers outside the continental United States must add $1.00 to the subscription price for postage.)

The 1964 bound volumes of ELECTROCHEMICAL TECHNOLOGY can be obtained at the prepublication price of $4.00 by adding this amount to your remittance. However, no orders will be accepted at this rate after *December 1, 1963,* when the price will be increased to $6.00 subject to prior acceptance. Bound volumes are *not* offered independently of your ECT subscription.

Manuscripts and Abstracts for Spring 1964 Meeting

Papers are now being solicited for the Spring Meeting of the Society, to be held at the Royal York Hotel, in Toronto, Ont., Canada, May 3, 4, 5, 6, and 7, 1964. Technical sessions probably will be scheduled on: Electric Insulation, Electronics (including Luminescence and Semiconductors), Electrothermics and Metallurgy, Industrial Electrolytic, Theoretical Electrochemistry

To be considered for this meeting, **triplicate copies of the usual 75-word abstract, as well as of an extended abstract of 500-1000 words** (see notice on page 234C of this issue), must be received at Society Headquarters, 30 East 42 St., Rm. 1806, New York, N. Y., 10017, *not later than December 13, 1963. Please indicate on abstract for which Division's symposium the paper is to be scheduled, and underline the name of the author who will present the paper.* No paper will be placed on the program unless one of the authors, or a qualified person designated by the authors, has agreed to present it in person. Clearance for presentation of a paper at the meeting should be obtained before the abstract is submitted. An author who wishes his paper considered for publication in the JOURNAL or ELECTROCHEMICAL TECHNOLOGY should send triplicate copies of the manuscript to the Managing Editor of the appropriate publication, 30 East 42 St., Rm. 1806, New York 17, N. Y.

Presentation of a paper at a technical meeting of the Society does not guarantee publication in the JOURNAL or in ELECTROCHEMICAL TECHNOLOGY. However, all papers so presented become the property of The Electrochemical Society, and may not be published elsewhere, either in whole or in part, unless permission for release is requested of and granted by the Editor. Papers already published elsewhere, or submitted for publication elsewhere, are not acceptable for oral presentation except on invitation by a Divisional program Chairman.

there is collected here a large quantity of experimental data, originally published in widely scattered journals over a period of many years. For all categories of readers, the phenomenological approach and the emphasis on experimentation and observation served as a timely reminder that the purpose of a theory is to explain and predict experimental observation.

The grouping of the papers is as follows: Vol. 1, low-pressure phenomena; vol. 2, heat transfer and incandescent tungsten; vol. 3, thermionic phenomena, including thermionics, vacuum pumps, electron emission, and adsorbed films; vol. 4, electrical discharge; vol. 5, plasma and oscillations; vol. 6, structure of matter, including atomic structure; vol. 7, protein structure; vol. 8, properties of matter, including fundamental properties of liquids and solids and interfacial phenomena; vol. 9, surface phenomena, including evaporation, condensation, and adsorption, and monomolecular films; vol. 10, atmospheric phenomena; vol. 11, cloud nucleation; and vol. 12, biography and philosophy.

At the price of $15 per volume, presumably, the publishers expected to sell only complete sets to libraries, although each volume starts with the same foreword, by Guy Suits. Unfortunately, libraries usually bury volumes of collected papers in the biographical sections. A lower price and a wider distribution would have been infinitely preferable. There is so much of value in each volume that it is a shame that the average chemist or student has been priced out of the market.

H. W. Salzberg

Positions Wanted

Please address replies to the box number shown, c/o The Electrochemical Society, 30 East 42 St., New York, N. Y., 10017.

Corrosion Chemist, Ph.D.—Seeks position in corrosion or related fields. Over twelve years experience in the various aspects of corrosion of a wide variety of metals and alloys. Numerous publications, honor societies, and patents pending. Metropolitan New Jersey area desired. *Reply to Box A 298.*

European citizen, five years experience in electrode kinetics, experience in techniques of polarography, electronic circuits for transients at electrodes, electron diffraction of metal deposits, various types of *in situ* microscopy on electrodes, crystal growth, *etc.* Has background academic qualifications equivalent to Masters Degree. Several publications. Two years experience American University. Intends U. S. citizenship. *Reply to Box A 299.*

Advertiser's Index

The Electrochemical Society

Patron Members

Aluminum Co. of Canada, Ltd.,
Montreal, Que., Canada
International Nickel Co., Inc.,
New York, N. Y.
General Electric Co.
Capacitor Dept., Hudson Falls, N. Y.
Chemical Laboratory, Knolls Atomic Power Laboratory, Schenectady, N. Y.
Chemical and Materials Engineering Laboratory, Advanced Technology Laboratories, Schenectady, N. Y.
Chemistry Research Dept., Schenectady, N. Y.
Direct Energy Conversion Operation, West Lynn, Mass.
Lamp Division, Cleveland, Ohio
Materials & Processes Laboratory, Large Steam Turbine-Generator Dept., Schenectady, N. Y.
Metallurgy and Ceramics Research Dept., Schenectady, N. Y.
Olin Mathieson Chemical Corp.,
Chemicals Div., Research Dept., New Haven, Conn.
Union Carbide Corp.
Divisions:
National Carbon Co., New York, N. Y.
Union Carbide Consumer Products Co., New York, N. Y.
Westinghouse Electric Corp., Pittsburgh, Pa.

Sustaining Members

Air Reduction Co., Inc., New York, N. Y.
Ajax Electro Metallurgical Corp.,
Philadelphia, Pa.
Allen-Bradley Co., Milwaukee, Wis.
Allied Chemical Corp.
General Chemical Div., Morristown, N. J.
Alloy Steel Products Co., Inc., Linden, N. J.
Aluminum Co. of America,
New Kensington, Pa.
American Metal Climax, Inc.
New York, N. Y.
American Potash & Chemical Corp.,
Los Angeles, Calif.
American Smelting and Refining Co.,
South Plainfield, N. J.
American Zinc Co. of Illinois,
East St. Louis, Ill.
American Zinc, Lead & Smelting Co.,
St. Louis, Mo.
M. Ames Chemical Works, Inc.,
Glens Falls, N. Y.
Ampex Corp., Redwood City, Calif.
Armco Steel Corp., Middletown, Ohio
Basic Inc., Maple Grove, Ohio
Bell Telephone Laboratories, Inc.,
New York, N. Y. (2 memberships)
Bethlehem Steel Co., Bethlehem, Pa.
(2 memberships)
Boeing Co., Seattle, Wash.
Burgess Battery Co., Freeport, Ill.
(2 memberships)
Burndy Corp., Norwalk, Conn.
Canadian Industries Ltd., Montreal,
Que., Canada
Carborundum Co., Niagara Falls, N. Y.
Consolidated Mining & Smelting Co. of
Canada, Ltd., Trail, B. C., Canada
(2 memberships)
Continental Can Co., Inc., Chicago, Ill.
Cooper Metallurgical Associates, Cleveland,
Ohio
Corning Glass Works, Corning, N. Y.
Diamond Alkali Co., Painesville, Ohio
Dow Chemical Co., Midland, Mich.
Wilbur B. Driver Co., Newark, N. J.
(2 memberships)
E. I. du Pont de Nemours & Co., Inc.,
Wilmington, Del.
Eagle-Picher Co., Chemical and Metals Div.,
Joplin, Mo.
Eastman Kodak Co., Rochester, N. Y.
Thomas A. Edison Research Laboratory, Div.
of McGraw-Edison Co., West Orange, N. J.
Electric Auto-Lite Co., Toledo, Ohio
C & D Div., Conshohocken, Pa.
Electric Storage Battery Co., Yardley, Pa.
Engelhard Industries, Inc., Newark, N. J.
(2 memberships)
The Eppley Laboratory, Inc., Newport, R. I.
(2 memberships)
Exmet Corp., Tuckahoe, N. Y.
Fairchild Semiconductor Corp., Palo Alto,
Calif.
FMC Corp.
Inorganic Chemical Div., Buffalo, N. Y.
Chlor-Alkali Div., South Charleston, W. Va.
Foote Mineral Co., Exton, Pa.
Ford Motor Co., Dearborn, Mich.
General Motors Corp.
Allison Div., Indianapolis, Ind.
Delco-Remy Div., Anderson, Ind.
Research Laboratories Div., Warren, Mich.
General Telephone & Electronics
Laboratories Inc., Bayside, N. Y.
(2 memberships)
Globe-Union, Inc., Milwaukee, Wis.
B. F. Goodrich Chemical Co.,
Cleveland, Ohio
Gould-National Batteries, Inc.,
Minneapolis, Minn.

(Sustaining Members cont'd)

Great Lakes Carbon Corp., New York, N. Y.
Hanson-Van Winkle-Munning Co.,
Matawan, N. J. (2 memberships)
Harshaw Chemical Co., Cleveland, Ohio
(2 memberships)
Hercules Powder Co., Wilmington, Del.
Hill Cross Co., Inc., West New York, N. J.
Hoffman Electronics Corp., Semiconductor
Div., El Monte, Calif.
Hooker Chemical Corp., Niagara
Falls, N. Y. (3 memberships)
HP Associates, Palo Alto, Calif.
Hughes Research Laboratories, Div. of
Hughes Aircraft Co., Malibu, Calif.
International Business Machines Corp.
New York, N. Y.
International Minerals & Chemical
Corp., Skokie, Ill.
International Resistance Co., Philadelphia,
Pa.
ITT Federal Laboratories, Div. of
International Telephone & Telegraph
Corp., Nutley, N. J.
Jones & Laughlin Steel Corp.,
Pittsburgh, Pa.
K. W. Battery Co., Skokie, Ill.
Kaiser Aluminum & Chemical Corp.
Div. of Chemical Research,
Permanente, Calif.
Div. of Metallurgical Research,
Spokane, Wash.
Kawecki Chemical Co., Boyertown, Pa.
Kennecott Copper Corp., New York, N. Y.
Leesona Moos Laboratories, Div. of Leesona
Corp., Jamaica, N. Y.
Libbey-Owens-Ford Glass Co., Toledo, Ohio
Lockheed Aircraft Corp.,
Missiles & Space Div., Sunnyvale, Calif.
Mallinckrodt Chemical Works, St. Louis, Mo.
P. R. Mallory & Co., Indianapolis, Ind.
Martin-Marietta Corp., Baltimore, Md.
Melpar, Inc., Falls Church, Va.
Merck & Co., Inc., Rahway, N. J.
Miles Chemical Co., Div. of Miles
Laboratories, Inc., Elkhart, Ind.
Minneapolis-Honeywell Regulator Co.,
Minneapolis, Minn.
Minnesota Mining & Manufacturing Co.,
St. Paul, Minn.
Monsanto Chemical Co., St. Louis, Mo.
M&T Chemicals Inc., Detroit, Mich.
National Cash Register Co., Dayton, Ohio
National Lead Co., New York, N. Y.
National Research Corp., Cambridge, Mass.
National Steel Corp., Weirton, W. Va.
North American Aviation, Inc., Rocketdyne
Div., Canoga Park, Calif.
Northern Electric Co., Montreal, Que.,
Canada
Norton Co., Worcester, Mass.
Owens-Illinois Glass Co., Toledo, Ohio
Pennsalt Chemicals Corp.,
Philadelphia, Pa.
Phelps Dodge Refining Corp., Maspeth, N. Y.
Philco Corp., Research Div., Blue Bell, Pa.
Philips Laboratories, Inc., Irvington-on-
Hudson, N. Y.
Pittsburgh Plate Glass Co., Chemical Div.,
Pittsburgh, Pa.
Potash Co. of America,
Carlsbad, N. Mex.
The Pure Oil Co., Research Center,
Crystal Lake, Ill.
Radio Corp. of America
Tube Div., Harrison, N. J.
RCA Victor Record Div., Indianapolis,
Ind.
Ray-O-Vac Co., Madison, Wis.
Raytheon Co., Waltham, Mass.
Remington Rand, Div. of Sperry Rand Corp.,
New York, N. Y.
Reynolds Metals Co., Richmond, Va.
Shawinigan Chemicals Ltd., Montreal, Que.,
Canada
Socony Mobil Oil Co., Inc.,
Dallas, Texas
Speer Carbon Co.
International Graphite & Electrode
Div., St. Marys, Pa.
Sprague Electric Co., North Adams, Mass.
Stackpole Carbon Co., St. Marys, Pa.
Stauffer Chemical Co., New York, N. Y.
Tennessee Products & Chemical Corp.,
Nashville, Tenn.
Texas Instruments, Inc., Dallas, Texas
Metals and Controls Corp.,
Attleboro, Mass.
Titanium Metals Corp. of America,
Henderson, Nev.
Udylite Corp., Detroit, Mich.
(4 memberships)
United States Borax & Chemical Corp.,
Los Angeles, Calif.
United States Steel Corp., Pittsburgh, Pa.
Universal-Cyclops Steel Corp.,
Bridgeville, Pa.
Upjohn Co., Kalamazoo, Mich.
Western Electric Co., Inc., Chicago, Ill.
Wyandotte Chemicals Corp.,
Wyandotte, Mich.
Yardney Electric Corp., New York, N. Y.